The mechanism and manipulation of PK-M alternative splicing

Thesis Dissertation

By
Zhenxun Wang

Watson School of Biological Sciences, Cold Spring Harbor Laboratory

Advisor: Dr. Adrian R. Krainer

December 2011

TABLE OF CONTENTS

TABLE OF FIGURES

1 CHAPTER 1: INTRODUCTION

1.1 Splicing and its importance in gene expression

Pre-mRNA splicing involves the precise excision of intervening RNA sequences known as introns, and the joining of flanking coding sequences, known as exons, during or immediately after the transcription of primary mRNA (Black, 2003). This process is widespread and is considered to be an obligate step for the expression of the vast majority of human genes. An analysis of all annotated human genes revealed that the transcribed genome consists of approximately 230000 exons and 210000 introns, roughly nine exons and eight introns per gene (Sakharkar et al., 2004).

1.2 Canonical splicing *cis*-elements

Exon-intron junctions on the pre-mRNA are demarcated by specific sequence motifs. The motifs are conserved yet degenerate, and consist of the branchpoint sequence (BPS), the 5' splice site (5'ss) and the 3' splice site (3'ss). The BPS is typically present 18-40 nucleotides upstream from the 3'ss (Will and Luhrmann 2011), and a polypyrimidine-rich tract (PPT) lies between both. These splicing elements are necessary for splicing of the pre-mRNA, and serve as binding sites for the step-wise recruitment and assembly of spliceosomal components, which carry out the actual splicing reaction.

1.3 The molecular mechanism of splicing

The spliceosome is a nuclear macromolecular complex consisting of small RNAs and proteins. Individual small RNA-protein complexes, termed small nuclear ribonuclear proteins (snRNPs) are sequentially recruited to exon-intron junctions by binding the canonical splicing elements present on the pre-mRNA (Hastings and Krainer, 2001).

The U1, U2, U4/U6 and U5 snRNPs are the main components of the spliceosome and are involved in the removal of most introns in the eukaryotic genome. In some metazoans and plants, a second, minor spliceosome, which consists of the U11/U12, U4atac/U6atac, and U5 snRNPs, is needed to process the rarer U12-class of introns (Patel and Steitz, 2003). Although minor spliceosome snRNP components recognize different splice sites and BPS sequences, they are analoglous to the major spliceosome in function, with the U5 snRNP being used by both kinds of spliceosomes.

These snRNPs have been characterized intensely *in vitro* and it has been found that the stepwise assembly and intramolecular rearrangements of snRNPs on the pre-mRNA are required to render the spliceosomal complex catalytically active and competent to perform the actual splicing reaction (Will and Luhrmann, 2011). Initial recognition of the intron-exon junctions occurs through the recruitment of U1 snRNP to the 5'ss via RNA:RNA interactions; protein components associated with the U2 snRNP bind to the BPS and 3'ss at the same time, forming the E complex. The A complex is formed when the U2 snRNA base-pairs with the BPS evicting the initially bound SF1 protein in the E complex. The U4/U6 and U5 tri-snRNP complex is then recruited to the B complex. The B complex is then rendered catalytically active through a series of arrangements that includes the eviction of U1 and U4

snRNPs forming the C complex, and it then carries out the first transesterification step of the splicing reaction,

In the first step, the 2'OH group of the adenosine branchpoint nucleotide attacks the phosphodiester bond of the 5'ss, cleaving it and ligating the 5'end of the intron to the adenosine, forming a lariat. Additional rearragements then occur, which render the spliceosome competent to carry out the second transesterification step.

In the second step, the free 3'OH group of the upstream exon attacks the 3'ss, forming a new phosphodiester bond that joins both exons, with the simultaneous removal of the intron lariat. After this step, the spliceosome dissociates, releasing the mRNA as an mRNP. The free snRNPs then reassembles elsewhere in the nascent pre-mRNA to carry out splicing reactions.

Although the details of snRNP rearrangements in the later steps of splicing are poorly understood, note that all rearrangements involve numerous individually weak RNA:protein and RNA:RNA interactions. These interactions collectively stabilize the spliceosomal complex, allowing it recognize degenerate splice signals with great fidelity, and catalyze the splicing reaction with great flexibility, even at long (>10 kb) intronic distances, in a regulated manner.

1.4 Splicing is linked to the downstream steps of gene expression

Splicing effector proteins that mediate post-transcriptional processes are usually deposited on the mature mRNA in a splicing-dependent manner (Moore and Proudfoot, 2009). This allows splicing to be coupled to these processes (Long and Caceres, 2009), which include mRNA export (Huang and Steitz, 2005), translation (Michlewski et al., 2008), and surveillance of premature stop codons by the nonsense-mediated decay machinery

(NMD) (McGlincy and Smith, 2008; Zhang and Krainer, 2004). In particular, the exon-junction (EJC) protein complex was found to be stably deposited on spliced mRNA about 20-24 nucleotides upstream of exon-exon junctions (Le Hir et al., 2000), where it participates in mRNA surveillance. The EJC complex accompanies the mRNA as it is transported into the cytoplasm, where it is removed by during the pioneer round of translation. In the event that a premature stop codon is present more than 50 nucleotides upstream of an EJC on the mRNA the EJC complex is not removed from the mRNA and this induces the recruitment of RNA decay machinery that leads to the inhibition of translation of, and to the eventual degradation of the transcript (Chang et al., 2007; Stalder and Muhlemann, 2008).

1.5 Alternative splicing is a major source of proteomic diversity in eukaryotes

By differentially splicing exons or exon segments from pre-mRNA, multiple mature mRNAs can be generated from the same pre-mRNA transcript (Black, 2003; Matlin et al., 2005). This process, known as alternative splicing, is a major source of protein isoform diversity in mammals (Black, 2000). An analysis of tissue-specific splicing via exon-junction micrarrays revealed that 74% of more than 10000 genes analyzed encode transcripts that result in multiple spliced isoforms (Johnson et al., 2003). Recent RNA deep-sequencing experiments also confirm and extend this analysis, estimating that nearly all (92% -95%) multi-exon genes undergo alternative splicing (Pan et al., 2008; Wang et al., 2008). Protein isoforms resulting from these alternatively spliced variants often have distinct or even antagonistic functions (Black, 2003; Cartegni et al., 2002; Matlin et al., 2005).

1.6 Types of alternative splicing outcomes

Alternative splicing outcomes are generally divided into 5 types (reviewed in (Black, 2003; Cartegni et al., 2002):

1. Use of alternative 5' or 3' splice sites, usually located near each other. This leads to a lengthening or shortening of an exon.

2. Alternative use of a promoter or a polyadenylation (poly(A)) site. This affects the 5' or 3' composition of a mature mRNA

3. Retention of an intron.

4. Cassette exons. The most commonly observed alternative splicing system in global genomic analyses (Pan et al., 2008; Wang et al., 2008), where a exon could be included or excluded, depending on the outcome of the competition between factors that activate or repress this exon.

5. Mutually exclusive exons. This is where only a single exon is selected from a pair, or an array of competing exons.

1.7 Mechanisms of alternative splicing: splicing *cis* elements

Although the canonical splicing elements are necessary for splicing to occur, they are not sufficient to specify alternatively spliced (AS) exons. Inclusion or exclusion of AS exons is thus regulated through an additional set of specific *cis*-regulatory elements – exonic or intronic splicing enhancers (ESE, ISE) and silencers (ESS, ISS) present on the pre-mRNA. This is because alternatively spliced exons tend to have weaker splice sites that deviate from

the consensus (Roca et al., 2005). This permits the regulation of alternative splicing through these motifs by binding cognate *trans*-acting factors in a combinatorial fashion to promote or inhibit the recruitment of spliceosomal machinery, resulting in the respective enhancement or suppression of splicing (Black, 2003). Note that splicing *cis*-element also contribute to the definition of constitutive exons through similar mechanisms.

1.8 *Trans* mediators of alternative splicing

The *trans*-acting factors that regulate alternative splicing are typically RNA-binding proteins, a subset of which are classified into two groups: the Ser/Arg-rich (SR) proteins (Graveley, 2000) and heterogeneous ribonucleoproteins (hnRNP), which generally recognize enhancers and silencers, respectively. Reflecting their function, both classes of proteins typically contain one or two RNA recognition motifs (RRM) and a domain that is involved in interactions with other *trans*-acting factors and/or spliceosomal components. SR and hnRNP proteins typically have opposing effects on the alternative splicing of exons, eliciting changes in splicing outcomes in a concentration-dependent manner (Black, 2003). Consequently, non-physiological changes in the global levels of SR and hnRNP proteins can potentially alter the splicing profile of cells and lead to aberrant splicing of multiple target genes.

1.9 Mechanisms of activation

The mechanistic basis of SR-protein mediated splicing activation has been well defined and can be reasonably applied to any other class of splicing activators. Splicing factor activation is thought to work in two modes.

Splicing factors that are bound to a enhancer element work to recruit spliceosomal components to weak 5' or 3'ss. For example, a SR protein bound to an exonic splicing enhancer typically activates the splicing of its cognate exon by stabilizing the interaction of the U2AF splicing factor, which is part of the U2 snRNP, with a weak 3'ss and/or BPS via its RS interaction domain (Graveley et al., 2001; Zuo and Maniatis, 1996). The same factor could also perform the same function by stabilizing U1 snRNP interactions with a downstream 5'ss, or through indirect interactions with a splicing co-activator such as Srm160, stabilize and recruit U1 snRNPs to the upstream 5'ss (Eldridge et al., 1999). In the intronic context, TIA1 binding to a downstream ISE in the FAS transcript activates the upstream exon by facilitating the recruitment of U1 snRNP to the upstream 5'ss (Matlin et al., 2005).

The second mode of activation involves antagonizing splicing repressor function by binding to a splicing enhancer site in the proximity of the silencer site. This mode explains the observations that the recruitment of a SR protein to an ESE is sufficient for splicing activation, even in the absence of a RS interaction domain (Kan and Green, 1999; Zhu et al., 2001).

1.10 Mechanisms of repression

As with SR proteins, the best-known mechanisms of repression come from mechanistic analysis of hnRNP-mediated splicing repression. In the first mode, a hnRNP protein binding to a splicing silencing site that is in the proximity of an splicing enhancer site antagonizes splicing activator function, destabilizing spliceosomal assembly on the pre-mRNA (Zhu et al., 2001). In the second mode, the splicing repressor binds to a high affinity

silencing element, inducing the cooperative binding of the same or additional inhibitory factors, eventually spreading across the exons and splice sites. This inhibits the recruitment to splicing activators to splicing enhancer sites and/or blocks the recruitment of spliceosomal components to splice sites. In the third mode, two splicing repressors are recruited to distant intronic silencer sites, and then dimerize, bringing the two sites in close proximity (Blanchette and Chabot, 1999; Wagner and Garcia-Blanco, 2001). This causes the intervening RNA sequence to be looped out and not be recognized by the splicing machinery.

1.11 Positional dependence of splicing factors on splicing outcomes

Recent genome-wide analysis of splicing factors through the isolation and deep sequencing of RNA that are UV-crosslinked to RNA binding proteins (Cross Linking and Immunoprecipitation-sequencing experiments, or CLIP-seq), combined with RNA-sequencing experiments or splicing micro-array data that correlate splicing factor-RNA interactions with splicing outcomes has generated RNA splicing maps that bring new insights on the positional dependence of splicing factors that influence splicing outcomes (Licatalosi and Darnell, 2010). For example, a variety of splicing factors, for example, Polypyrimidine tract binding protein (PTB) (Xue et al., 2009) and Nova (Licatalosi et al., 2008) splicing factors repress exon inclusion by binding at positions close to canonical splice sites or within exons, but activate exon inclusion when bound downstream of exons. It has also been found that splicing factors also exert their effects on distal exons; for example, the splicing factor TIA1 has been demonstrated to silence inclusion of downstream alternatively-spliced exons when bound near the 5'ss of preceding exons (Wang et al., 2010). A mechanistic basis of

these observations has not been elucidated thus far, but most likely requires a rethinking of the above-mentioned classical splice site competition mechanisms.

1.12 Emerging models of splicing regulation

There are two main models of splicing regulation that could explain the positional dependent effects of splicing factors, which are not mutually exclusive. Both take into account the observations that transcriptional elongation and chromatin affect splicing. In the recruitment model, the C terminal domain (CTD) of RNA polymerase II and local chromatin architecture recruit specific splicing factors to nascent RNA. In support of this hypothesis, it has been observed that recruitment of SR proteins to RNA is CTD dependent, and that antibodies against CTD also coimmunoprecipitate SR proteins (Caceres and Kornblihtt, 2002). Specific modifications of histone H3 have also been demonstrated to bind PTB (Luco et al., 2010). The specific position-dependent outcome of splicing factors could thus depend on specific, local, extra-RNA variables such as promoter identity, post-translational modifications to the CTD, and histone modifications (Luco et al., 2011) that recruit a specific repertoire of factors that influences a splicing decision. However, since splicing decisions depend on combinatorial outputs, how much of a role these extra-RNA variables play in influencing a splicing outcome of a particular exon remains to be seen.

In the second model, it is postulated that splicing factors binding to distal sites could affect the kinetics of spliceosomal assembly from the E to C complexes (Witten and Ule, 2011) . In particular, a decrease in the rate of spliceosomal assembly at an upstream splice site could allow more time for a downstream splice site to recruit splicing enhancers that activate the downstream exon. In support of this model, expression of a slow RNA pol II

mutant leads to an increased usage of an upstream 5' ss in the Adenovirus E1a splicing system as the slower elongation of RNA pol II presumably leads to a slower spliceosomal assembly at the 5'ss, allowing a longer window for splicing factor mediated use of the 5'ss (de la Mata et al., 2003). Similarly in the example of TIA, recruitment of TIA to the upstream 5'ss could accelerate the rate of spliceosomal assembly at the 5'ss, decreasing the window of time for splicing factors to stabilize U2 snRNP interaction at the downstream 3'ss of the downstream exon, leading to suppression of exon inclusion (Wang et al., 2010). However, the exact mechanism by which these splicing factors affect spliceosomal assembly remains to be elucidated.

1.13 Mechanistic questions in mutually exclusive splicing

Mutually exclusive splicing by definition mandates the selection of only one exon out of an array of two or more exons. Two major questions are then evident in a mutually exclusive splicing system. 1) What prevents two mutually exclusive exons from being spliced together? 2) How is one exon preferentially included over the other? Four mechanisms have been proposed for the first question (Smith, 2005). The first is that there are minimum spacing requirements (~50 bps) between the 5'ss and BPS in the introns for splicing. Below this threshold, steric interference prevents the complete spliceosome complex from being recruited to the intron and for splicing to occur. The second is that inclusion of both exons leads to altering of the reading frame and the introduction of premature stop codons (PTC) in the transcript, leading to degradation of the transcript by NMD. The third is splice site incompatibility. The consensus splice sites recognized by the minor spliceosome are different from those of the major spliceosome, such that an intron

with a U11 5'ss and a U2 3'ss (or vice versa) cannot be spliced. This has been observed in intron 6 of the mutually exclusive exons 6 and 7 in the JNK gene. The last mechanism involves the formation of long-distance intramolecular secondary structures (Graveley, 2005; Kreahling and Graveley, 2005; May et al., 2011; McManus and Graveley, 2011; Olson et al., 2007). This has been observed in Drosophila through the comparison of conserved sequences present around the mutually exclusive exon 6 cluster of exons. These exons were found to be constitutively repressed, but exon selection requires the pairing of a selector site sequence found upstream of each exon with a doctor site found in intron 5 between the constitutive exon 5 and the first ME exon in the exon 6 cluster. Mutations in the docking site lead to the complete skipping of the exon 6 cluster, while mutations of the selector site that weakened or strengthened the base pairing interactions between these two sites decreased or increased the inclusion of the particular exon, respectively (May et. al. 2011). Although this mode of ME maintenance has been well characterized in Drosophila DSCAM, it remains to be seen whether similar intramolecular base pairing-mediated exon selection mechanisms could occur in other splicing systems.

1.14 Altered splicing in cancer

Since alternative splicing often modulates the activities of oncogenes and tumor suppressors, aberrant splicing is strongly correlated with cancer. This happens either through mutations that change *cis*-acting splicing sequences in genes, or through changes in levels of splicing regulators in cells. In the former, mutations that affect the alternative splicing of tumor suppressors, such as *BRCA1/2* (Venkitaraman, 2002), *WT1* (Hammes et al., 2001), *LKB1* (Hastings et al., 2005), *APC*, *TP73*, and *TSC1/2* (Venables, 2004) account for sporadic

or hereditary susceptibility to cancer. In the latter case, aberrant expression of SR proteins has been implicated in tumorigenesis (Fischer et al., 2004; Ghigna et al., 2005; He et al., 2004).

1.15 SR proteins in cancer

In particular the prototypical SR protein SRSF1 was recently found to be highly expressed in a variety of tumor samples. Overexpression of SRSF1 *in vitro* was sufficient to transform immortal rodent fibroblasts by altering splicing in a number of key genes involved in apoptosis and metabolism, including a dominant-negative form of the apoptosis mediator protein, *BIN1* (Ge et al., 1999; Sakamuro et al., 1996), and a novel, oncogenic isoform of a key regulator of global protein translation, *RPS6KB1*.

Similar to its paralog SRSF1, SRSF3 has also been implicated in tumorigenesis. SRSF3 is overexpressed in ovarian cancers (He et al., 2004) and cervical cancer cell lines, whereas in normal cervical tissue its expression is restricted to the basal proliferating layers (Jia et al., 2009). SRSF3 is also a downstream target of the oncogenic β-catenin/TCF-4 pathway in colorectal cancer cells (Goncalves et al., 2008). Moreover, overexpression of SRSF3 was recently found to be sufficient for transformation of NIH-3T3 immortal mouse fibroblasts (Jia et al., 2010).

1.16 The Warburg effect and tumorigenesis

When Warburg observed that cancer cells exhibited a high rate of glycolysis and produced lactic acid avidly even under aerobic conditions, he proposed that cancer was

initiated through the impairment of oxidative phosphorylation (Warburg, 1956). Although this hypothesis has since been discredited, the plethora of oncogenes (see below) that maintain and reinforce the "Warburg effect" - the metabolic switch from oxidative phosphorylation to aerobic glycolysis - implies that this event is undoubtedly important.

1.17 Oncogenes and the Warburg effect

1.17.1 Phosphatidylinositol 3-kinase signaling pathway

This signaling pathway connects upstream growth factor signaling pathways to downstream pathways that mediate cellular growth and survival. As such, constitutive activation of this pathway is a common feature in cancers (Cairns et al., 2011). The downstream effector of PI3K, AKT1, is an important mediator of tumor glycolysis. It stimulates glycolysis by stimulating glucose uptake and activating rate-limiting glycolytic enzymes (Elstrom et al., 2004). AKT also stimulates anabolic metabolism by activating the mammalian target of rapamycin (mTOR) kinase (Robey and Hay, 2009), which controls global mRNA translation and ribosome biogenesis (Guertin and Sabatini, 2007).

1.17.2 Oncogenic transcription factors

The oncogene Myc plays an important role in controlling cell cycle and differentiation. Together with Hypoxia-inducible factor 1 (HIF1α), it also stimulates glycolysis by directly upregulating the expression of glyolytic enzymes, including the pyruvate kinases (PK-M, PK-R, PK-L) and glucose transporters (Dang et al., 2008; Semenza, 2010). Crucially, HIF1 also activates the expression of pyruvate dehydrogenase

kinase 1 (PDK1), which shunts pyruvate away from the mitochondrial oxidative phosphorylation pathways (Kim et al., 2006; Papandreou et al., 2006). In normal oxygen conditions, HIF1 undergoes an oxygen-dependent hydroxylation on its α-subunit that results in its ubiquitination by the von Hippel-Lindau tumor suppressor, and is subsequently degraded (Kaelin, 2008). As a result, HIF1 is only stabilized in hypoxic conditions, but it is constitutively stabilized in normal oxygen conditions in cancer cells due to activated oncogenic signaling pathways, including PI3K, or through the inactivation of tumor suppressors involved in its destabilization (Cairns et al., 2011).

1.18 Pyruvate kinase isoforms and the Warburg effect

What advantages does aerobic glycolysis confer to transformed cells? Recent studies by Christofk and colleagues illuminate a possible *raison d'être* for the Warburg effect: conferring a proliferative advantage by facilitating anabolic metabolism (Christofk et al., 2008a; Christofk et al., 2008b).

Pyruvate kinase is a key rate-limiting enzyme in the glycolytic pathway that is tightly regulated in cells and catalyzes the conversion of its substrate phosphoenolpyruvate (PEP) to pyruvate (Mazurek et al., 2005). The pyruvate kinase-m *(PK-M)* gene encodes two splice isoforms that differ by the inclusion of one of two mutually exclusive exons. The authors first discovered that in mouse and human tumor samples, expression of the fetal M2 isoform, together with the concurrent downregulation of the adult M1 isoform, correlated with tumor development. A further screen of established cancer cell lines using isoform-specific antibodies confirmed this correlation. They then knocked down endogenous PKM2 by RNAi

in cancer cell lines and re-expressed mouse versions of either PKM2 or PKM1 and compared their metabolic and proliferation profiles.

Although PKM1 and PKM2-expressing cells were indistinguishable under normoxic conditions, strong differences were observed in hypoxia. M2-expressing cells grew at a higher rate, consumed less oxygen, and produced more lactate than M1 cells, all of which are hallmarks of the Warburg effect. Strikingly, ATP levels in both cell lines under either normal or simulated hypoxic conditions were similar, suggesting that these differences were not due to energy levels. Proliferation differences between M1 and M2 cells in xenograft tumor models also reflected *in vitro* differences: larger tumors developed with a shorter latency from M2 cells compared to M1 cells. Most importantly, tumors arising from M1 xenografts all re-expressed endogenous PKM2, and tumors that arose from an M1/M2 mixed xenograft originated only from M2 cells. These observations strongly suggested that expression of PKM2 during tumorigenesis confers a proliferative advantage to cancer cells.

1.19 Inhibition of PKM2 kinase activity is important for the Warburg effect

How does PKM2 confer this advantage? The authors found that only the PKM2 isoform bound phosphotyrosine residues. This catalyzed the release of its activator fructose bisphosphate (FBP) from its allosteric site, effectively inhibiting its enzymatic activity in vitro. This effect could be mimicked in cells by stimulating a growth factor receptor tyrosine kinase (RTK) signaling pathway or overexpressing a constitutively active tyrosine kinase. Although cells expressing either M2 or a phosphotyrosine binding mutant (M2KE) exhibited comparable glycolytic rates, M2 cells grew faster, implying that the inhibition of PKM2 by RTK signaling was necessary for this to occur. Finally, the authors hypothesized that

inhibition of PKM2 led to an accumulation of upstream glycolytic intermediates that could serve as substrates in anabolic processes, and validated this by demonstrating through radioisotope labeling, that M2 but not M2KE cells, exhibited a higher, and phosphotyrosine peptide-dependent rate of lipid synthesis (Christofk et al., 2008b).

In addition, PKM2 has been observed to exist mostly in an inactive dimerized form in tumor cells, as opposed to a more active tetrameric configuration in normal cells, further enhancing anabolic metabolism (Mazurek et al., 2005). Growth-signalling mediated phosphorylation (Hitosugi et al., 2009), and acetylation (Lv et al., 2011) of PKM2 also inhibit its kinase activity, facilitating tumor cell proliferation and growth. PKM2 has also been demonstrated to be induced by the mammalian target of rapamycin (mTOR) complex, an important regulator of cell growth and proliferation, through transcriptional activation by the hypoxia-inducible factor 1α (HIF-1α), a known mTOR downstream target (Sun et al., 2011). PKM2 also functions in a positive-feedback loop with HIF-1α by acting as a coactivator of HIF-1, thereby reinforcing its overexpression in tumor cells (Luo et al., 2011; Luo and Semenza, 2011).

The above observations implicate the Warburg effect in cellular anabolism, linking it directly to the growth of transformed cells, and provide a mechanistic link between growth factor signaling, cellular anabolism and aerobic glycolysis, highlighting the importance of the Warburg effect as a *cooperative* event in tumorigenesis.

1.20 Alternative splicing of the PKM gene

Although the importance of PKM2 has been repeatedly demonstrated, the mechanism of the mutually exclusive (ME) mode of PK-M alternative splicing, which favors the apparent inclusion of exon 10 over exon 9 in tumors and exon 9 over exon 10 in normal

tissues, remains poorly understood. Understanding the splicing regulation of the PK-M gene is as crucial, if not more so, than understanding its transcriptional regulation, because the process of tumorigenesis not only requires an increase in the amount of PK-M transcripts, but also a change in the *type* of transcript that is produced from the mutually exclusive splicing of PK-M.

1.21 Preliminary analyses of the PK-M gene

An earlier study based on a rat minigene system (Takenaka et al., 1996) concluded that 1) the 5' splice sites of both exons were weak; and 2) conserved elements in intron 8 did not affect M2/M1 splicing. Although the first conclusion failed to address why exon 10 is preferentially included in cultured cells, the data suggested the presence of splicing enhancer/suppressor elements present within both exons and intron 9. In addition, since both conclusions were based on crude deletion and exon swapping experiments, a major caveat is that the altering of the original context in these constructs could potentially mask regulatory elements otherwise present in the wild-type context, or create new regulatory elements that are irrelevant, confounding the intepretation of the results.

1.22 PK-M Exon 9 repression in tumor cells

Recently, we and others demonstrated that the exon-10-included M2 isoform is the default choice in cancer and proliferating cells, and also implicated two pairs of splicing-repressor paralogs—PTB/nPTB and hnRNPA1/A2—in repression of exon 9 (Clower et al., 2010; David et al., 2010). In addition, hnRNPA1/A2 and PTB have been reported to bind at the exon 9 5'ss and in intron 8 near the exon 9 splice sites (David et al., 2010) respectively.

However, because the conclusions were derived from in vitro UV-crosslinking experiments, it is unclear whether these sites are *bona fide* ESSs in the context of intact pre-mRNAs *in vivo*, because it is not known how well hnRNPA1 binding to a motif that is part of a 5'ss can compete with binding of spliceosomal components, such as U1 and U6 snRNPs.

1.23 Critical *cis*-elements and the question of Exon 10 definition

In addition, these experiments did not precisely map the elements involved in M2/M1 splicing *in vivo*, making functional follow-up experiments to unearth cognate *trans*-acting factors and the mechanism(s) of action (MOA) difficult. In particular, the crucial question of where the critical *cis*-elements responsible for the characteristic PK-M2 splicing pattern in proliferating cells are distributed, i.e., are these elements present in the exons, the introns, or both, remained unanswered. It also remained unclear how exon 10 is the "default" exon in proliferating cells, i.e., is selection of exon 10 actively promoted, or is exon 10 included simply as a consequence of repression of exon 9?

1.24 Splicing Antisense Oligonucleotides

A method to screen for functional splicing elements, as well as to manipulate splicing outcomes in endogenous pre-mRNA involves the use of antisense oligonucleotides (ASO). These short oligonucleotides were initially used to downregulate mRNA expression by homing to target mRNAs via Watson-Crick base pairing and inducing nuclease mediated-degradation of nucleotide:RNA hybrids (Crooke, 2001). Their therapeutic potential was first demonstrated by Zamecnik and Stephenson, who used ASO to target viral replication in cell

culture. More recently, chemical modification has led to a class of nuclease-resistant ASOs that have high affinity for their RNA targets. A wide range of backbone-modified ASOs with differing chemical properties engineered for different applications include 2′-*O*-methyl phosphorothioate (2OMe) RNA, 2-*O*-methoxyethyl (MOE) RNA, peptide nucleic acid (PNA), locked nucleic acid (LNA) and phosphorodiamidate morpholino (PMO) variants. These ASOs work by direct sequence-specific annealing to target mRNA to either block splicing *cis*-elements, or block ribosome recruitment to inhibit translation (Muntoni and Wood, 2011; Opalinska and Gewirtz, 2002).

Splicing ASOs have been used to manipulate and correct aberrantly spliced transcripts implicated in disease. They work in two ways: (1) restore the splicing of an aberrantly spliced transcript; and 2) manipulate the splicing of a transcript from one isoform to another.

1.25 ASO-mediated splicing correction in disease

The Kole lab first used ASOs to block cryptic intronic splice sites in the β-globin gene that were activated due to mutations that occur in some β-thalassemia patients, essentially restoring the normal splicing of the β-globin transcript (Sazani and Kole, 2003). Since then, ASOs have been used in the context of other genetic diseases in which a mutation of a single gene alters its splicing. In the example of Duchenne muscular dystrophy (DMD), missense mutations and deletions in the dystrophin gene (*DMD*) cause the generation of premature termination codons and frameshifted transcripts, specifically in the central portion of the gene that encodes a large rod domain made up of 24 large spectrin-like repeats and four flexible hinge regions (Hammond and Wood, 2011). Mutations can be compensated by removing the mutated or neighboring exons through the use of splicing ASO to produce a

shorter mature mRNA transcript and restoring the translational reading frame. The internally deleted protein retains many of its crucial functions, enabling it to reduce disease severity when used in mouse models of DMD (Alter et al., 2006; Lu et al., 2003; Lu et al., 2005).

In the example of spinal muscular atrophy (SMA), the therapeutic use of ASOs involves restoring the inclusion of the constitutively skipped exon 7 of the SMN2 gene. The SMN1 gene is mutated in SMA, giving rise to atrophy of proximal muscles and the subsequent degeneration of motor neurons in patients. SMN2 is a paralog of SMN1 and differs from SMN1 only by a nucleotide transition in the sequence of exon 7. This A to T sequence change induces the skipping of exon 7, producing a truncated and unstable SMN protein. ASOs were used to induce the inclusion of SMN2 by targeting splicing silencers found in or in the vicinity of exon 7, increasing the expression of the SMN protein. ASOs have been used in vivo and have been found to rescue phenotypes in SMA mouse models (Hua et al., 2010; Hua et al., 2011; Passini et al., 2011).

Splicing ASOs have also been used against targets that are important in cancer. The most notable example involves the use of ASOs to target the BCL-X gene (Sazani and Kole, 2003). The Bcl-X gene codes for two splice isoforms with antagonistic functions, through the use of two alternative 5'ss. The longer isoform, Bcl-xL has an anti-apoptotic function, while the shorter isoform, Bcl-xS, is pro-apoptotic. In cancer cells, the splicing of the Bcl-x gene has been demonstrated to be skewed towards the anti-apoptotic Bcl-xL isoform as it facilitates cellular survival. ASOs that target enhancer elements near the xL (proximal) 5'ss in order to restore the splicing of the xS isoform have been demonstrated to sensitize cells to chemotherapeutic agents (Taylor et al., 1999) or to induce apoptosis in cancer cells

(Mercatante et al., 2001). Further work is needed to demonstrate the efficacy of these ASOs in the *in vivo* context.

1.26 Application of splicing ASO technology to PKM2 splicing in cancer cells

The successful use of a splicing ASO to switch PKM2 transcripts into PKM1 transcripts in cancer cells would potentially represent a major therapeutic advance in targeting the Warburg effect in solid tumors; it would also be useful in uncovering the mechanism by which PKM2 confers a proliferative advantage to cancer cells, through the analysis of cellular phenotypes as a result of ASO-mediated loss of PKM2 protein.

2 CHAPTER 2: Exon-Centric Regulation of Pyruvate Kinase M Alternative Splicing via Mutually Exclusive Exons

Zhenxun Wang[1,2], Deblina Chatterjee[1,3], Hyun Yong Jeon[1,3],

Martin Akerman[1], Matthew G. Vander Heiden[4], Lewis C. Cantley[5],

and Adrian R. Krainer[1]

Running title: Exon-Centric Regulation of PK-M Alternative Splicing

[1] Cold Spring Harbor Laboratory, Cold Spring Harbor, NY 11724

[2] Watson School of Biological Sciences, Cold Spring Harbor, NY 11724

[3] Graduate Program in Molecular and Cellular Biology, Stony Brook University, Stony Brook, NY 11794

[4] Koch Institute for Integrative Cancer Research at MIT, Cambridge, MA 02139

[5] Division of Signal Transduction, Beth Israel Deaconess Medical Center and Department of Systems Biology, Harvard Medical School, Boston, MA 02115

Correspondence:
Adrian R. Krainer, Ph.D.
Cold Spring Harbor Laboratory
PO Box 100
Cold Spring Harbor, NY 11724
Tel: 516 367 8417
Fax: 516 367 8453
Email: krainer@cshl.edu

2.1 Manuscript and Contributions

This manuscript was published in the Journal of Molecular Cell Biology in November 2011. Z.W and A.R.K conceived and designed the experiments. Z.W, H.Y.J and D.C performed the experiments. M.A performed bioinformatics analysis. Z.W, A.R.K wrote the manuscript.

2.2 Abstract

Alternative splicing of the pyruvate kinase M gene to generate the M2 isoform promotes aerobic glycolysis and tumor growth. However, the cancer-specific alternative splicing regulation of *PK-M* is not completely understood. Here, we demonstrate that *PK-M* is regulated by reciprocal effects on the mutually exclusive exons 9 and 10, such that exon 9 is repressed and exon 10 is activated in cancer cells. Strikingly, exonic, rather than intronic, *cis*-elements are key determinants of *PK-M* splicing isoform ratios. Using a systematic sub-exonic duplication approach, we identify a potent exonic splicing enhancer in exon 10, which differs from its homologous counterpart in exon 9 by only two nucleotides. We identify SRSF3 as one of the cognate factors, and show that this SR protein activates exon 10 and mediates changes in glucose metabolism. These findings provide mechanistic insights into the complex regulation of alternative splicing of a key regulator of the Warburg effect, and also have implications for other genes with a similar pattern of alternative splicing.

2.3 Introduction

Cancer cells exhibit a metabolic phenotype termed aerobic glycolysis, or the Warburg effect, characterized by increased glycolysis with lactate generation, regardless of oxygen availability (Vander Heiden et al., 2009). Expression of the type II isoform of the pyruvate-kinase-M gene (*PKM2*, referred to here as *PK-M*) mediates this metabolic phenotype, and confers a proliferative advantage to tumor cells *in vivo* (Christofk et al., 2008a).

Pyruvate kinase (PK) catalyzes the final step in glycolysis, generating pyruvate and ATP from phosphoenolpyruvate and ADP (Dombrauckas et al., 2005). The *PK-M* gene consists of 12 exons; exons 9 and 10 are alternatively spliced in a mutually exclusive fashion to give rise to M1 and M2 isoforms, respectively (Noguchi et al., 1986). Exons 9 and 10 each encode a 56-amino-acid segment that confers distinctive properties to the PK-M isozymes. PK-M1 is constitutively active, whereas PK-M2 is allosterically regulated by fructose-1,6-bisphosphate (FBP) levels and interaction with tyrosine-phosphorylated signaling proteins (Christofk et al., 2008b).

The growth-signal-mediated inhibition of *PK-M2* activity is thought to contribute to cancer-cell growth by decreasing carbon flux through the catabolic glycolytic pathway, allowing accumulated upstream intermediates to be shunted to anabolic pathways and thereby facilitating cell proliferation (Hitosugi et al., 2009). Consistent with this hypothesis, PK-M2 is expressed in a broad range of cancer cells, as well as in fetal and undifferentiated adult tissues, whereas PK-M1 is expressed predominantly in terminally differentiated tissues

(Clower et al., 2010). Despite increasing evidence demonstrating the significance of PK-M2 isoform expression in cancer-cell metabolism and tumorigenesis, the mechanisms governing alternative splicing of the PK-M pre-mRNA are not well understood.

Alternative splicing via a pair of mutually exclusive (ME) exons accounts for □2% of alternative splicing in human genes (Chacko and Ranganathan, 2009). ME exons often show sequence homology—as is the case for *PK-M* exons 9 and 10—indicating an exon-duplication origin (Letunic et al., 2002). Although several mechanisms involved in the selection of ME exons in mammalian genes have been described, how these pairs of exons are coordinately regulated in a ME fashion is not well understood (Smith, 2005). The mechanism underlying the ME splicing pattern of *PK-M* appears to be novel: for example, the length (401 bp) and sequence of intron 9 rules out steric interference effects that could prevent double splicing due to the spacing of the branch site and the 5' splice site (5'ss) (Smith and Nadal-Ginard, 1989).

We have begun to dissect the molecular mechanisms underlying *PK-M2* alternative splicing regulation. Recently, we and others demonstrated that the exon-10-included M2 isoform is the default choice in cancer and proliferating cells, and also implicated two pairs of splicing-repressor paralogs—PTB/nPTB and hnRNPA1/A2—in repression of exon 9 (Clower et al., 2010; David et al., 2010). However, it remains unclear whether there are additional repressors that also block the use of exon 9, and whether exon 10 is the "default" exon in proliferating cells, i.e., is selection of exon 10 actively promoted, or is exon 10 included simply as a consequence of repression of exon 9? In addition, though hnRNPA1/A2 and PTB

have been reported to bind in the intronic regions near the exon 9 splice sites (David et al., 2010), it remains unclear where the critical *cis*-elements responsible for the characteristic PK-M2 splicing pattern in proliferating cells are distributed, i.e., are these elements present in the exons, the introns, or both?

To address these questions, we constructed a *PK-M* minigene that recapitulates the splicing-regulatory features of the endogenous gene. Using this minigene and derivatives thereof, we demonstrate that exon 10 is activated in cancer cells independently of exon 9 repression. By duplicating or swapping exons 9 or 10, we further show that exonic, but not intronic *cis*-elements, are the key determinants of *PK-M* alternative splicing. Using a novel sub-exonic duplication strategy, we then mapped an exonic splicing enhancer (ESE) in exon 10, and found that SRSF3 (formerly SRp20), an oncogenic member of the serine/arginine-rich (SR) protein family of splicing activators, is its cognate binding factor. Knockdown of SRSF3 in cancer cells leads to the rescue of *PK-M1* expression and a decrease in lactate production and cellular proliferation.

2.4 Results

2.4.1 A *PK-M* minigene recapitulates alternative splicing of the endogenous gene

The ME exons 9 and 10 of *PK-M* are identical in length, and highly homologous at both the nucleotide and amino-acid sequence levels (Fig. 1A). One crucial difference is that only exon 10 codes for a key lysine residue within the FBP-binding pocket, and this lysine mediates binding to tyrosine-phosphorylated proteins to release FBP and inhibit enzymatic activity (Fig. 1A;

To analyze the mechanism of ME splicing of *PK-M* pre-mRNA, and facilitate the discovery of splicing *cis*-elements, we generated a minigene transcribed from a CMV promoter (Fig. 1B). The minigene consists of the genomic region encompassing the ME exons 9 and 10, introns 8, 9 and 10, and proximal portions of the flanking exons 8 and 11. Detection and analysis of minigene-derived transcripts utilized a modified RT-PCR and restriction-digestion strategy, as described for endogenous *PK-M* transcripts (Fig. 1B; (Clower et al., 2010)). To characterize all possible minigene-derived species after transfection into cell lines, we selectively amplified them from total cDNA using a forward primer specific for an upstream vector sequence, together with a reverse primer annealing to constitutive exon 11 (Fig. 1B).

Fig. 1C shows the profiles of endogenous and minigene-derived transcripts in HEK-293 cells (similar data not shown for HeLa, A172, and SKNBE). The minigene predominantly expressed the exon-10-included *PK-M2* isoform, paralleling endogenous *PK-M2/M1* splicing

ratios. Two additional, minor minigene RNAs not found in endogenous *PK-M* transcripts were also reproducibly detected: an RNA lacking both exons 9 and 10, and comprising only the flanking exons (Fig. 1C; double-skipped species **d**) and a variant *PK-M2* transcript spliced via a cryptic 3'ss upstream of the authentic 3'ss of exon 10 (Fig. 1C and Suppl. Fig. 1; exon 10 3'ss cryptic species **c**).

2.4.2 Blocking exon 10 inclusion does not fully rescue exon 9 inclusion

Given the predominant *PK-M2* splicing of endogenous and minigene transcripts in proliferating cells, we tested whether blocking exon 10 inclusion by inactivating or weakening its splice sites might force a corresponding increase in exon 9 inclusion. The 5'ss or 3'ss of exon 10 were inactivated by mutating the invariant G residues at the intron borders, and the 3'ss was separately weakened by transversions within its upstream polypyrimidine tract (PPT) (Fig. 2A).

Mutating the exon 10 5'ss resulted in a larger mRNA with an extended exon 10 (Fig. 2A and Suppl. Fig. 1, lanes 5-8; exon 10 5'ss cryptic species **e**). This mRNA resulted from splicing via a cryptic 5'ss 105 nt downstream of the authentic 5'ss of exon 10. There was no significant increase in the double-skipped RNA species **d**. Thus, exon 10 definition was essentially preserved, even though the normal 5'ss was inactivated.

In contrast, mutating the exon 10 3'ss largely abrogated exon 10 definition, as seen from the large increase in double-skipped transcripts (Fig. 2A and Suppl. Fig. 1, lanes 9-12; species

d). A small increase in the exon 10 cryptic 3'ss species **c** was also observed. These results suggest that the exon 10 3'ss is essential for exon 10 definition. Similarly, weakening the exon 10 PPT led to some loss of exon 10 definition, as seen from the large increases in double-skipped RNA and in the use of the upstream cryptic 3'ss (Fig. 2A, lanes 13-16; species **c** and **d**). This result implies that exon 10 inclusion is an active process, such that the loss of exon 10 activation results in non-productive splicing of the PK-M transcript.

With all three minigene mutants, there was only marginal recovery of exon 9 inclusion (Fig. 2A, lanes 5-16). In addition, deleting exon 10 from the minigene also led to a similar increase in double-skipped mRNA, with the mutant displaying a phenotype identical to that of exon 10 3'ss inactivation (data not shown). Therefore, exon 9 inclusion in proliferating cells is repressed independently of exon 10 splicing.

2.4.3 Strengthening the splice sites of exon 9 leads to aberrant *PK-M* splicing

Because blocking exon 10 splicing did not lead to a significant rescue of M1 splicing in transformed cells, we tested whether directly strengthening the exon 9 splice sites might do so. We therefore mutated the exon 9 5'ss to the consensus 5'ss sequence (Fig. 2B, lanes 5-8), and strengthened the exon 9 3'ss by increasing the pyrimidine content of its upstream PPT (Fig. 2B, lanes 9-12).

As expected, strengthening either the exon 9 5'ss or 3'ss led to an increase in M1 splicing. However, a new exon 9 plus exon 10 doubly-included mRNA species was also observed in both cases (Fig, 2B and Suppl. Fig. 1; double-spliced species **f**). Mutating the 5'ss to the

consensus resulted in a large increase in the amount of M1 RNA and in high levels of the double-spliced mRNA (Fig. 2B, lanes 5-7), whereas slightly increasing the 3'ss strength gave somewhat lower levels of these two mRNAs (lanes 9-11). The concurrent appearance of the double-spliced mRNA suggests that exon 10 definition—and by extension, exon 10 activation—is largely independent of exon 9 splicing.

2.4.4 Exonic splicing silencers and enhancers are key determinants of *PK-M* splicing ratios

To prioritize *PK-M* regions for *cis*-element analysis, we next asked whether intronic or exonic *cis*-elements play critical roles in activating exon 10 and/or repressing exon 9. First, we duplicated exon 10 in place of exon 9 in the minigene (Fig. 3, lanes 9-12; Suppl. Fig. 1). If exon 9 repression depends on *cis*-elements present in introns 8 or 9, there should be inefficient use of the upstream copy of exon 10, because it would be under the influence of these repressive elements, and the pattern should be similar to that of the wild-type minigene. Instead, we observed the striking appearance of a doubly-included exon 10 mRNA species (Fig. 3, lane 9; exon 10 double-included species **g**) indicating that the upstream exon 10 was still activated, regardless of its position. This finding strongly suggests that splicing enhancer elements involved in exon 10 definition are present in the exon itself.

Similarly, we duplicated exon 9 in place of exon 10 in the minigene (Fig. 3, lanes 5-8). If exon 10 splicing is normally activated through flanking *cis*-elements in introns 9 or 10, there should be a strong increase in exon-9-included transcripts, compared to the wild-type minigene, because the downstream copy of exon 9 would now be under the influence of such

elements. However, there was no such increase from the exon-9-duplicated minigene transcripts (Fig. 3, lanes 5-8). This finding suggests that splicing-silencing elements involved in repressing exon 9 are located in the exon itself.

When the positions of exons 9 and 10 were swapped, leaving all the introns unchanged (Fig. 3, lanes 13-16), the M1 and M2 isoform ratio was similar to that of the wild-type minigene, although there was a decrease in M1 abundance, and an expected decrease in the use of the cryptic 3'ss upstream of the original exon 10 (i.e., in intron 9), because this 3'ss is now juxtaposed with the repressed exon 9 3'ss. This finding indicates that exon 10, when moved to exon 9, is spliced as efficiently as in its original location. This striking result suggests that exonic *cis*-elements involved in *PK-M* splicing are sufficient to activate exon 10 and repress exon 9, in a manner that is independent of their respective positions along the gene and the influence of their flanking introns.

To confirm the above results, and to determine the role of the splice sites in ME exon use, we swapped the 3'ss or 5'ss of both exons. Computational analysis of these splice sites (Yeo and Burge, 2004) suggested that the 3'ss of exon 9 is weaker than those of exons 10 and 11 (Suppl. Fig. 2). Exon 9 inclusion was therefore expected to increase when its 3'ss was replaced by the stronger one from exon 10. Instead, we observed a decrease in M1 isoform abundance, suggesting that proper definition of exon 9 requires its native, albeit weaker, 3'ss, for contextual reasons (Suppl. Fig. 2, lanes 3 and 11). There were no significant changes when the 5'ss were swapped (lanes 3 and 7). These observations again indicate that exonic, rather intronic, *cis*-elements are the key determinants of PK-M splicing ratios.

2.4.5 A strong ESE in exon 10 is necessary and sufficient for activation of the exon

To test the hypothesis that there are critical ESEs in exon 10, we systematically searched for such elements. Taking advantage of the high nucleotide-sequence identity between exons 9 and 10, and their identical lengths (Fig 1A), we duplicated 15-30 nt stretches of exon 10 into the corresponding location in exon 9, in order to find sub-exonic regions that are sufficient to activate exon 9 inclusion (Fig. 4A).

We found that the last 30 nt, but not the last 15 nt of exon 10 strongly increased exon 9 inclusion, suggesting that a strong ESE is present within, or overlaps with, the penultimate 15 nt of exon 10 (Fig. 4B, compare lanes 4-6 with lanes 7-9). We then analyzed the entire 30-nt stretch using SFmap (Akerman et al., 2009; Paz et al., 2010), a method to predict splicing-regulatory motifs based on their inter-species conservation and sequence environment. This analysis yielded a near-consensus, conserved SRSF3 motif (Schaal and Maniatis, 1999) within the penultimate 15-nt segment (Suppl. Fig. 3). To determine whether this SRSF3 motif alone can account for the observed M1 splicing activation, we duplicated the 7-nt SRSF3 motif from exon 10 into exon 9, by mutating the only two nucleotides that differ between exons 9 and 10 within this heptamer. Remarkably, duplicating only the SRSF3 motif, but not the flanking 8-nt or the final 15-nt region, activated exon 9 to a similar extent as that achieved by duplicating the entire 30-nt region (Fig. 4B, compare lanes 10-12 with lanes 7-9 and 13-15). This result strongly suggests that the SRSF3 motif is an actual exon 10 ESE.

We then reciprocally abrogated the motif in exon 10 by mutating it into the corresponding exon-9 sequence (Fig. 4C). This resulted in a decrease in exon 10 splicing, as inferred by the large increase in double-skipped RNA (Fig. 4D, lanes 10-12; species **d**), together with the concomitant increase in M1 isoform abundance (Fig. 4D, lanes 10-12; species **a**). Taken together, these data suggest that the SRSF3 motif is a *bona fide* ESE that is both necessary and sufficient for exon 10 activation.

2.4.6 SRSF3 binds specifically to the exon-10 ESE

Because the mapped ESE resembles a consensus SRSF3 motif, we used RNA-affinity pulldowns to ask whether SRSF3 indeed binds to this RNA sequence. Synthetic 24-nt RNAs were covalently linked via their 3'ends to agarose beads, incubated with HeLa nuclear extract under splicing conditions, and then washed at two different salt concentrations. Bound proteins were then eluted and analyzed specifically for SRSF3 binding by Western blotting (Fig. 5). We initially compared RNA sequences 6 to 29 nt upstream from the last 3' nucleotide in both exons (Fig. 5B). As an additional control, we mutated the exon 10 SRSF3 motif to the consensus (1-nt A to C mutation, AUCGUCC to CUCGUCC). Coomassie-Blue staining and mass spectrometry analysis revealed a different composition of bound proteins between exon 9 and exon 10 RNAs (Fig. 5A, compare lanes 2 and 3). We observed similar patterns of bound proteins under more stringent washing conditions (300 mM instead of 150 mM KCl; data not shown). More importantly, SRSF3 bound strongly to the exon 10 RNA. Because hnRNPA1 bound to all RNAs tested—presumably non-specifically—we used

hnRNPA1 as an internal loading control for subsequent analyses. Immunoblotting unambiguously revealed that SRSF3 bound only to the exon 10 and consensus SRSF3 RNAs, but not to the exon 9 RNA, at both salt concentrations (Fig. 5B).

To pinpoint the precise location of SRSF3 binding in exon 10, we mutated the SRSF3 motif to the corresponding exon 9 sequence (Fig. 5C). This resulted in a large decrease in SRSF3 binding (Fig. 5C), indicating that the motif is necessary for strong SRSF3 binding to these short exon 10 RNA fragments.

2.4.7 SRSF3 is necessary for exon 10 inclusion

Although abrogating the SRSF3 motif in exon 10 led to greater exon 9 inclusion (Fig. 4D), we could not rule out the presence of functional *cis*-elements in the corresponding exon 9 sequence that might influence the observed PK-M1 inclusion ratio. To better assess the effect of SRSF3 on exon 10 inclusion, we tested whether knocking down SRSF3 in the context of both the wild-type minigene and the duplicated SRSF3 motif minigene mutant (10 SR minigene, Fig. 4B) would enhance exon 9 inclusion, as exon 10 inclusion would be expected to decrease. Indeed, knocking down SRSF3 using two different siRNAs (Fig. 5D) led to an increase in M1 inclusion and in the abundance of the double-skipped RNA for the wild-type minigene (Fig. 5E, lanes 1-6), similar to what we observed when we mutated the SRSF3 ESE (9 SR minigene, Fig. 4D). We also observed a strong decrease in exon 10 inclusion, and a corresponding increase in exon 9 inclusion with the 10 SR minigene (Fig. 5E, lanes 7-12). These data indicate that SRSF3 is necessary for exon 10 inclusion.

2.4.8 SRSF3 affects endogenous *PK-M* splicing

We next tested whether SRSF3 could affect endogenous *PK-M* alternative splicing; we used knockdown and overexpression, which, as expected, gave reciprocal effects. Knocking down SRSF3 in HEK-293 cells led to a 12-fold increase in PK-M1 mRNA, which was also reflected at the protein level (Fig. 6A,B). A previous study found that knocking down SRSF3 led to a smaller increase in PK-M1, which was deemed not significant (David et al., 2010), but this could have been due to weaker knockdown and/or negative selection resulting from the use of a stably transfected shRNA. Interestingly, knocking down SRSF3 additionally resulted in some double skipping of both exons 9 and 10 (Fig. 6A)—supporting the notion that SRSF3 promotes the definition of exon 10. As a reciprocal experiment, we overexpressed SRSF3 in the glioblastoma cell line A172 (Supp. Fig. 4B), which expresses relatively high levels of PK-M1 (Clower et al., 2010) and has low levels of endogenous SRSF3 protein (Suppl. Fig. 4D). As expected, overexpression of SRSF3 promoted an increase in M2 levels, and therefore led to a 5-fold decrease in M1 levels (Fig. 6C).

2.4.9 SRSF3 activates endogenous PK-M exon 10

To determine whether the above effect of SRSF3 overexpression (Fig. 6C) is due to increased activation of exon 10 and/or repression of exon 9, we first rescued M1 inclusion by knocking down hnRNPA1/A2 and PTB in HEK-293 cells, and then we overexpressed SRSF3 and assessed its effects on endogenous *PK-M* transcripts (Fig. 6D and Suppl. Fig.

4A). SRSF3 overexpression partially restored the level of PK-M2 mRNA (Fig. 6D). This observation suggests that SRSF3 only activates PK-M exon 10. Indeed, overexpression of SRSF3 did not elicit a change in splicing of the duplicated-exon-9 minigene, and knockdown of SRSF3 in the context of the 9 SR minigene had no significant effect on PK-M1/M2 splicing ratios, further suggesting that SRSF3 does not directly affect exon 9 splicing (Suppl. Fig. 5).

2.4.10 SRSF3 is necessary for aerobic glycolysis and cellular proliferation

PK-M isoform ratios influence aerobic glycolysis (Christofk et al., 2008a) , and therefore, we determined the effect of SRSF3 knockdown on this process, as assayed by the extent of cellular lactate production. SRSF3 knockdown in HEK-293 cells resulted in a significant 2-fold decrease in lactate production (Fig 6E). Because the Warburg effect also strongly influences the rate of cellular proliferation (Christofk et al., 2008a), we next assayed the effect of SRSF3 knockdown on cell growth and viability. A 3-(4,5-dimethylthiazol-2-yl)-2,5-diphenyltetrazolium bromide (MTT) assay was performed over the course of 7 days in HEK-293 cells. Strikingly, SRSF3 knockdown significantly decreased the cellular proliferation rate. We conclude that SRSF3 promotes cellular proliferation and aerobic glycolysis at least in part by influencing PK-M isoform ratios. Moreover, because the effect of SRSF3 knockdown was primarily to increase PK-M1 at the protein level (Fig. 6B), this suggests that the increase in PK-M1, rather than a decrease in PK-M2, is responsible for the effects on metabolism and proliferation.

2.5 Discussion

We have demonstrated that *PK-M* ME splicing involves a two-component circuit: exon 9 is repressed and exon 10 is activated in proliferating cells, and these two effects are essentially independent of each other (Fig. 7).

By duplicating and swapping ME exons in a *PK-M* minigene, we showed that the most important *cis*-elements controlling *PK-M* alternative splicing are located within the ME exons themselves. This is the first demonstration of exon-centric alternative splicing regulation via ME exons. As a first proof of this principle, we mapped a *bona fide* SRSF3 ESE in exon 10 that proved sufficient to activate exon 9 splicing in cancer cells when placed in this exon. Although double inclusion of exon 10 was not the major product from the exon-10-duplication minigene (Fig. 3), this cannot be due to repression via the flanking intron 8 and 9 regions, because exon 10 was spliced efficiently when it was cleanly swapped with exon 9. Instead, we speculate that intronic elements are likely involved in the ME exon selection properties of PK-M.

Remarkably, the SRSF3 ESE motif in exon 10 differs from the corresponding exon 9 sequence by only two nucleotides (Suppl. Fig. 3B). Both nucleotides correspond to wobble bases in the corresponding codons (Suppl. Fig. 3A). The first wobble base is highly conserved, which might reflect the importance of this nucleotide in mediating SRSF3 recruitment and functionality. The corresponding two nucleotides in exon 9 are also conserved, suggesting strong selection against the creation of an exon 9 SRSF3 activation

motif (Suppl. Fig. 3B), However, because we used exon 9 sequences to replace exon 10 when abrogating the exon 10 SRSF3 ESE, we cannot rule out the existence of a corresponding exonic splicing silencing (ESS) element in exon 9. The co-evolution of splicing signals in both exons exemplifies the requirement for these exons to be coordinately regulated in order to maintain the ME properties of the system. Additionally, the use of two wobble nucleotides to code for a key splicing signal illustrates the impact of sequence changes that are expected to be translationally neutral, but that nevertheless drastically affect the structure of the resulting protein by changing alternative splicing of the entire exon (reviewed in (Cartegni et al., 2002)).

Although mutating just two wobble nucleotides in exon 10 to the corresponding exon 9 sequence (9 SR minigene) gave rise to more double-skipped and PK-M1 mRNAs, this was not the case when the surrounding exon 9 sequence was also duplicated (9 1530 and 9 30 minigenes). This probably reflects the presence of as yet uncharacterized *cis*-elements in exon 9, such as putative ESEs that may compensate for the loss of exon definition upon mutation of the SRSF3 motif.

Whereas the 5'ss of exons 9 and 10 do not play a dominant role in exon selection in this system—considering that the levels of M1 and M2 mRNAs do not change upon swapping the 5'ss of the ME exons (Suppl. Fig. 2B)—mutational analysis indicates that the 3'ss are necessary for definition of their respective exons, and they compete with each other. It appears that exon definition, and ultimately, proper ME exon selection in the *PK-M* gene, are dependent on the outcome of competition between the alternative 3' ss. We speculate that the

recovery of endogenous PK-M1 transcripts upon SRSF3 knockdown may be due to this competition mechanism, resulting in a loss of exon 10 definition, and allowing the basal splicing machinery to be recruited to the exon 9 3'ss. Loss of exon 10 definition is also supported by the increase in the abundance of double-skipped minigene transcripts from the wild-type minigene upon SRSF3 knockdown. However, it is unclear why the extent of PK-M1 inclusion is weaker in minigene transcripts than in endogenous transcripts, leading to the accumulation of unproductively spliced double-skipped transcripts.

We were surprised to find no rescue of exon 9 inclusion when its 5'ss was swapped with that of exon 10—even though it has been reported that hnRNPA1 represses exon 9 inclusion by binding to the exon 9 5'ss (David et al., 2010)—as this swap presumably removed the repressive hnRNPA1 binding site; perhaps this lack of rescue reflects contextual effects. However, our results confirm and extend the data from an earlier study that duplicated the exon 10 5'ss in a heterologous minigene reporter system, and found no change in *PK-M* splicing (Takenaka et al., 1996). Moreover, in the context of intact pre-mRNAs, it is not known how well hnRNPA1 binding to a motif that is part of a 5'ss can compete with binding of spliceosomal components, such as U1 and U6 snRNPs. Given that hnRNPA1 does have strong effects on exon 9 inclusion *in vivo* (Clower et al., 2010; David et al., 2010), hnRNPA1-induced exon 9 repression could occur either indirectly—through hnRNPA1-mediated regulation of a splicing factor that in turn regulates *PK-M* alternative splicing—or through additional *cis*-elements located elsewhere on the *PK-M* pre-mRNA.

The change in endogenous levels of PK-M1 when SRSF3 was knocked down was roughly comparable to the effects of knocking down the known repressors of exon 9, hnRNPA1/A2 and PTB (Clower et al., 2010; David et al., 2010). However, knocking down these factors did not completely rescue exon 9 inclusion, and as in other systems, we anticipate the existence of several additional activators of exon 10 and/or repressors of exon 9 that contribute to maintaining exon 10 definition in proliferating cells. With respect to the enhancer region we identified in exon 10, knockdown of other candidate splicing factors identified by RNA-affinity chromatography, namely hnRNPK, and RBM3, did not change PK-M splicing ratios (data not shown).

We have demonstrated that the SR protein SRSF3 promotes the inclusion of the *PK-M2*-specific alternative exon 10 in transformed cells by binding to an ESE near the 3' end of the exon. Consistent with its expected ability to facilitate cellular proliferation by altering glycolytic metabolism, *SRSF3* is overexpressed in ovarian cancers (He et al., 2004) and cervical cancer cell lines, whereas in normal cervical tissue, its expression is restricted to the basal proliferating layers (Jia et al., 2009). SRSF3 is also a downstream target of the oncogenic β-catenin/TCF-4 pathway in colorectal cancer cells (Goncalves et al., 2008). Moreover, overexpression of SRSF3 was recently found to be sufficient for transformation of NIH-3T3 immortal mouse fibroblasts (Jia et al., 2010), indicating that similar to its paralog, SRSF1 (Karni et al., 2008), SRSF3 is an oncoprotein. Given the multitude of potential SRSF3 downstream target genes, we expect that SRSF3-mediated tumorigenesis reflects splicing changes in multiple effector genes, including *PK-M*.

Important questions that remain unanswered include: What are the additional factors that govern exon 9 and exon 10 usage in tumor cells? Can the PK-M2 isoform be completely switched to the PK-M1 isoform by manipulating the levels of splicing factors in tumor cells? How is exon 9 selected as the default spliced exon in quiescent cells? Are there tissue-specific differences in the mechanisms of exon 9 selection in differentiated cells? Answers to these questions will contribute to a better understanding of the regulation of PK-M isoform expression in the context of tumorigenesis, which could provide the basis to develop splicing-targeted cancer therapeutics.

2.6 Experimental Procedures

2.6.1 Cells and transfections

HeLa and HEK-293 cells were grown in DMEM, supplemented with 10% (v/v) FBS, penicillin and streptomycin, at 37 °C and 5% CO_2. 5 μg of minigene plasmid per 10-cm dish, or 1 μg per well of a 6-well plate, was transiently transfected using Lipofectamine 2000 (Invitrogen). Total RNA from transfected cells was harvested after 36 hr.

2.6.2 RNA interference

Two siRNAs targeting human *SFRS3* were obtained from Sigma Genosys, and have the sense-strand sequences 5'-CGAUCUAGGUCAAAUGAAA-3' (SR3#1) and 5'-CGUAGUCGAUCUAGGUCAA-3' (SR3#2). siRNAs against hnRNPA1, hnRNPA2, and PTB were used as described (Cartegni et al., 2006). 10^6 HEK-293 cells in 6-well plates were transfected with 200 pmol of siRNA duplex using Lipofectamine 2000 (Invitrogen). Cells were harvested 48 hr later.

2.6.3 Immunoblotting

Cells were lysed in SDS, and total protein concentration was measured by the Bradford assay. 30 μg of total protein was separated by SDS-PAGE and transferred onto nitrocellulose, followed by blocking with 5% (w/v) milk in Tris-buffered saline with Tween-

20, probing with the indicated antibodies, and visualization by enhanced chemiluminescence (Roche). Primary antibodies were: β-tubulin (Genscript rAb, 1:5000); hnRNPA1 (mAb UP1-55, culture supernatant (Hua et al., 2008)); SRSF3 (Zymed mAb, 1:1000); PK-M2 (rabbit, 1:2000) and PK-M1 (rabbit, 1:2000; (Christofk et al., 2008b)). Secondary antibodies were goat anti-mouse or anti-rabbit HRP conjugates, 1:20,000 (Bio-Rad).

2.6.4 Plasmids

DNA oligonucleotides were obtained from Sigma Genosys. The *PK-M2* minigene was constructed by amplifying a 6.4-kb *PK-M* exon 8-11 fragment from human genomic DNA (Promega) using Phusion High-Fidelity DNA Polymerase (Finnzymes) and primers PKMinigeneF (5'-GGGGAAGATATCAATTCCCCATTCTGTCTTCCCATGT-3') and PKMinigeneR (5'-GGGGAACTCGAGCTAGACATTCATGGCAAAGTTCACC-3'). The product was then digested and cloned between the BamHI and XhoI sites of pcDNA3.1+ (Invitrogen). Site-directed mutagenesis using Pfu polymerase (Strategene) was used to generate the mutant minigene constructs in Fig. 2. For the constructs in Figs. 3-6, the upstream KpnI site 1552 nt downstream of exon 8 was removed by a 1-nt deletion, and an EcoRV restriction site was generated 90 nt upstream of exon 9 by a 2-nt insertion to create a modified wild-type minigene. See Supplementary experimental procedures for the generation of exonic and sub-exonic duplication, exon-swap, and splice-swap constructs.

2.6.5 RT-PCR

2-5 μg of total RNA was extracted from cell lines using Trizol (Invitrogen). Contaminating DNA was removed with DNAase I (Promega). Reverse transcription was carried out using ImPromp-II reverse transcriptase (Promega). Semiquantitative PCR using Amplitaq polymerase (Applied Biosystems) was performed by including [α-^{32}P]-dCTP in the reactions. The human-specific primer sets used to amplify endogenous transcripts anneal to *PK-M* exons 8 and 11, and their sequences are: hPKMF: 5'-AGAAACAGCCAAAGGGGACT-3'; hPKMR: 5'-CATTCATGGCAAAGTTCACC-3'. To amplify minigene-specific transcripts, the forward primer was replaced with a primer annealing to the pcDNA3.1(+) vector, pcDNAF: 5'-TAATACGACTCACTATAGGG-3'. After 26 amplification cycles for minigene-derived transcripts, and 24 cycles for endogenous transcripts, the reactions were divided into four aliquots for digestion with NcoI, PstI (New England Biolabs), both, or neither. The products were analyzed on a 5% native polyacrylamide gel, visualized by autoradiography, and quantified on a FLA-5100 phosphoimager (Fuji Medical Systems) using Multi Gauge software Version 2.3. The % M1 mRNA in endogenous transcripts was calculated using the GC-content-normalized intensities of the top undigested band (M1, A) and the bottom two digested bands (M2, B1 B2) in the PstI-digest lanes. The % M1 mRNA from minigene-transcripts was calculated using the GC-content-normalized intensities of the top undigested band (**a,** M1) and other higher-mobility digested bands corresponding to M2 and its variant species (**b – g**, as described above) in the PstI-digest lanes. All the PCR products were gel-purified, cloned, and sequenced to verify their identities.

2.6.6 RNA-affinity chromatography and mass spectrometry

RNA-affinity chromatography was performed as described (Caputi et al., 1999; Hua et al., 2008). RNA oligonucleotides were obtained from Sigma Genosys. 10 nanomoles of each RNA was oxidized with sodium *m*-periodate in a 24-μl reaction and mixed with 100 μl (1:1 slurry) of adipic-acid-dihydrazide agarose beads (Sigma) by rotation overnight at 4 °C. A 250-μl in vitro splicing reaction mix including 100 μl of HeLa nuclear extract was added to 50 μl RNA-bound beads equilibrated with buffer D (Mayeda and Krainer, 1999) containing 0.1 M KCl. Mixtures were incubated at 30 °C for 40 min and divided into two aliquots for washing three times with buffer D containing either 150 mM or 300 mM KCl. After the final wash, the beads were resuspended in 75 μl of 4× Laemmli buffer and boiled for 5 min to elute bound proteins. 5 μl of each protein sample was loaded on a 12 % SDS polyacrylamide gel for immunoblotting. 15 μl of sample was used for Coomassie-Blue staining. Prominent bands were excised for in-gel trypsin digestion. The samples were then processed and analyzed by mass spectrometry at the Cold Spring Harbor Proteomics Core.

2.6.7 Lactate assay

For measurements of lactate secretion, cells were transfected with siRNA in 6-well plates. 24 hr later, the cells were replated (three replicates per condition) at subconfluent density (25,000 cells/well) in 12-well dishes, and after 24 hr, the cells were switched to serum-free medium without phenol red for 20 min, and lactate secreted into the medium over this time was measured, in triplicate for each sample, using the colorimetric mode of a Lactate Assay Kit II (Biovision Inc.). Optical density readings at 450 nm were averaged for each sample replicate

set, then averaged for each condition replicate set, and finally normalized to the cell number measured from parallel wells.

2.6.8 MTT assay

3×10^6 HEK-293 cells were transfected with 400 pmol of luciferase control or SRSF3 siRNA in a 6-cm dish. After 24 hr, cells were seeded into 96-well plates (2500 cells/well). The next day, and every two days thereafter, MTT (Sigma) was added to fresh medium at a final concentration of 0.5 mg/ml. Cells were then incubated at 37 °C for 4 hr and then solubilized with DMSO. Optical density at 560 nm was then determined for each well and averaged.

2.7 Supplementary Experimental Procedures

Table 2.7-1 Site-directed mutagenesis.

Mutant Name	Sequences of Mutagenesis Primer Pairs
Exon 10 5'ss mutant	F: 5'-AAGTCTGGCAGATAGGAGGCGGCAG-3' R: 5'-CTGCCGCCTCCTATCTGCCAGACTT-3'
Exon 10 3'ss mutant	F: 5'-GTTGCTCCCCTAAATTGCCCGTGAGG-3' R: 5'-CCTCACGGGCAATTTAGGGGAGCAAC-3'
Exon 10 Py Down mutant	F: 5'-CCCTCTGGACGGATGTTGGAGAGATAGATTGCCCGTGAGGCAG-3' R: 5'-CTGCCTCACGGGCAATCTATCTCTCCAACATCCGTCCAGAGGG-3'
Exon 10 5'ss consensus mutant	F: 5'-CGGAGTCTGGCAGGTAAGTGCCTAAGGGCAGGTAAC-3' R: 5'-GTTACCTGCCCTTAGGCACTTACCTGCCAGACTCCG-3'
Exon 10 3'ss Py Up mutant	F: 5'-GCCCCCTCTTCCCCTTTTCCTTACAGATAGCTCG-3' R: 5'-CGAGCTATCTGTAAGGAAAAGGGGAAGAGGGGGC-3'
EcoRV insertational minigene mutant	F: 5'-CTTCCTCTCTGATATCAATTCCCCATTCTG-3' R: 5'-AGAATGGGGAATTGATATCAGAGAGGAAG-3'
KpnI inactivation minigene mutant	F: 5'-GAGCCAAGATGGACCAGCCTAGGTG-3' R: 5'-CACCTAGGCTGGTCCATCTTGGCTC-3'

Site-directed mutagenesis using Pfu polymerase (Strategene) was used to generate the mutant minigene constructs in Figure 2. For the constructs in Figures 3-6, the upstream KpnI site 1552 nt downstream of exon 8 was removed by a 1-nt deletion, and an EcoRV restriction site was generated 90 nt upstream of exon 9 by a 2-nt insertion to create a modified wild-type minigene.

Table 2.7-2 Exon duplication and swaps

Exon 9 Duplication	**Sequence of Primer Pairs**
Fragment A (exon 9 + flanking exon 10)	F: 5'-TGGACGGATGTTGCTCCCCTAATAGCTCGTGAGGCTGAGGC-3' R: 5'-GGTACCACTGAGCAGGGCATTCCAGGGAGCCGCTGCCGCCTCCTACCTGCCAGACTCCGTCAGAAC-3'
Fragment B	**FEcoRV:** 5'-GGGGAAGATATCAATTCCCCATTCTGTCTTCCCATGT-3' R: 5'-CTAGGGGAGCAACATCCGTCCA-3'

Exon 10 Duplication	**Sequence of Primer Pairs**
Fragment A (exon 10 + flanking) exon 9)	F: 5'-TTCCCCATTCTGTCTTCCCATGTGTTGTGTCTCGTTTTTTTCCTCCTCCTTCCCTCTTCCTTGCCCCCTCTTCCCCTAAACCTTACAGATTGCCCGTGAGGCAGAG-3' R: 5'-GTGTTACCTGCCCTTAGGGCCCTACCTGCCAGACTTGGTGAGGAC-3'
Fragment B	F: 5'-GTAGGGCCCTAAGGGCAGGTAACAC-3' **RKpnI**: 5'-GGGGAAGGTACCACTGAGCAGGGCATT-3'

Exon Swap	**Sequence of Primer Pairs**
Fragment A (Template: exon 9 duplication)	F: 5'-GTAGGGCCCTAAGGGCAGGTAACAC-3' **RKpnI**: 5'-GGGGAAGGTACCACTGAGCAGGGCATT-3'
Fragment B (Template: exon 10 duplication)	**FEcoRV:** 5'-GGGGAAGATATCAATTCCCCATTCTGTCTTCCCATGT-3' R: 5'-CTAGGGGAGCAACATCCGTCCA-3'
OE PCR End Primers	**FEcoRV:** 5'-GGGGAAGATATCAATTCCCCATTCTGTCTTCCCATGT-3' **RKpnI:** 5'-GGGGAAGGTACCACTGAGCAGGGCATT-3'

Fragments A and B were individually generated using the primer pairs indicated in the table, with Phusion High-Fidelity polymerase (Finnzymes), and then gel-purified (Qiagen). Both fragments were then joined by OE PCR using Pfu polymerase (Stratagene). OE PCR end

primers are indicated in bold in the table. The chimeric fragment (A+B) was then digested with KpnI and EcoRV, gel-purified and ligated between the EcoRV and KpnI restriction sites in the modified *PK-M* minigene. For generation of the exon-swap minigenes, the same procedure was carried out, except that different templates (indicated in the table) were used to generate Fragments A and B.

Table 2.7-3 Splice site swaps

Exon 9 5'ss duplication	**Sequences of Primer Pairs**
Fragment A	FEcoRV R: 5'- GGGGAAGGTACCACTGAGCAGGGCATTCCAGGGAGCCGCTGCCGGGCC CTACCTGCCAGACTTGGTGAGGACGATTATGGCC-3'
Exon 10 5'ss duplication	
Fragment A	FEcoRV R: 5'-TAACAGTGTTACCTGCCCTTAGCCT CCTACCTGCCAGACTCCGTCAGAA-3'
Fragment B	F: 5'- AGGCTAAGGGCAGGTAACACTGTTAGGATAACCAGCCTCTTGCTCCAC CT-3' RKpnI
5'ss swap	Same primer pairs as for exon swap. Template for Fragment A is exon 9 5'ss A+B duplication fragment; template for Fragment B is exon 10 5'ss duplication A+B fragment.
Exon 9 3'ss duplication	**Sequences of Primer Pairs**
Fragment A	FEcoRV R:5'-CTCTGCCTCACGGGCAATCTGTAAGGTTTACATCCGTCCAGAGGG ACGAGAGGGGGACAGAGCTTT-3'
Fragment B	F: CCCTCTGGACGGATG TAAACCTTACAG ATTGCCCGTGAGGCAGAG- 3' RKpnI
Exon 10 3'ss duplication	F: 5'- TTCCCCATTCTGTCTTCCCATGTGTTGTGTCTCGTTTTTTTCCTCCTCCTT CCCTCTTCCTTGCCCCCTCTTCCCC TTGCTCCCCTAG ATAGCTCGTGAGGCTGAGGCAG-3' RKpnI
3'ss swap	Same primers pairs as for exon swap. Template for Fragment A is exon 9 3'ss duplication A+B fragment; template for Fragment B is exon 10 3'ss duplication A+B fragment.

Construction procedures are identical to II. Templates for 5'ss and 3'ss swap are indicated in the above table.

Table 2.7-4 Sub exonic duplications

Name	Oligonucleotide sequence
Exon9Fwd	5’-CCCTAAACCTTACAGATAGCTCGTGAGGCTGAG GCAGCCATGTTCCACCGCAAGCTGTTTGAAGAA CTTGTGCGAGCCTCAAGTCACTCCACAGACCTC ATGGAAGCCAT-3’
10 15	5’-CCCTTAGGGCCCTACCTGCCAGACTTGGT GAGAACTATCAAAGCTGCTGCTAAACACT TATAAGAAGCCTCCACGCTGCCCATGGCC ATGGCTTCCATGAGGTCTG-3’
10 30	5’-CCCTTAGGGCCCTACCTGCCAGACTTGGT GAGGACGATTATGGCCGCTGCTAAACACT TATAAGAAGCCTCCACGCTGCCCATGGCC ATGGCTTCCATGAGGTCTG-3’
10 SR	5’-CCCTTAGGGCCCTACCTGCCAGACTCCGT CAGGACGATCAAAGCTGCTGCTAAACACT TATAAGAAGCCTCCACGCTGCCCATGGCC ATGGCTTCCATGAGGTCTG-3’
10 5’	5’-CCCTTAGGGCCCTACCTGCCAGACTCCGT CAGAACTATTATGGCTGCTGCTAAACACTT ATAAGAAGCCTCCACGCTGCCCATGGCCA TGGCTTCCATGAGGTCTG-3’
Exon10Fwd	5’-ATGTTGCTCCCCTAGATTGCCCGTGAGGC AGAGGCTGCCATCTACCACTTGCAATTAT TTGAGGAACTCCGCCGCCTGGCGCCCAT TACCAGCGACCCCACAGAAGCCAC-3’
9 30	5’-CGCTGCCGCCTCCTACCTGCCAGACTCC GTCAGAACTATCAAAGCTCCACTGCAGCA CTTGAAGGAGGCCTCCACGGCACCCACG GCGGTGGCTTCTGTGGGGTCGCT-3’
9 1530	5’-CGCTGCCGCCTCCTACCTGCCAGACTTG GTGAGAACTATCAAAGCTCCACTGCAGC ACTTGAAGGAGGCCTCCACGGCACCCAC GGCGGTGGCTTCTGTGGGGTCGCT-3’
9 SR	5’-CGCTGCCGCCTCCTACCTGCCAGACTTG GTGAGAACTATTATGGCCCCACTGCAGC ACTTGAAGGAGGCCTCCACGGCACCCAC GGCGGTGGCTTCTGTGGGGTCGCT-3’

For exon 10 sub-exonic duplications, a 110-nt oligonucleotide (Exon9Fwd) that includes the 5' sense DNA sequence of exon 9, was annealed with a variable106-nt oligonucleotide that includes the 3' antisense DNA sequence of exon 9, and amplified using the following OE PCR primer pairs: Ex10ADupF: 5'-TTCCCCATTCTGTCTTCCCATGTGTTGTGTCTCGTTTTTTTCCTCCTCCTTCCCTCTTCCTTGCCCCCTCTTCCCCTAAACCTTACAG-3' and Ex10ADupR: 5'-AGTGTTACCTGCCCTTAGGGCCCTAC-3'. The 106-nt oligonucleotide carries mutations that duplicate specific stretches of exon 10 over the corresponding region of exon 9. The sequences of these oligonucleotides are shown below. Another fragment was amplified from the wild-type minigene using the following primer pairs: Ex10BF: 5'-GTAGGGCCCTAAGGGCAGGTAACAC-3' and RKpnI. Both fragments were then subject to a second OE PCR reaction using the same procedures and primers as those used for exon swaps.

For exon 9 sub-exonic duplications, a 110-nt oligonucleotide (Exon10Fwd) that includes the 5' sense DNA sequence of exon 10, was annealed with a variable 108-nt oligonucleotide that includes the 3' antisense DNA sequence of exon 10, and amplified using the OE PCR primer pairs: Ex9ADupF: 5'-TGGACGGATGTTGCTCCCCTAG-3' and Ex9ADupR: 5'-GGTACCACTGAGCAGGGCATTCCAGGGAGCCGCTGCCGCCTCCTAC-3'. The 108-nt oligonucleotide carries mutations that duplicate specific stretches of exon 9 over the corresponding region in exon 10. The sequences of these oligonucleotides are shown below. Another fragment was amplified from the wild-type minigene using the following primer pairs: FEcoRV and Ex9BR: 5'-GTAGGGCCCTAAGGGCAGGTAACAC-3'. Both

fragments were then subjected to a second OE PCR reaction using the same procedures and primers as those used for exon swaps.

Oligonucleotide sequences used for exon 9 and 10 sub-exonic duplications. The variable 106-nt and 108-nt sequences were used in the construction of specified sub-exonic duplication mutants and are named after them.

2.8 Figures and Figure Legends

Figure 2.8-1

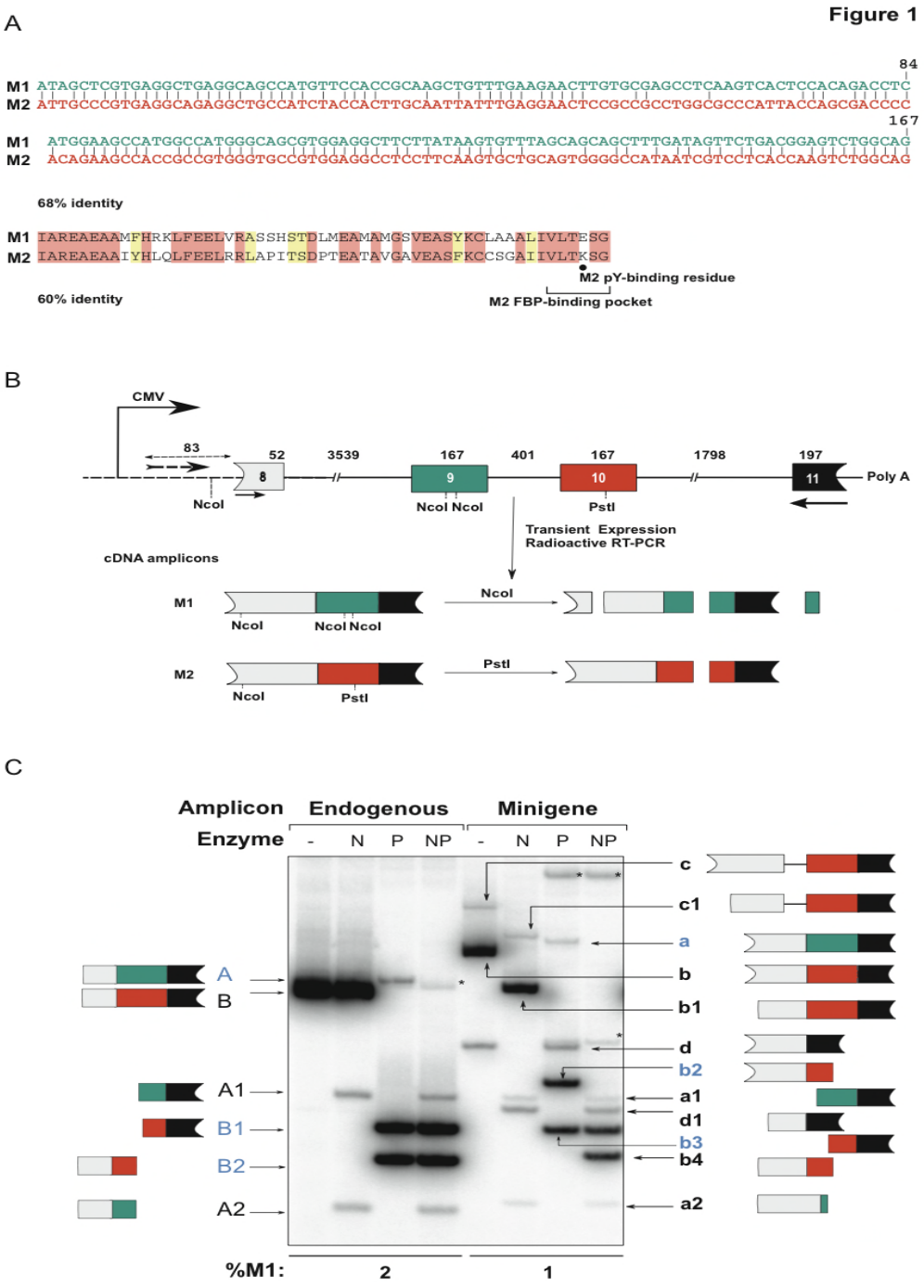

2.8.1 Figure 1. Detection of endogenous and minigene-specific *PK-M* spliced isoforms

(A) Nucleotide (top) and amino-acid (bottom) sequence alignments of ME exons 9 (M1) and 10 (M2). Identical nucleotides are shown by vertical dashes. Identical and similar amino acids are highlighted in red and yellow, respectively. The key phosphotyrosine-binding residue and the fructose-1,6-bisphosphate (FBP)-binding pocket of PK-M2 are indicated. The percentages of nucleotide and amino acid identity are shown.

(B) Diagram of the human *PK-M* minigene. The minigene comprises the intact introns 8, 9, and 10, the intact alternative exons 9 and 10, and portions of the flanking constitutive exons 8 and 11. The numbers above each exon and intron show the length in nucleotides. A vector-specific forward primer (dashed arrow) and a reverse primer annealing to exon 11 were used to amplify minigene-derived transcripts; to amplify endogenous transcripts in untransfected cells, a forward primer annealing to exon 8 (solid arrow) was used instead. To distinguish between exon-9-included (M1 isoform) and exon-10-included (M2 isoform) transcripts, cDNA amplicons were cleaved with NcoI (N), PstI (P) or both (NP), as described (Clower et al., 2010). Note the additional NcoI site at the 5' end of the PK-M minigene, which is absent from the endogenous gene.

(C) Radioactive RT-PCR and restriction digest of endogenous and minigene-derived *PK-M* transcripts in HEK-293 cells. RNA was isolated from untransfected cells or 48 hr after transfection of the plasmid minigene. Bands marked with asterisks (*) indicate restriction fragments corresponding to unspliced *PK-M* pre-mRNA. cDNAs and fragments from endogenous mRNAs are indicated on the left in uppercase font; those derived from minigene-specific transcripts are shown on the right in lowercase bold font. The most important bands are indicated in blue font. The bands correspond to: uncut M1 fragment (A, 398 nt; **a**, 481 nt); uncut M2 fragment (B, 398 nt; **b**, 481 nt); NcoI-cleaved M1 3' fragment

(A1, 248 nt; **a1,** 248 nt); NcoI-cleaved M1 5' fragment (A2, 144 nt; **a2**, 150 nt); PstI-cleaved M2 5' fragment (B2, 185 nt; **b2**, 268 nt); PstI-cleaved M2 3' fragment (B1, 213 nt; **b3,** 213 nt). Minigene M2 cDNA is cleaved by NcoI, giving rise to **b1** (404 nt). Two additional species are observed from minigene-specific transcripts: a spliced mRNA that skips both exons 9 and 10 (**d**, 314 nt) and is cleaved by NcoI (**d1,** 237 nt), and an M2 transcript that uses a cryptic 3' splice site 115 nt upstream of the authentic 3'ss of exon 10 (**c,** 596 nt), and whose 3' fragment after PstI digestion is identical to **b3**. Due to its low abundance, the corresponding 5' end after PstI digestion can only be detected with certain mutant minigenes (see Fig. 2A). The 5' end of the PstI-cleaved M2 fragment, **b2**, is additionally cleaved by NcoI to a shorter fragment (**b4,** 194 nt) plus a 74-nt fragment that runs off the gel. See Suppl. Fig. 1 for a detailed description of these M2-variant species. The numbers below the gel indicate the percentage of exon 9-included transcripts (% M1); standard deviations (s.d.) are $\leq 0.2\%$ ($n \geq 3$).

Figure 2.8-2

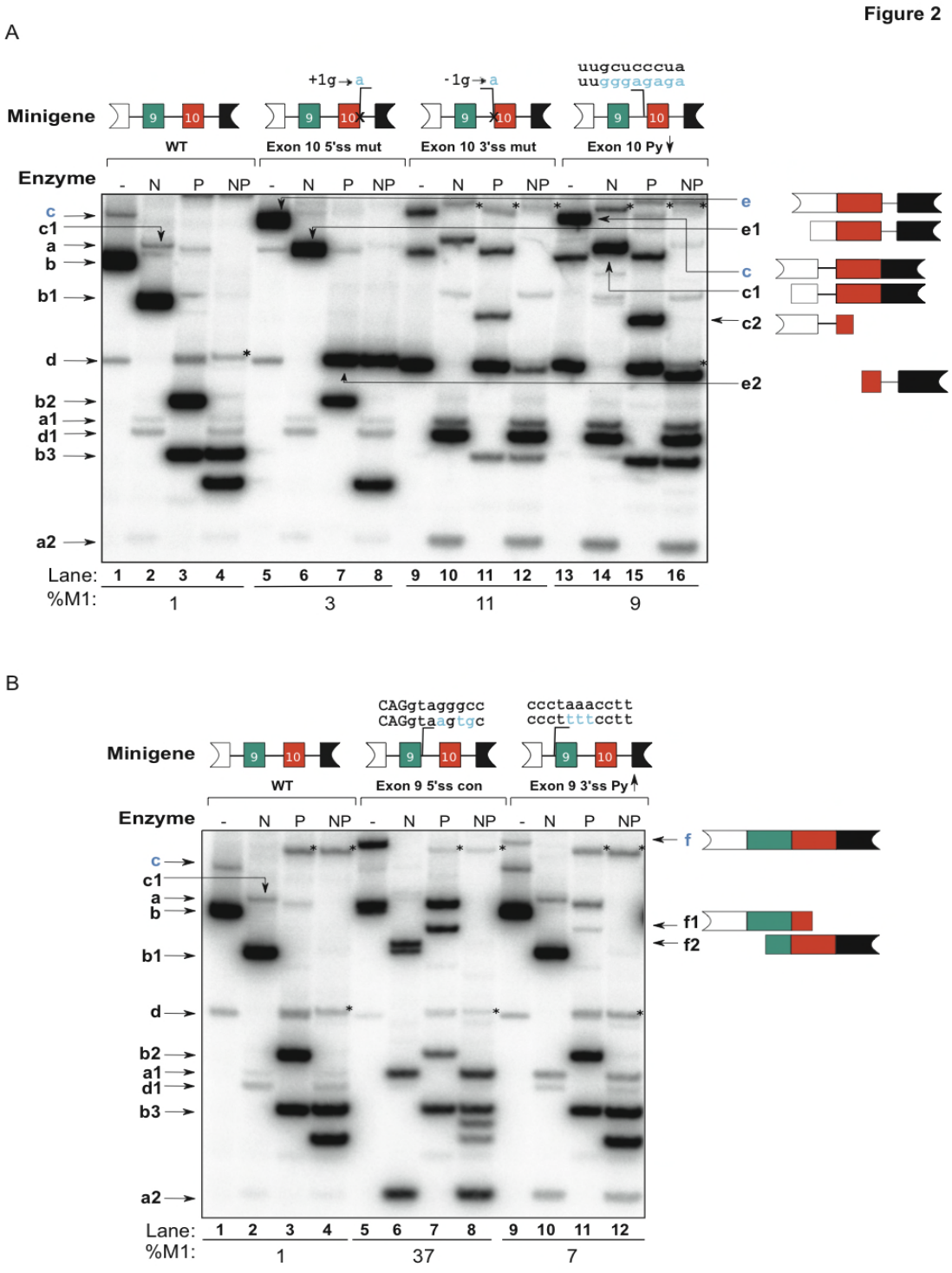

2.8.2 Figure 2. Effects of splice-site relative strengths on inclusion of exon 9

Mutant minigenes were analyzed by transient transfection into HEK-293 cells, followed by radioactive RT-PCR and restriction digests, as in Fig. 1C.

(A) Mutations that inactivate or weaken the splice sites (ss) of exon 10. The mutated 5'ss, 3'ss, or PPTnucleotides are indicated in light blue. Numbers indicate the position of the mutated nucleotide, either upstream (+), or downstream (-) of the exon. Bands marked with asterisks (*) are fragments of *PK-M* pre-mRNA, as in Fig. 1C. Bands already described in Fig. 1C are indicated on the left. New and/or important bands are indicated on the right, and the key bands are labeled in blue font (see also Suppl. Fig. 1). The 5'ss mutation gives rise to a new M2 variant (**e**, 586 nt) derived from use of a cryptic 5'ss 105 nt downstream of the authentic 5'ss; this band is cleaved by NcoI (**e1**, 509 nt), and PstI digestion generates a longer 3' fragment (**e2**, 318 nt). The increase in the M2 3'ss cryptic variant (**c**, as described in Fig. 1C) upon mutation of the PPT or 3'ss allows detection of the 5' PstI fragment (**c3**, 383 nt). The % M1 inclusion is indicated at the bottom; s.d.: 0.2% (WT); 0.3% (Exon 10 5'ss mut); 2% (Exon 10 3'ss mut); and 2% (Exon 10 Py↓) (n≥3).

(B) Mutations that strengthen the splice sites of exon 9. The mutated 5'ss and PPT nucleotides are indicated in light blue. Uppercase and lowercase letters indicate exonic and intronic sequences, respectively. Bands are labeled as in panel A. A new exon 9 – exon 10 doubly-included mRNA is indicated on the right (**f**, 648 nt). This band is sensitive to both PstI (**f1**, 435 nt) and NcoI (**f2**, 415 nt) digestion. See also Suppl. Fig. 1. The % M1 inclusion is indicated at the bottom; s.d.: 0.2% (WT), 4% (Exon 9 5'ss con) and 3% (Exon 9 3'ss Py↑) (n≥3).

Figure 2.8-3

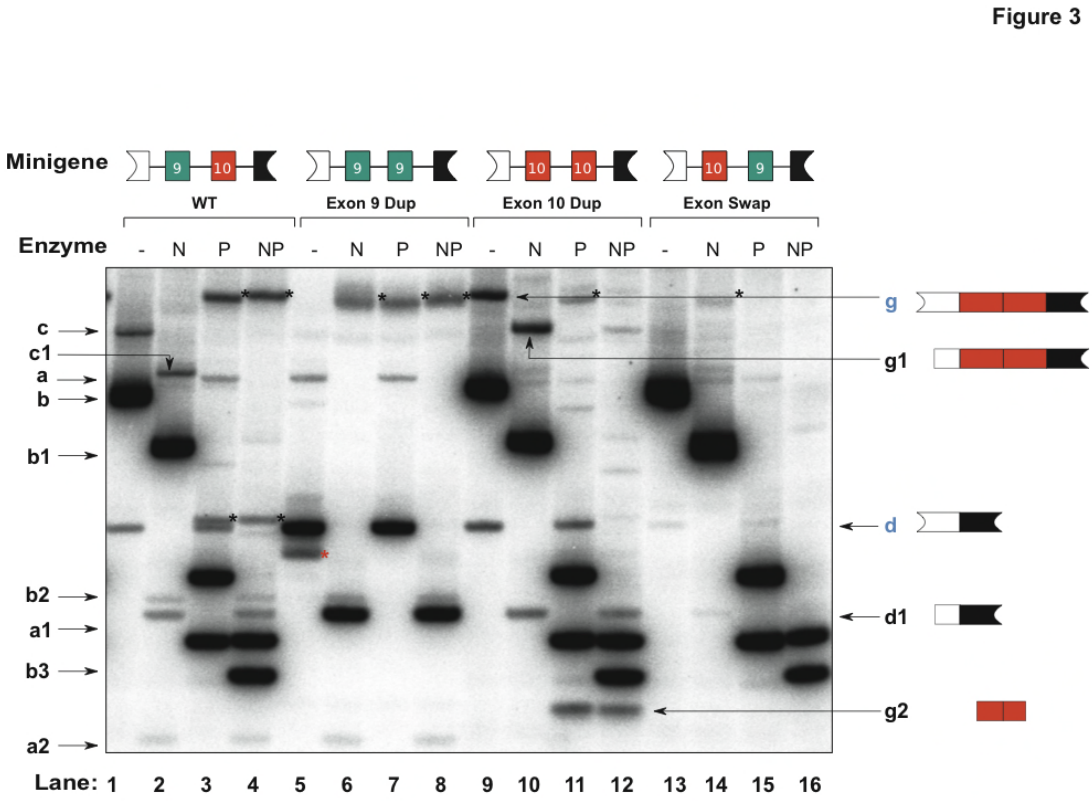

2.8.3 Figure 3. Effects of exonic *cis*-elements on *PK-M* alternative splicing

Mutant minigenes were analyzed by transient transfection into HEK-293 cells, followed by radioactive RT-PCR and restriction digests, as in Fig. 1C.

Minigenes were constructed with clean duplications or swaps of exons 9 and 10, as shown schematically at the top. Bands marked with black asterisks (*) or labeled on the left are as described in Fig. 1C. Key bands are labeled in blue font. The band marked with a red asterisk indicates a non-reproducible PCR artifact. A new exon 10 – exon 10 doubly-included mRNA

expressed from the Exon 10 Dup minigene is indicated on the right (**g**, 648 nt). It generates unique fragments upon NcoI (**g1**, 571 nt) and PstI (**g2**, 167 nt) digestion. See also Suppl. Fig. 1.

Figure 2.8-4

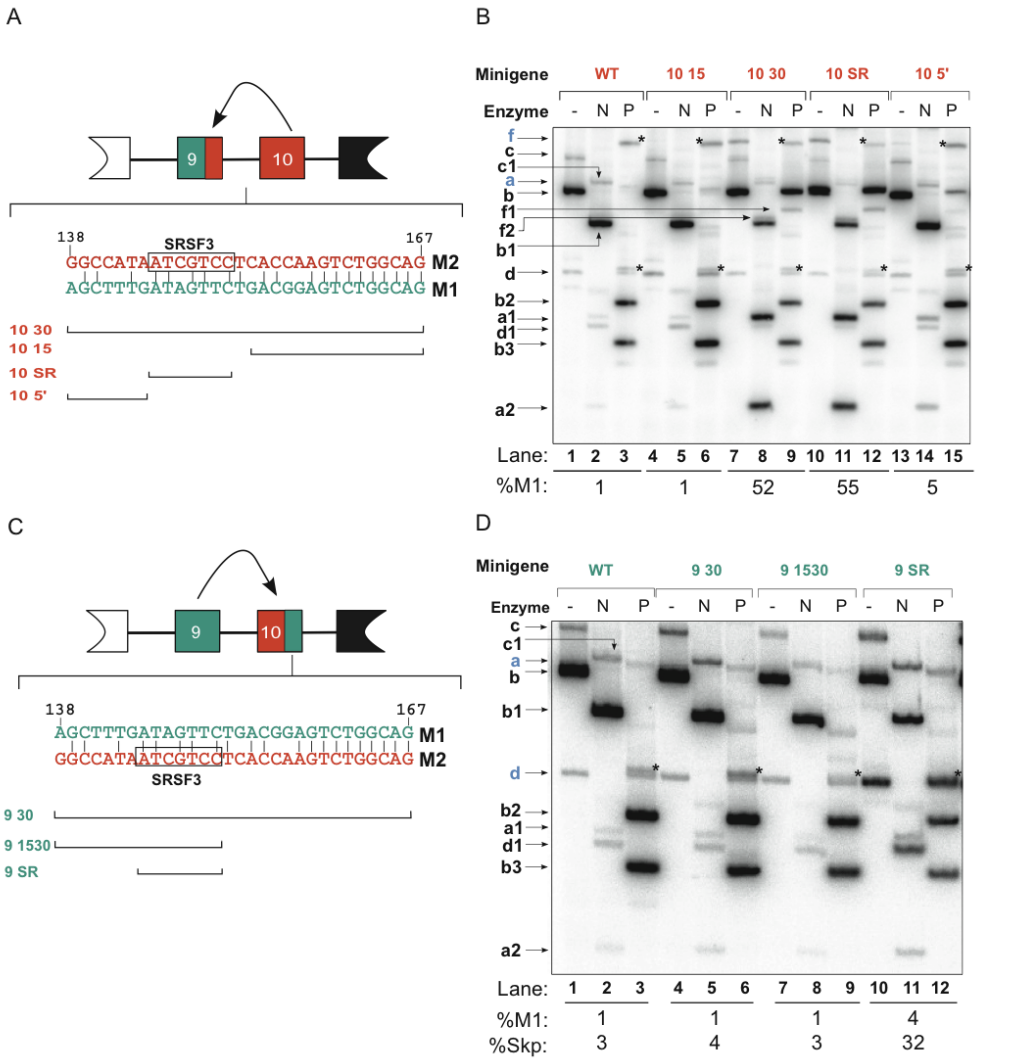
Figure 4
A
9
10
138
SRSF3
167
GGCCATAATCGTCCTCACCAAGTCTGGCAG M2
AGCTTTGATAGTTCTGACGGAGTCTGGCAG M1
10 30
10 15
10 SR
10 5'
B
Minigene
WT
10 15
10 30
10 SR
10 5'
Enzyme
- N P - N P - N P - N P - N P
f
c
c1
a
b
f1
f2
b1
d
b2
a1
d1
b3
a2
Lane: 1 2 3 4 5 6 7 8 9 10 11 12 13 14 15
%M1: 1 1 52 55 5
C
9
10
138
167
AGCTTTGATAGTTCTGACGGAGTCTGGCAG M1
GGCCATAATCGTCCTCACCAAGTCTGGCAG M2
SRSF3
9 30
9 1530
9 SR
D
Minigene
WT
9 30
9 1530
9 SR
Enzyme
- N P - N P - N P - N P
c
c1
a
b
b1
d
b2
a1
d1
b3
a2
Lane: 1 2 3 4 5 6 7 8 9 10 11 12
%M1: 1 1 1 4
%Skp: 3 4 3 32

2.8.4 Figure 4. Mapping an ESE in exon 10

(A) Method used to map an ESE within the last 30 nt of exon 10. The indicated exon 9 (green) nucleotides were mutated to corresponding exon 10 (red) sequences. The last 30 nt of exon 10, when moved to exon 9, activated inclusion of exon 9. An SRSF3 SELEX motif (Schaal and Maniatis, 1999) identified by a SFmap (Akerman et al., 2009) is shown by a black rectangle. Exon-10 candidate regions that were duplicated into exon 9 are indicated at the bottom, and the construct names (red) are given on the left.

(B) The SRSF3 motif is the ESE in the last 30 nt of exon 10. The constructs from (A) are indicated at the top. Labeled bands are as in Fig. 1C. The % M1 inclusion is shown at the bottom ($n \geq 3$). Duplication of the exon 10 SRSF3 motif into exon 9 was sufficient to rescue exon 9 inclusion. The % M1 inclusion is indicated at the bottom; s.d.: 0.2% (WT), 0.1% (10 15), 5% (10 30), 4% (10 SR), 1% (10 5') (n=3).

(C) Replacing the SRSF3 motif in exon 10 by duplicating exon 9 sequences. The indicated exon 10 (red) nucleotides were mutated to the corresponding exon 9 (green) sequences. Exon 9 regions that were duplicated into exon 10 are indicated below, and the construct names (green) are given on the left.

(D) Inactivating the SRSF3 motif in exon 10 causes skipping of exon 10. Candidate exon 9 regions duplicated into exon 10 are indicated at the top. Labeled bands are as in Fig. 1C. % M1-included and % double-skipped (% Skp) transcripts are indicated below. Inactivating the SRSF3 motif in exon 10 is sufficient to increase the abundance of the double-skipped RNA species Transcript-level changes are indicated at the bottom; s.d.: 0.3% (WT), 0.3% (9 30), 1% (9 15 30), 2% (9 SR) (n=3).

Figure 2.8-5

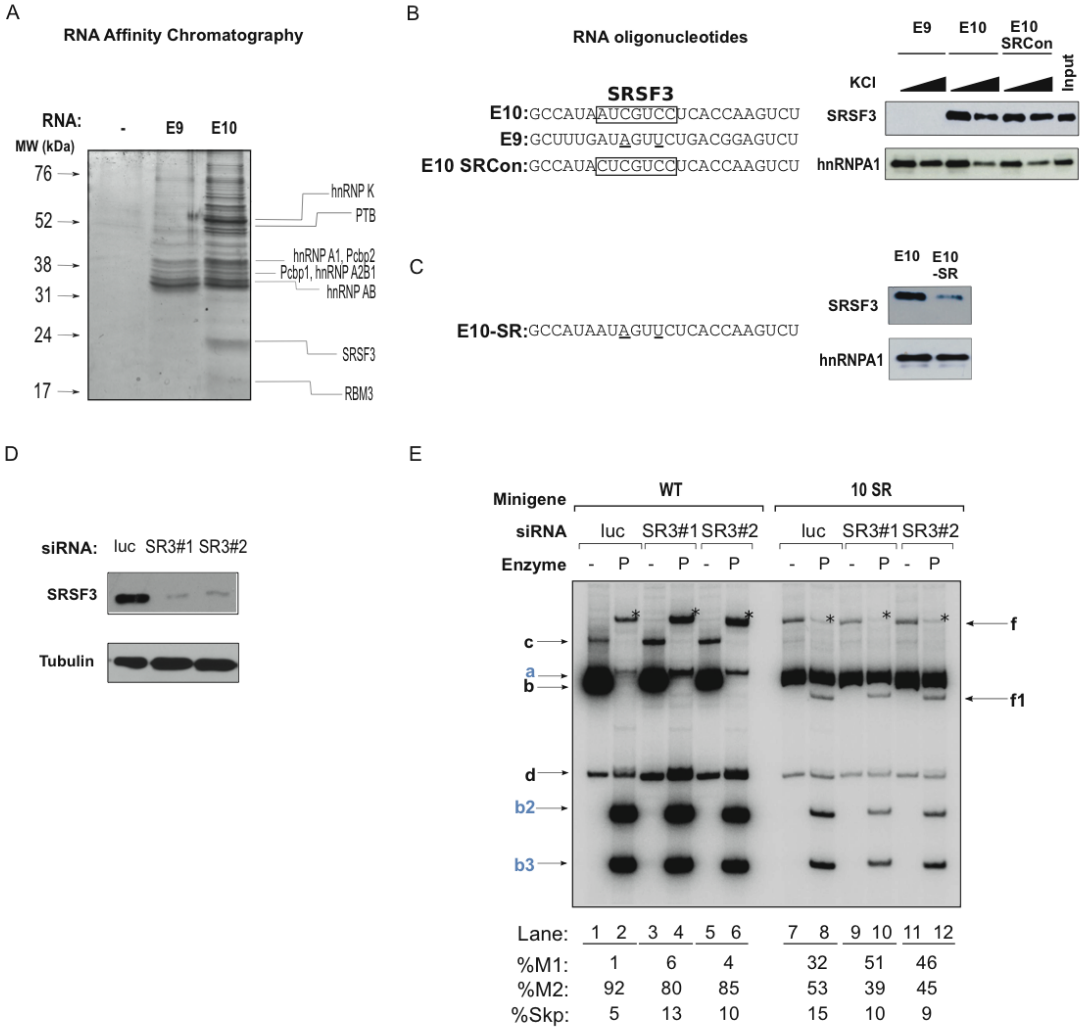
Figure 5
A
RNA Affinity Chromatography
RNA:
-
E9
E10
MW (kDa)
76
52
38
31
24
17
hnRNP K
PTB
hnRNP A1, Pcbp2
Pcbp1, hnRNP A2B1
hnRNP AB
SRSF3
RBM3
B
RNA oligonucleotides
SRSF3
E10:GCCAUAAUCGUCCUCACCAAGUCU
E9:GCUUUGAUAGUUCUGACGGAGUCU
E10 SRCon:GCCAUACUCGUCCUCACCAAGUCU
E9
E10
E10 SRCon
KCl
Input
SRSF3
hnRNPA1
C
E10-SR:GCCAUAAUAGUUCUCACCAAGUCU
E10
E10 -SR
SRSF3
hnRNPA1
D
siRNA:
luc
SR3#1
SR3#2
SRSF3
Tubulin
E
Minigene
WT
10 SR
siRNA
luc
SR3#1
SR3#2
Enzyme
- P - P - P - P - P - P
c
a
b
d
b2
b3
f
f1
Lane: 1 2 3 4 5 6 7 8 9 10 11 12
%M1: 1 6 4 32 51 46
%M2: 92 80 85 53 39 45
%Skp: 5 13 10 15 10 9

2.8.5 Figure 5. SRSF3 binds to the motif in exon 10 and is necessary for exon 10 inclusion

(A) The indicated RNAs covalently linked to agarose beads were incubated with HeLa cell nuclear extract under splicing conditions, and the beads were washed three times with buffer containing 150 mM KCl. Bound proteins were eluted with SDS and analyzed by SDS-PAGE and Coomassie-Blue staining. The mobilities of size markers (M) are indicated. Prominent bands were excised and analyzed by mass spectrometry; the identified proteins are indicated on the right.

(B) (C) Sequences of synthetic RNA oligonucleotides used for affinity pulldowns, and Western-blotting analysis. Descriptive names of RNAs are indicated on the left. The SRSF3 motif are enclosed by rectangles. Underlined nucleotides indicate the differences between the SRSF3 motif and the corresponding sequences in exon 9. Western blots of eluted proteins are shown on the right of each set of sequences. The RNAs used and wash conditions are indicated at the top. Antibodies against SRSF3 and hnRNPA1 were used. HeLa nuclear extract was used as a positive control; hnRNPA1 was used as a loading control, as it binds to these short RNAs to similar extents.

(D) (E) The indicated SRSF3 siRNA or control luciferase siRNA was co-transfected into HEK-293 cells with the wild-type or 10 SR minigene. Knockdown of SRSF3 was verified by immunoblotting, as shown in (D). Minigene-specific transcript-level changes for *PK-M1* and *PK-M2* are shown in (E). siRNAs used are indicated at the top. Labeled bands are as in Fig. 1C. Asterisks indicate PstI-cleaved pre-mRNA. % M1-included, % M2-included, and % double-skipped (% Skp) transcripts are indicated below, with the following s.d.: 0.3% (WT/luc), 1.2% (WT/SR3#1), 1.5% (WT/SR3#2), 5.7% (10SR/luc), 3.5% (10SR/SR3#1),

2.7% (10SR/SR3#2) (n=4). *P*-values (Student's t-test) comparing % M2 from luc siRNA to that from SR3#1 and SR3#2 siRNAs co-transfected with the 10 SR minigene were 0.01 and 0.02, respectively.

Figure 2.8-6

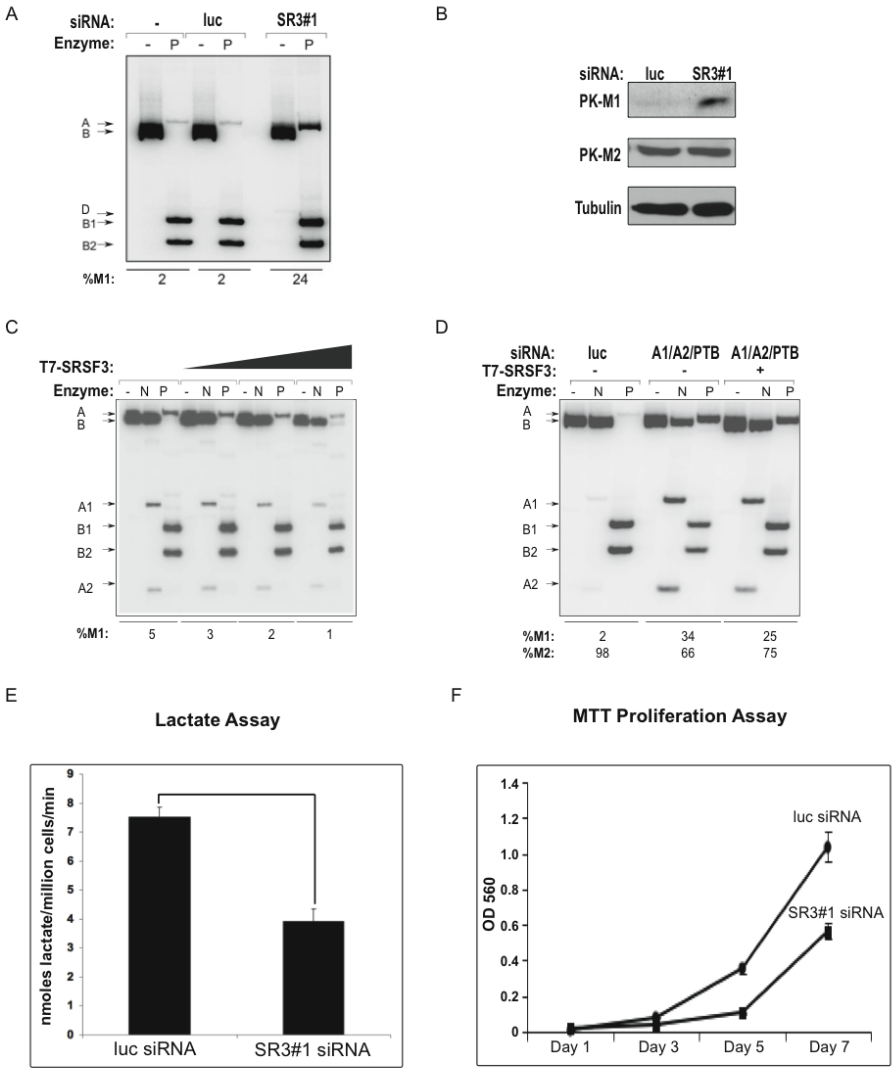
Figure 6
A
siRNA: - luc SR3#1
Enzyme: - P - P - P
A
B
D
B1
B2
%M1: 2 2 24
B
siRNA: luc SR3#1
PK-M1
PK-M2
Tubulin
C
T7-SRSF3:
Enzyme: - N P - N P - N P - N P
A
B
A1
B1
B2
A2
%M1: 5 3 2 1
D
siRNA: luc A1/A2/PTB A1/A2/PTB
T7-SRSF3: - - +
Enzyme: - N P - N P - N P
A
B
A1
B1
B2
A2
%M1: 2 34 25
%M2: 98 66 75
E
Lactate Assay
nmoles lactate/million cells/min
0 1 2 3 4 5 6 7 8 9
luc siRNA
SR3#1 siRNA
F
MTT Proliferation Assay
OD 560
0 0.2 0.4 0.6 0.8 1.0 1.2 1.4
luc siRNA
SR3#1 siRNA
Day 1
Day 3
Day 5
Day 7

2.8.6 Figure 6. SRSF3 affects endogenous levels of PK-M1/M2, aerobic glycolysis, and cellular proliferation

(A) (B) The indicated SRSF3 siRNA or control luciferase siRNA was transfected into HEK-293 cells. (A) shows transcript-level changes for *PK-M1* and *PK-M2*. % M1 is indicated at the bottom, with the following s.d.: ≤ 0.2% (luc); 0.3 % (SRSF3) (n = 3). (B) shows changes at the protein level, as seen in a representative blot.

(C) T7-tagged SRSF3 cDNA was transfected in increasing amounts into A172 cells. Cells were harvested after 48 hr. *PK*-M mRNA level was determined by RT-PCR. s.d. ≤1% in all cases (n=5).

(D) hnRNPA1/A2/PTB siRNAs were co-transfected into HEK-293 cells, followed by transfection of SRSF3 cDNA 24 hr later. Cells were harvested 36 hr after the second transfection. Transcript-level changes are indicated at the bottom, with the following s.d.: 1% (A1/A2/PTB siRNA); 3% (A1/A2/PTB siRNA + SRSF3) (n=5). p-value (Student's t-test) comparing A1/A2/PTB siRNA with A1/A2/PTB+SRSF3 is 0.002.

(E) The indicated SRSF3 siRNA or luciferase siRNA was transfected into HEK-293 cells. Lactate production was measured 48 hr after transfection. Error bars represent s.d.; n = 3. * $P<0.05$ (Student's t-test).

(F) Analysis of cell proliferation by standard MTT Assay. HEK-293 cells were transfected with luciferase or SRSF3 siRNA and plated into 96-wells. Error bars represent the standard error of the mean. Day 1 is the next day after seeding.

Figure 2.8-7

Figure 7

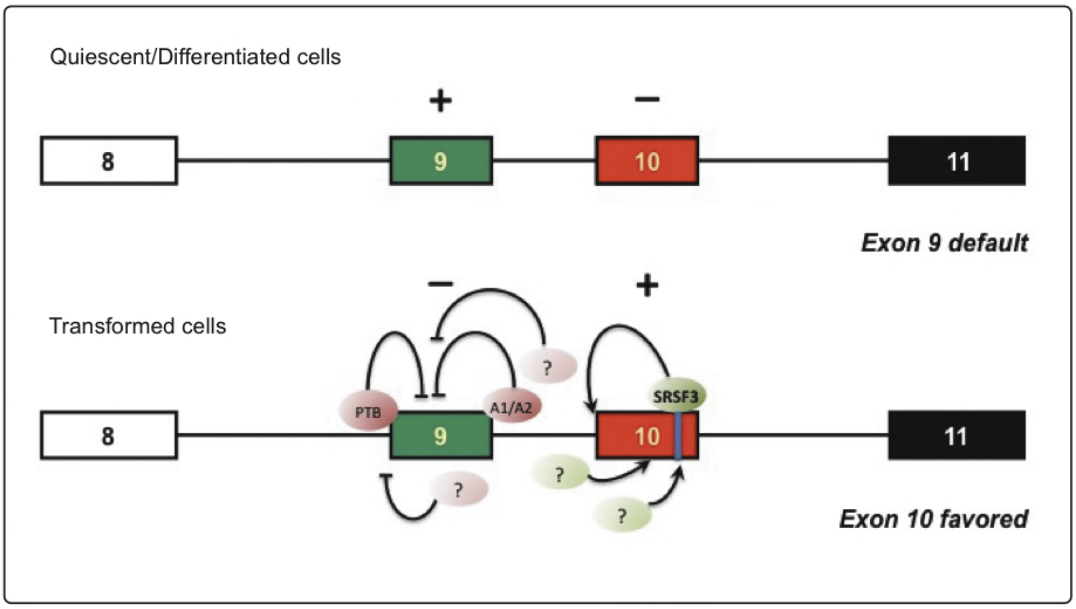

2.8.7 Figure 7. Regulation of *PK-M* splicing in cancer cells

In quiescent or differentiated cells, exon 9 is the default spliced exon. In transformed cells, overexpression of oncogenic splicing factors leads to the simultaneous repression of exon 9 and activation of exon 10. Binding of SRSF3 to the activation motif near the 3' end of exon 10 is proposed to enhance exon definition by facilitating spliceosomal recruitment to the 3'ss of this exon. Additional, unknown activators (green ovals) likely contribute to exon 10 recognition. Upregulated splicing repressors (pink ovals) that presumably act through silencing motifs in exon 9 and introns 8 and 9, including hnRNPA1/A2 and PTB (Clower et al., 2010; David et al., 2010), further reinforce exon 10 selection in transformed cells by repressing exon 9 inclusion. When SRSF3 is less abundant (or when we mutated the SRSF3 activation motif), loss of exon 10 definition occurs, and leads to increased exon 10 skipping. The exon 9 3'ss is then able to compete more effectively for spliceosomal components, leading to an increase in exon 9 inclusion.

Figure 2.8-8

Supplementary Figure 1

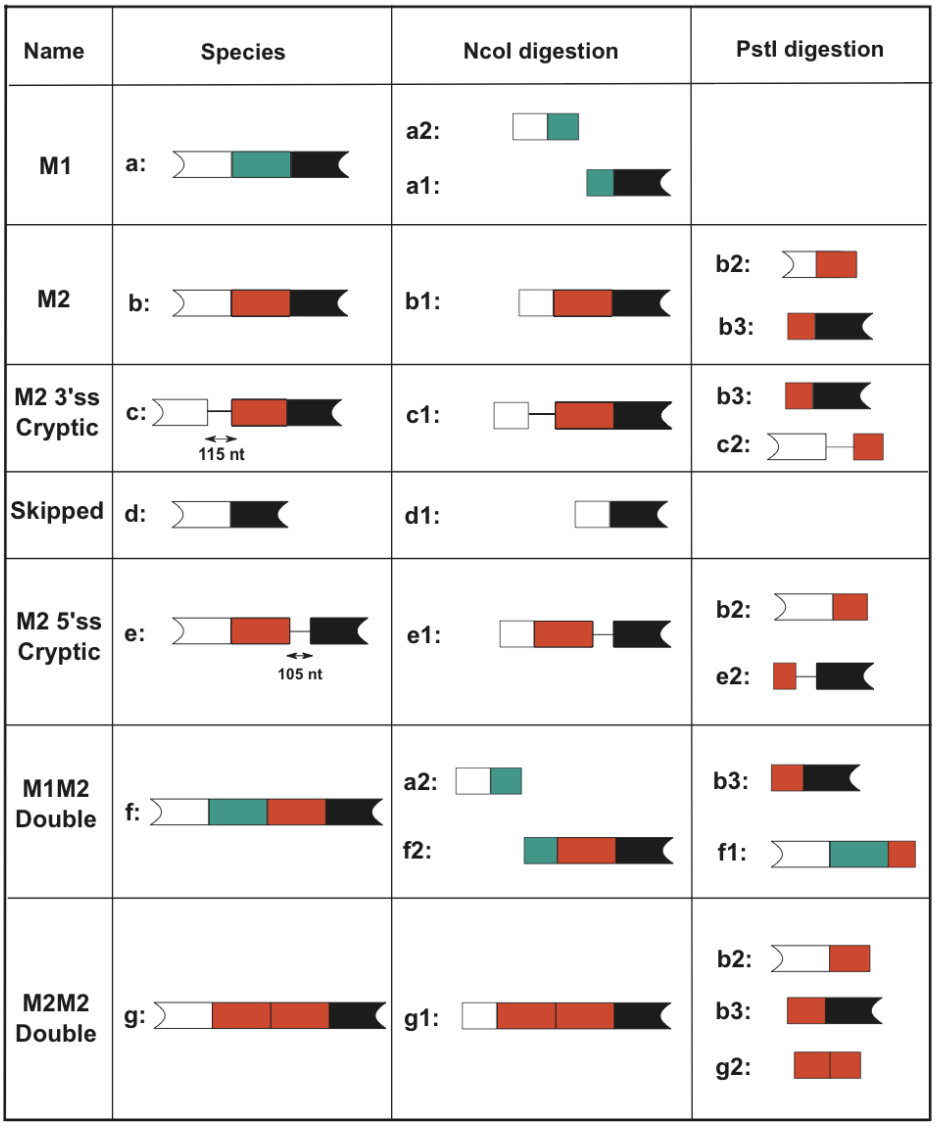

2.8.8 Supplementary Figure 1. Diagram of *PK-M* minigene-specific RNA species in Figs. 1-4.

Names of transcript species are indicated in the first column, and their structures are shown in the second column. Shorthand band designations used in the figures are indicated on the left of each diagram. Boxes filled in white, green, red, and black represent exons 8, 9, 10 and 11, respectively. Lines linking boxes indicate retained intronic sequences, and numbers with arrows below the lines specify their length. Fragments arising from NcoI (third column) or PstI (last column) digestion are given a unique designation (e.g., fragment **g2** from PstI digestion of PCR product from RNA species **g**) if they are not identical to already-named fragments (e.g., fragment **b2** also occurs from PstI digestion of PCR product **g**). Double digestion with NcoI and PstI results in cleavage of band **b2**, as described in the legend to Fig. 1C. All species were cloned and sequenced to confirm their identities.

Figure 2.8-9

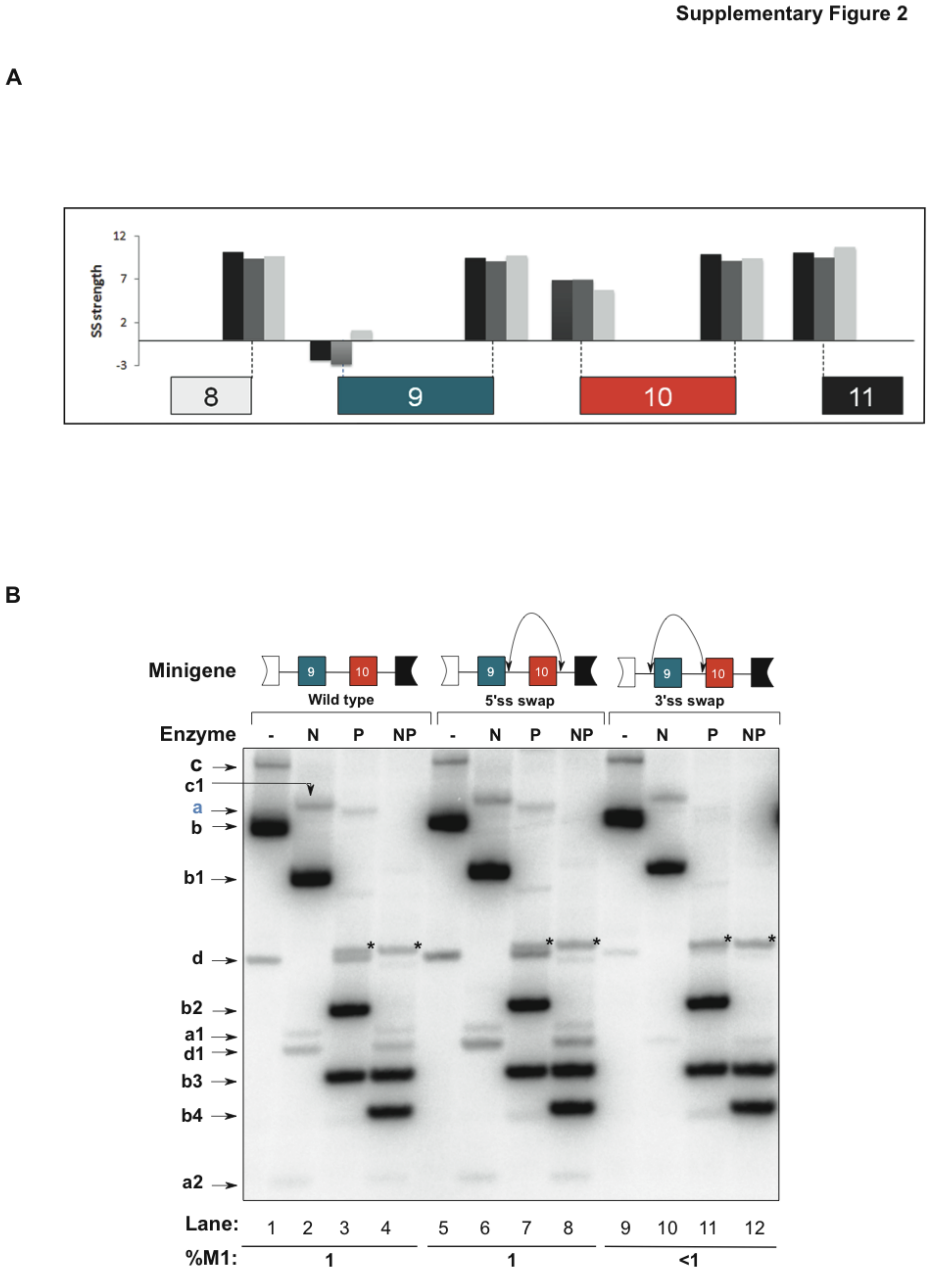
Supplementary Figure 2
A
SS strength
12
7
2
-3
8
9
10
11
B
Minigene
9
10
Wild type
5'ss swap
3'ss swap
Enzyme
- N P NP - N P NP - N P NP
C
c1
a
b
b1
d
b2
a1
d1
b3
b4
a2
Lane: 1 2 3 4 5 6 7 8 9 10 11 12
%M1: 1 1 <1

2.8.9 Supplementary Figure 2. The splice sites of exons 9 and 10 play only a minor role in *PK-M* alternative splicing .

(A) Bioinformatic analysis of *PK-M* splice-site strengths. Normalized 5'- and 3'-splice-site strengths of exons (as indicated by dashed lines) were plotted on the Y-axis using a published method (Yeo and Burge, 2004).

(B) The splicing patterns of *PK-M* minigene splice-site-swap mutants do not differ much from that of the wild-type minigene. 5'ss- and 3'ss-swap mutants are schematically indicated at the top. 9 nt comprising the 5'splice site (3 nt of the exon and 6 nt of the intron) and 12 nt comprising the 3'splice site (2 nt of the exon and 10 nt of the intron) were swapped, respectively. Labeled bands are as in Fig. 1 and Suppl. Fig. 1. The numbers below the panels indicate the percentage of exon-9-included (% M1) transcripts ($n \geq 3$).

Figure 2.8-10

Supplementary Figure 3

A

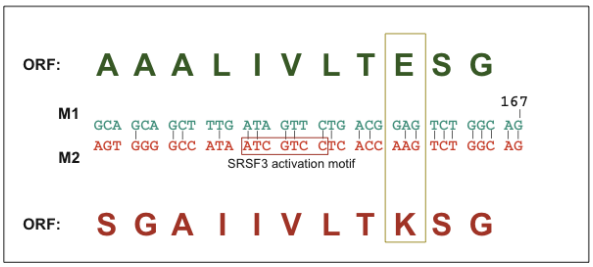

B

Exon 10 alignment

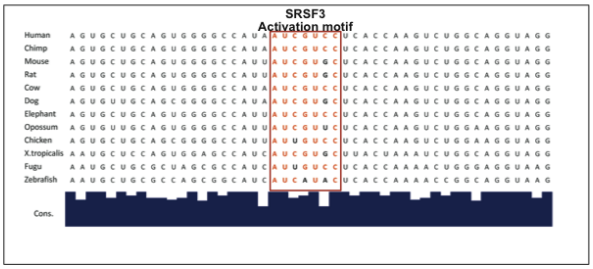

Exon 9 alignment

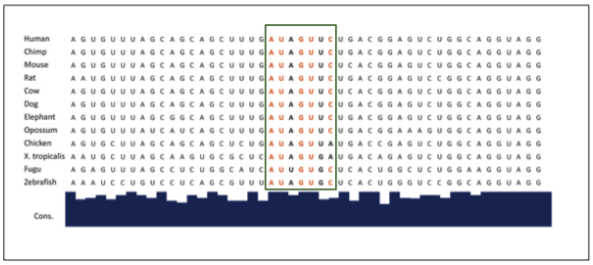

2.8.10 Supplementary Figure 3. Codon and conservation analysis of *PK-M* exons 9 and 10.

(A) Two wobble nucleotides define the exon 10 SRSF3 activation motif. Alignment of *PK-M* exon 9 (top) with exon 10 (bottom) DNA sequences. The SRSF3 activation motif is indicated by the red rectangle. The sequences were grouped into codons to indicate the reading frame. Amino acids coded by the *PK-M1* and *M2* open reading frames are shown at the top and bottom, respectively. The gold rectangle highlights the key phosphotyrosine-binding lysine residue that functionally differentiates the PK-M2 from the PK-M1 isozyme.

(B) Conservation analysis of SRSF3 motif. Alignment of *PK-M* exon 10 (top) and *PK-M* exon 9 (bottom) RNA sequences from different species. The exon 10 alignment shows the SRSF3 motif, indicated with red letters and enclosed by a red box, and partial surrounding sequence. The exon 9 alignment shows the region corresponding to the exon 10 SRSF3 motif, indicated with red letters and enclosed by a green box, and partial surrounding sequence. Bold black letters highlight the nucleotide differences between the SRSF3 motif in exon 10 and the corresponding region in exon 9. The conservation index of each nucleotide is indicated below by the black histogram.

Figure 2.8-11

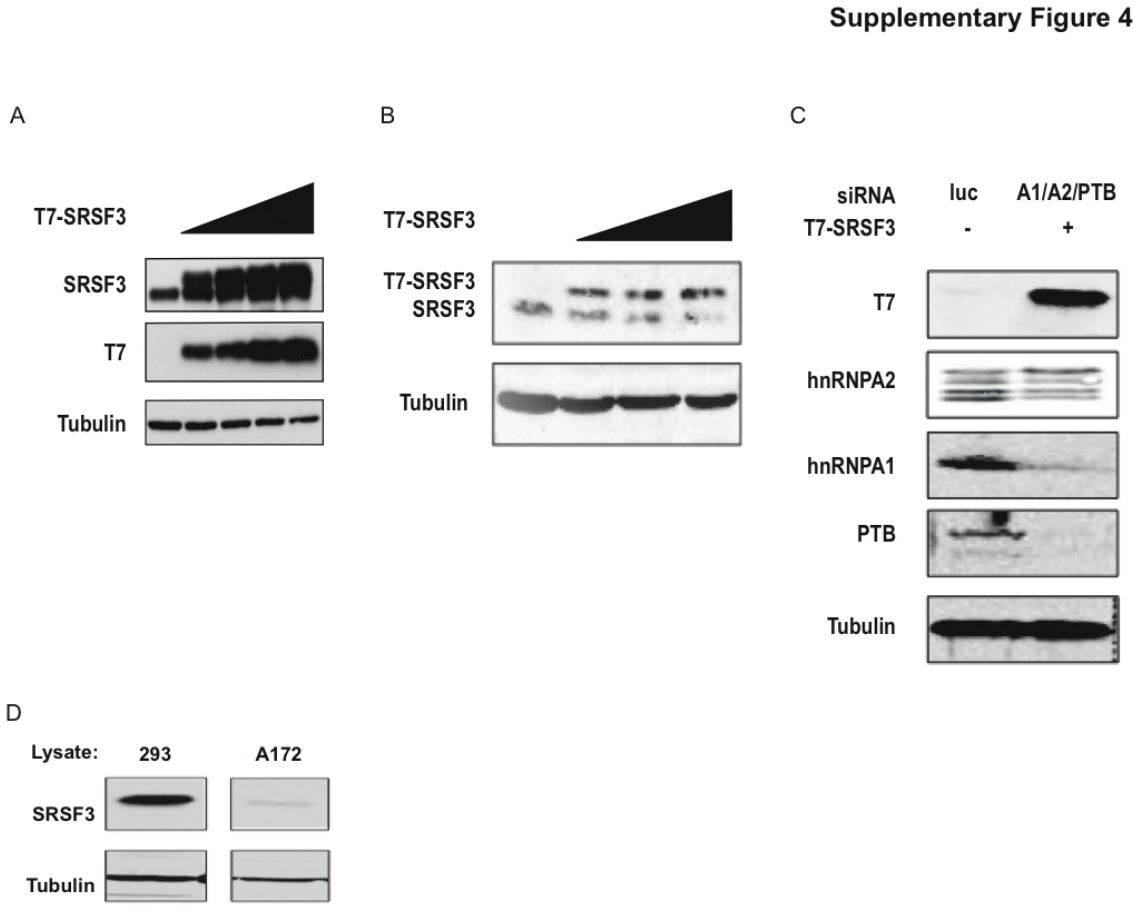
Supplementary Figure 4
A
T7-SRSF3
SRSF3
T7
Tubulin
B
T7-SRSF3
T7-SRSF3
SRSF3
Tubulin
C
siRNA
luc
A1/A2/PTB
T7-SRSF3
-
+
T7
hnRNPA2
hnRNPA1
PTB
Tubulin
D
Lysate:
293
A172
SRSF3
Tubulin

2.8.11 Supplementary Figure 4. Western blots for overexpression and knockdown experiments in Figure 6.

(A,B) Overexpression of SRSF3 in HEK-293 (A) and A172 (B) cells. Cells were transfected with plasmids encoding T7-tagged SRSF3 cDNA (Cáceres et al., 1998) in increasing amounts. Cell lysates were prepared after 48 hr, and overexpression was verified by immunoblotting with monoclonal antibodies against SRSF3 or the T7 tag, and tubulin as a loading control.

(C) Overexpression of SRSF3 combined with triple-knockdown of hnRNPA1/hnRNPA2/PTB in HEK-293 cells. hnRNPA1/A2 /PTB siRNAs and T7-tagged SRSF3 cDNA were co-transfected into HEK-293 cells. Cell lysates were prepared after 72 hr, and knockdown and overexpression were verified by immunoblotting with monoclonal antibodies against the T7 tag (for SRSF3) and hnRNPA1, A2, and PTB, as well as tubulin as a loading control.

(D) SRSF3 protein level was measured by Western blotting of HEK-293 and A172 cell lines.

Figure 2.8-12

Supplementary Figure 5

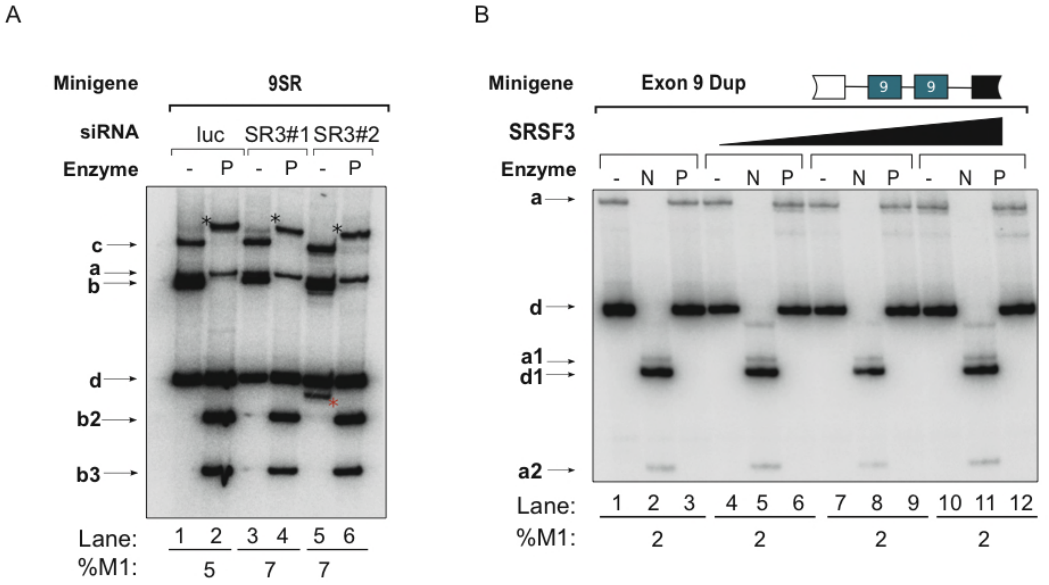

2.8.12 Supplementary Figure 5. SRSF3 does not repress splicing of exon 9.

(A) The indicated SRSF3 siRNA or control luciferase siRNA was co-transfected into HEK-293 cells with the 9 SR minigene. Knockdown of SRSF3 was verified by immunoblotting, as shown in Fig. 5D. Minigene-specific transcript-level changes for *PK-M1* and *PK-M2* are shown. Labeled bands are as in Fig. 1C. Black asterisks indicate PstI-cleaved pre-mRNA. The red asterisk indicates a non-reproducible PCR artifact. % M1-included transcripts are indicated below the gel, with the following s.d: 2% (9S/luc), 1% (9S/SR3#1), 0.5% (9S/SR3#2).

(B) Exon-9 duplication minigenes were co-transfected with increasing amounts of T7-tagged SRSF3 cDNA, as in Suppl. Fig. 4. Green and red boxes represent exons 9 and 10, respectively. A representative gel from a total of 3 replicates is shown. Labeled bands are as described in Fig. 1C and Suppl. Table 4. % M1 is indicated below the gel.

3 CHAPTER 3

Rescue of PK-M Exon 9 inclusion by antisense oligonucleotides targeting PK-M in cancer cells

3.1 Introduction

Cancer cells preferentially use the glycolytic pathway with lactate generation, even in normal oxygen conditions (Vander Heiden et al., 2009). This metabolic feature is termed the Warburg effect. This expression of the type II isoform of the pyruvate-kinase-M gene (*PKM2*, referred to here as *PK-M*) has been shown to mediate the Warburg effect, and facilitate the *in vivo* proliferation of cancer cells (Christofk et al., 2008a).

The *PK-M* gene consists of 12 exons; exons 9 and 10 are alternatively spliced in a mutually exclusive fashion to give rise to M1 and M2 isoforms, respectively (Noguchi et al., 1986). As do other paralogs, pyruvate kinase-M (PK-M) catalyzes the final step in glycolysis to generate pyruvate and ATP from phosphoenolpyruvate (PEP) and ADP (Dombrauckas et al., 2005). Exons 9 and 10 each encode a 56-amino-acid segment that confers distinctive properties to the PK-M isozymes. PK-M1 is constitutively active, whereas PK-M2 is allosterically regulated by fructose-1,6-bisphosphate (FBP) levels and interaction with tyrosine-phosphorylated signaling proteins (Christofk et al., 2008b).

Consistent with the correlation between proliferation and PK-M2 expression, PK-M2 is highly expressed in a broad range of cancer cells, whereas PK-M1 is predominantly expressed in terminally differentiated tissues (Christofk et al., 2008a; Clower et al., 2010). In particular, the mammalian target of rapamycin (mTOR) pathway, which is a central mediator of cellular growth and proliferation, transcriptionally induces PK-M2 expression through its downstream target, the transcription factor hypoxia inducible factor-1α (HIF-1α; (Sun et al., 2011)).

Paradoxically, inhibition of PK-M2 kinase activity is required cancer-cell growth. This decreases carbon flux through the catabolic glycolytic pathway, allowing upstream

intermediates to be shunted to anabolic pathways, facilitating proliferation (Christofk et al., 2008a), and detoxification of reactive oxygen species (ROS; (Anastasiou et al., 2011)). Apart from allosteric regulation, PK-M2 kinase activity can be suppressed in many other ways. These include growth-signaling-mediated inhibition through the binding of phosphorylated tyrosine proteins to its allosteric pocket (Christofk et al., 2008b), direct phosphorylation at Y105 (Hitosugi et al., 2009), acetylation at K305 (Lv et al., 2011), and oxidation at C358 via ROS (Anastasiou et al., 2011). The multitude of avenues leading to PK-M2 inhibition underlies the importance of PK-M2 and glycolysis in tumorigenesis.

PK-M2 has also been demonstrated to have critical functions beyond its kinase activity. In particular, PK-M2 has been shown to translocate into the nucleus and act as a co-activator for HIF-1α (Luo et al., 2011), and β-catenin (Yang et al., 2011) in mediating transactivation of targets important for tumor growth and proliferation. In spite of the importance of PK-M2 in tumorigenesis, little is known regarding the alternative splicing of the PK-M gene that predominantly generates the PK-M2 isoform in cancer cells.

We and others have shown that the exon 9 inclusion that generates the PK-M1 isoform is actively repressed in cancer cells via the well-characterized PTB/nPTB and hnRNPA1/A2 splicing repressors (Clower et al., 2010; David et al., 2010). We have also shown that critical *cis*-elements that mediate the PK-M2 dominant splicing pattern in cancer cells are located in the exons and have found a potent exon 10 ESE that recruits the splicing factor SRSF3 to exon 10 and activates it (Wang et al., 2011).

Because of the importance of PK-M2 as a cancer drug target, and in order to systematically find new splicing elements mediating the PK-M2 dominant splicing patterns, we conducted a systematic antisense oligonucleotide screen targeting endogenous PK-M

exons 9 and 10 to find new splicing *cis*-elements and to discover ASOs that switch the expression of the PK-M2 isoform back to PK-M1 isoform in cancer cells.

Short oligonucleotides were initially used to downregulate mRNA expression by homing to target mRNAs via Watson-Crick base pairing and inducing ribonuclease H mediated-degradation of nucleotide:RNA hybrids (Crooke, 2001). More recently, chemical modification has led to a class of nuclease-resistant ASOs that have high affinity for their RNA targets. A wide range of backbone-modified ASOs with differing chemical properties engineered for different applications include 2′-*O*-methyl phosphorothioate (2OMe) RNA, 2-*O*-methoxyethyl (MOE) RNA, peptide nucleic acid (PNA), locked nucleic acid (LNA) and phosphorodiamidate morpholino (PMO) variants. These ASOs work by direct sequence-specific annealing to target mRNA to either block splicing *cis*-elements, or block ribosome recruitment to inhibit translation (Muntoni and Wood, 2011; Opalinska and Gewirtz, 2002).

Our splicing ASO screen uncovered potent oligonucleotides that increase PK-M1 inclusion in cancer cells. We show that the effective ASOs principally target a new ESE in exon 10, and treatment with these ASOs in a glioblastoma cell line induces apoptosis. We then show that this phenotype is caused by the ASO-mediated downregulated of PK-M2, highlighting the viability and therapeutic potential of PK-M2 as an ASO drug target.

3.2 Results

3.2.1 An exon-centered ASO screen uncovers potent oligonucleotides that increase PK-M1 inclusion in cancer cells

Previously we reported that the critical *cis*-elements involved in the characteristic M2-dominant splicing pattern in proliferating cells are located in exons 9 and 10. To pinpoint the locations of these elements, we performed a systematic antisense oligonucleotide (ASO) walk along the entire length of PK-M exons 9 or 10. These ASOs contain 2′-*O*-methoxy-ethyl ribose (MOE) phosphodiester backbones that allow them to bind to RNA targets with high affinity, while remaining resistant to both endogenous nucleases and the cleavage of resultant RNA:DNA hybrids by RNaseH (McKay et al., 1999; Monia et al., 1993). 48 and 45 overlapping 15-mer ASOs were synthesized in 5-nt steps from 5’ to 3’ and are complementary to exons 10 and 9 respectively. The exon 10 ASOs cover the intron 9 region 96 nt from exon 10, through the entire 167 nt exon 10 and until 42 nt into intron 10 (Fig 1A). Similarly, the 45 overlapping 15-mer Exon 9 ASOs cover the intron 8 region 77 nt from exon 9, through the entire 167 nt exon 9, and end 16 nt downstream of exon 9 (Fig 2A).

To examine the effects of individual ASOs on endogenous PK-M transcripts, we transfected each ASO with Lipofectamine into HEK-293 cells at a final concentration of 30 nM and analyzed the splicing of the PK-M transcripts by radioactive RT-PCR 48 hours after transfection (Fig 1B and 2B). No strong increase in PK-M1 transcripts was observed when exon 9 ASOs were used; instead, some exon 9 ASOs led to an increase in the abundance of the exon 9-exon 10 double-skipped species (Fig 2B; species D), implying that these ASOs were interfering with the recognition of both exons. In contrast, some exon 10 ASOs strongly

increased the proportion of PK-M1 transcripts, with a concurrent increase in the amount of double-skipped species, suggesting that these ASOs were targeting ESEs in exon 10. The two most potent ASOs were the H11 and G7 ASOs. H11 targets the previously characterized exon 10 SRSF3 motif (Wang et. al. 2011) while the G7 ASO targeted a novel 15 nt region in the middle of exon 10. Because of the strong effect of G7 on PK-M splicing, we decided to characterize the G7 ASO and its target 15 nt region (termed as the G7 region).

3.2.2 The G7 ASO targets a novel activation region of PK-M exon 10

To map the enhancer elements present in the G7 region, we took advantage of the high sequence identity between exon 9 and 10, and duplicated the entire exon 10 G7 region into the corresponding region in exon 9 (Fig 3A). We also split the G7 region and duplicated only the first 7-nt subregion (termed the 10F region) and the last 8-nt subregion (termed the 10B region). Duplication of the exon 10 G7 region increased exon 9 inclusion (Fig 3B, lanes 1-4). However, only the duplication of the B7 region, but not the F7 region increased exon 9 inclusion, to an even greater extent than when the entire G7 region was duplicated (Fig 3B, compare lanes 5-6 with lanes 7-8). This suggests that the G7 region is a bona fide exon 10 ESE.

3.2.3 The G7 ASO interferes with exon 10 definition

To characterize the mechanism of action of the G7 ASO, we transfected exon 10 ASOs G7, G6 and an exon 9 ASO, B7, that targets the corresponding G7 region in exon 9, together with the previously characterized PK-M wildtype, exon 9 duplication, and exon 10 minigenes (Fig 3C). The wild-type minigene consists of the portions of the flanking exons 8

and 11 (Fig 3D), and the complete genomic region between both exons, whereas the duplication constructs have exon 10 (Fig 3E) or exon 9 (Fig 3F) entirely duplicated into the native exon 9 or exon 10 location, respectively.

As expected, G7 and G6 ASOs increased %M1 inclusion from the wild-type minigene transcripts (Fig 3D, lanes 3-6). The G7 ASO increased %M1 inclusion to a greater extent than G6, presumably because it completely targets the 10B region as opposed to G6, which targets only part of the region (Fig 3C). In agreement with RT-PCR of endogenous RNA, the exon 9 ASO B7 had no effect on minigene %M1 inclusion (Fig 3D, lanes 7-8).

Co-transfection of the G7 and G6 ASOs with the exon 10 duplication minigene led to a large increase in double-skipped species (Fig 3E, lanes 3-6), strongly suggesting that ASOs that target the G7 region act mainly by interfering with exon 10 activation, allowing spliceosomal components to be recruited to exon 9. However, transfection of G7 and G6 ASOs with the exon 9 duplication minigene also led to a slight increase in PK-M1 inclusion (Fig 3F, lanes 3-6). Since the B7 ASO did not increase PK-M1 inclusion from the exon 9 duplication minigene and instead reduced it (Fig 3F, Lanes 7-8) we ruled out the possibility that the G7/G6 ASOs were binding to the homologous exon 9 region. We hypothesized that there was a second site along the genomic region that could be targeted by G7.

3.2.4 The second binding site for the G7 ASO is located in PK-M intron 9.

Alignment of the G7 region with the PK-M exon 8 – 11 genomic region revealed a highly homologous region in intron 9 (Fig 4A). To interrogate the region for enhancer activity, we performed a supplementary intron 9 walk centered on the G7 homologous region. Nine overlapping ASOs targeting this region were synthesized, and we found that the

intron 9 B12 ASO strongly increased %M1 inclusion. This B12 ASO targeted exactly the G7-homologous region in intron 9, suggesting that this B12 region could also be an exon 10 enhancer element or exon 9 silencing element.

3.2.5 The exon 10 G7 region is more important for ASO-mediated PK-M1 inclusion

Because B12 is nearly identical to the G7 ASO, B12 could potentially also target the exon 10 G7 region (3 mismatches between the B12 and G7 target regions). To weigh the importance of the G7 and B12 regions in the G7 ASO-mediated recovery of endogenous PK-M1 transcripts, we made combinatorial minigene mutations that elminated the G7 or B12 binding sites, and determined the effect of these ASOs on the mutant minigenes. Three mutants were generated (Fig 4C). We mutated the exon 10 G7 region by duplicating the corresponding exon 9 region (termed the 9G7 construct); we made a 15 nt deletion in intron 9 that removed the B12 target region (termed the dB12 construct), and we introduced both mutations in the same minigene (termed the DMGB construct). The 9G7 minigene gave a slight increase in minigene PK-M1 inclusion (Fig 4D, lanes 3-4), suggesting that the duplicated exon 9 region contains enhancer elements, albeit weaker than the elements found in the exon 10 G7 region. There was a slight increase in exon 9-exon 10 doubly-spliced transcripts from dB12, with a decrease in the amount of PK-M1 transcripts (Fig 4D, lanes 5-6), suggesting that this region is involved in repressing the splicing of exon 9 to exon 10, and is not directly involved in the repression of exon 9 per se. Co-transfection of the B12 ASO with the three mingenes revealed that B12-mediated PK-M1 inclusion is largely dependent on the integrity of both the exon 10 G7 region (Fig 4D, lanes 13-18) and its intron 9 own binding site, as removal of both binding sites largely abrogated PK-M1 inclusion (Fig 4D,

lanes 16-18). In contrast, only the loss of the G7 binding site largely abrogated G7-mediated PK-M1 inclusion (Fig 4D, lanes 7-12). When both G7 and B12 binding sites were removed, G7-mediated PK-M1 inclusion was then completely abrogated (Fig 4E). The above results suggest that the G7 ASO largely mediates PK-M1 inclusion through the cognate exon 10 G7 region, though it could exert smaller effects through its supplementary intron 9 B12 binding region.

3.2.6 G7 ESE region centered ASO microwalks

To find the optimal ASO that targets the exon 10 G7 region, we performed an ASO microwalk along both regions (Fig 5A). Overlapping 15-nt ASOs targeting the G7 ESE were synthesized in 1 nt steps in the 5'-3' direction. A total of 20 ASOs were synthesized for the G7 regions (Fig 5A), and transfected into HEK-293 cells at a final concentration of 60 nM. We found that the C7 ASO was the most potent among the candidate microwalk ASOs, in terms of increasing endogenous PK-M1 transcript abundance (Fig 5B). This ASO targeted the B7 region to a similar extent as G7. To objectively compare the performance of ASOs targeting the G7 region and the previously characterized SRSF3 regions, we performed side-by-side ASO transfections at different doses, with final concentrations of 60 and 120 nM. We found that both G7 ASOs was the most potent in eliciting PK-M1 transcript inclusion, compared to the H11 and C7 ASOs (Fig 5C, compare lanes 3-6 with lanes 7-14), with H11 performing slightly better than C7. We also found that the effects of combining two ASOs were not additive (Fig 5C, lanes 15-18). Since targeting the G7 region gave the most %M1 inclusion, we decided to test the G7 or C7 ASOs in other cancer cell lines.

3.2.7 ASOs targeting the exon 10 G7 region induce apoptosis in glioblastoma cells.

Because normal brain tissue mainly expresses PK-M1, while a characteristic splicing switch to PK-M2 occurs during tumorigenesis (Bluemlein et al., 2011; Clower et al., 2010), we decided to focus on glioblastoma cells. In addition, due to mutation of the PTEN tumor suppressor, there is a characteristic overactivation of the mTOR pathway in glioblastoma cells (Verhaak et al., 2010), which makes them susceptible to glucose-withdrawal induced cell death (Choo et al., 2010).Thus, targeting of PK-M2 and by extension, the glycolytic pathway, could potentially be a viable strategy for glioblastoma treatement. Lastly, because there is generally a higher basal level of PK-M1 in glioblastoma cells (Clower et al., 2010), it might be easier to effect an ASO-mediated splicing switch back to the PK-M1 isoform.

We first tested the G7 and C7 ASOs in the PTEN-mutant A172 and U87-MG glioblastoma cell lines, transfecting at final concentrations of 60 nM and 120 nM (Fig. 6A). As expected, there was a dose-dependent increase in PK-M1 inclusion in these cell lines, with G7 ASO performing better than C7 ASO. In addition, there was greater %M1 inclusion in these cells, compared to HEK-293 cells. We also noticed that transfecting these ASOs into both of these cell lines induced apoptosis as early as 24 hours after transfection, even at the relatively lower dose (Fig 6B). Because C7 was less effective at inducing apoptosis, compared to G7, we used this ASO to facilitate the downstream analysis of these cells.

We found that upon transfection of C7 ASO, expression of PK-M2 protein was downregulated, concurrent with the appearance of cleaved PARP as an apoptotic marker (Fig 6B). Apoptosis was only partially rescued upon the addition of the exogenous FLAG-tagged mouse PKM2 cDNA into A172 cells; however, the FLAG signal was also decreased after 48

hours, implying that the C7 ASO might interfere with translation of the mouse PKM2 cDNA, presumably by binding to the completely homologous mouse cDNA region (Fig. 6B).

3.2.8 ASO-mediated apoptosis is caused by the downregulation of endogenous PK-M2 expression in glioblastoma cells.

Upon ASO transfection, there was; 1) an increase in PK-M1 inclusion; 2) an increase in the abundance of double-skipped (Skp) mRNA species; and 3) a decrease in PK-M2 inclusion. We wanted to find out which event was responsible for inducing apoptosis in glioblastoma cells. To do so, we made stable A172 cell lines that express human PK-M1 or human Skp isoform in a doxycyclin(dox)- dependent manner (Fig 6C), or knocked down PK-M2 expression using siRNA, and probed for the appearance of apoptotic markers after 48 hours (Fig 6D). We found that apoptosis was observed upon siRNA transfection, but not upon dox-induction of PK-M1 or Skp isoforms (Fig 6D). This implies that the ASO-mediated apoptosis was due to the downregulation of PK-M2 expression in glioblastoma cells.

3.3 Discussion

We have performed a systematic ASO screen of exons 9 and 10, and have discovered potent ASOs that rescue the inclusion of PK-M1 in cancer cells. We also show that these ASOs are effective in glioblastoma cells, and induce apoptosis upon ASO treatment. Finally, we show that it is the downregulation of PK-M2 expression that causes this apoptosis.

3.3.1 Apoptotic effects of PK-M2 isoform switching in glioblastoma cells

Glioblastomas are known to exhibit a high rate of glycolysis, even in normal oxygen conditions (Clower et al., 2010). Consistent with this phenomenon, the splicing profile of glioblastoma cell lines, as with other cancer cell lines, is PK-M2 dominant. In particular, since the splicing profile of PK-M in normal brain tissue is PK-M1 dominant (Bluemlein et al., 2011), there is a splicing switch from PK-M1 to PK-M2 during gliomagenesis. In addition, because it is known that glioblastoma cells freely take up ASOs *in situ* (Dean et al., 1996), and that minimally-invasive methods of ASO delivery into the central nervous system (CNS) via intrathecal means (Belverud et al., 2008), ASO-mediated PK-M1 rescue could be a viable strategy in the treatment of glioblastoma multiforme.

We observed that ASO treatment led to apoptosis of glioblastoma cell lines. Because PK-M2 is a rate-limiting glycolytic enzyme, targeting PK-M2 might target the entire glycolytic pathway, leading to apoptotic effects as observed by glucose withdrawal in glioblastoma cells *in vitro* (Jelluma et al., 2006). The replacement of PK-M2 in tumor cells with PK-M1 could lead to a shunting of metabolites into the mitochondria (Christofk et al., 2008b), phenocopying the apoptotic phenotype that is displayed by glioblastoma cells after treatment

with dichloroacetic acid (DCA), as a result of increased ROS production (Bonnet et al., 2007; Michelakis et al., 2010). Lastly, because PK-M2 also functions as a co-activator of HIF-1 (Luo et al., 2011) and β-catenin (Yang et al., 2011) transactivation, targeting the expression level of PK-M2, as opposed to inhibiting its kinase function, might also interfere with anti-apoptotic (Sendoel et al., 2010) and pro-proliferative functions mediated by these factors.

3.3.2 Translational inhibition of PK-M2 mRNA

We observed that restoring the level of PK-M2 in ASO-treated cells by exogenous addition of mouse PK-M2 cDNA was not sufficient to fully rescue the observed apoptotic phenotype. This is due to an ASO-dependent decrease in the amount of protein expressed from the mouse cDNA. This is a favorable outcome of ASO treatment, in that residual PK-M2 transcripts are translationally inhibited by the ASO, leading to a reinforcement of the PK-M2 to PK-M1 splicing switch at the protein level. As ASOs are also known to bind to mRNA and interfere with the recruitment of the translational machinery (Muntoni and Wood, 2011), further work must be done to confirm the apparent ASO-mediated translational inhibition of PK-M2 mRNA.

3.3.3 Mechanism of ASO-mediated PK-M2 to PK-M1 switch

How does blocking the activation of the exon 10 G7 region lead to an activation of PK-M exon 9? Although this could be explained in terms of 3'ss competition, in which the loss of exon 10 definition leads to increased recognition of the exon 9 3'ss by the splicing

machinery, it is not known at present which splicing factor(s) bind to this G7 ESE. Because ASOs targeting G7 also lead to inhibition of translation, the splicing factor binding to this region could be part of a RNP e involved in downstream post-splicing processes, such as mRNA transport, translation and stability.

3.3.4 Failure of exon 9 ASOs to rescue PK-M1 inclusion

Because we have demonstrated that exon 9 is enriched in ESS elements in the context of cancer cells, it was surprising that not one exon 9 ASO tested could rescue PK-M1 inclusion, as some ASOs were expected to block an ESS and facilitate the recognition of exon 9 by the splicing machinery. We speculate that ASO binding to the putative ESS could interfere with the second splicing step, i.e the ligation of exon 8 and exon 9, leading to the use of the alternate exon 11 3'ss and resulting in the observed increase in abundance of double-skipped RNA species. Another possibility is that distal regions (i.e, sequences that are outside of the ASO screening region) could be involved in exon 9 silencing, which would not have been revealed in the previous exon-duplication and swap experiments (Wang et al., 2011).

3.3.5 Use of ASOs in mouse models of glioblastoma

Because the ASOs we have screened are potent enough to switch the PK-M splicing profile of glioblastoma cells from PK-M1 to PK-M2 *in vitro*, the next step to demonstrate the therapeutic potential of these ASOs will be to test these ASOs in the context of allogenic xenograft or orthotopic models of glioblastoma.

3.4 Experimental Procedures

3.4.1 Cells and transfections

HEK-293, U87-MG and A172 cells were obtained from ATCC and grown in DMEM, supplemented with 10% (v/v) FBS, penicillin and streptomycin, at 37 °C and 5% CO_2. 5 μg of minigene plasmid per 10-cm dish, or 1 μg per 6-cm dish, was transiently transfected using Lipofectamine 2000 (Invitrogen). For ASO transfections, $4x10^6$ cells were first plated, and then ASO transfections were performed using a ASO:Lipofectamine 2000 ratio of 25 pmol:1 μl. Total RNA and protein from transfected cells was harvested after 48 hr. For doxycyline induction, doxycyline was added to the media at a final concentration of 100 ng/ml for 3 days before harvest.

3.4.2 Oligonucleotide synthesis

Synthesis and purification of chimeric 2′-*O*-methoxyethyl–modified oligonucleotides with a phosphodiester backbone were performed at ISIS Pharmaceuticals using an Applied Biosystems 380B automated DNA synthesizer (Applied Biosystems, Foster City, California, United States) as described previously (Hua et. al. 2011). The oligonucleotides were dissolved in water.

3.4.3 RNA interference

4 siRNAs targeting exon 10 of human *PKM2* were obtained from Sigma Genosys, and have the sense-strand sequences 5’-CCAUAAUCGUCCGCACCAA-3’ (M2si1), 5’-

CAUCUACCACUUGCAAUUA-3' (M2si2), 5'-CCGUGGAGGCCUCCUUCAA-3' (M2si3) and 5'CUUGCAAUUAUUUGAGGAA-3' (M2si4). $4x10^6$ A172 cells in 6-well plates were transfected with 400 pmol of siRNA duplex using Lipofectamine 2000 (Invitrogen). Cells were harvested 48 hr later.

3.4.4 Retrovirus transduction

To generate FLAG-tagged mPKM1 or mPKM2 overexpressing transductants, A172 cells were infected with pLHCX-mPKM1 or mPKM2 retrovirus (Christofk et al) and selected in 300 μg/ml of hygromycin for 2 weeks. To generate tet-on cell lines that overexpress human PKM1 (A) or human Skp (D) isoforms in a doxycylin-dependent manner, A172 cells were first infected with MSCV-rtTA-hygro virus, and selected in hygromycin for 2 weeks. Human PKM1 and Skp cDNA were amplified from A172 cells transfected with C7 ASO using the following primer pair hPKT7cDNAF (5'-GGGGAACTCGAGATGGCTTCTAGGATGGCATCGATGACAGGTGGCCAACAGATGGGCATGTCGAAGCCCCATAGTGAAGCCG-3') and hPKT7cDNAR (5'-GGGGAAGAATTCTCACGGCACAGGAACAACACGCATG-3') with Phusion High-Fidelity DNA Polymerase (Finnzymes). The resultant amplicons containing the T7 tag were then gel-purified and cloned between the EcoRI and XhoI sites of the retroviral TtiGP plasmid. Plasmids were sequenced to confirm their identities. A172-rTT cells were then infected with TtiGP-PKM1 or TtiGP-Skp virus and selected with 100 μg/ml of puromycin for 3 days.

3.4.5 Immunoblotting

Cells were lysed in SDS, and total protein concentration was measured by the Bradford assay. 30 μg of total protein was separated by SDS-PAGE and transferred onto nitrocellulose, followed by blocking with 5% (w/v) milk in Tris-buffered saline with Tween-20, probing with the indicated antibodies, and visualization by enhanced chemiluminescence (Roche). Primary antibodies were: β-tubulin (Genscript rAb, 1:5000); PK-M2 (Cell Signalling Technology, rAb, 1:2000); PARP (Cell Signalling Technology, rAb 1:1000); FLAG (Sigma, mAb 1:5000) and PK-M1 (rabbit, 1:2000 (Christofk et al., 2008b)). Secondary antibodies were goat anti-mouse or anti-rabbit HRP conjugates, 1:20,000 (Bio-Rad).

3.4.6 Minigene construction

DNA oligonucleotides were obtained from Sigma Genosys. The *PK-M2* minigene was constructed by amplifying a 6.4-kb *PK-M* exon 8-11 fragment from human genomic DNA (Promega) using Phusion High-Fidelity DNA Polymerase (Finnzymes) and primers PKMinigeneF (5'-GGGGAAGATATCAATTCCCCATTCTGTCTTCCCATGT-3') and PKMinigeneR (5'-GGGGAACTCGAGCTAGACATTCATGGCAAAGTTCACC-3'). The product was then digested and cloned between the BamHI and XhoI sites of pcDNA3.1+ (Invitrogen). For exon duplication and intron deletion constructs, the upstream KpnI site 1552 nt downstream of exon 8 was removed by a 1-nt deletion, and an EcoRV restriction site was generated 90 nt upstream of exon 9 by a 2-nt insertion to create a modified wild-type minigene. To generate the 10G7, 10B7 and 1010F7 constructs, modified Exon 9 fragments

were generated by annealing the following oliognucleotides 10G7F (5'-CCCTAAACCTTACAGATAGCTCGTGAGGCTGAGGCAGCCATGTTCCACCGCAAGCTGTTTGAGGAACTCCGCCGAGCCTCAAGTCACTCCACAGACCTCATGGAAGCCAT-3'), 10F7F (5'-CCCTAAACCTTACAGATAGCTCGTGAGGCTGAGGCAGCCATGTTCCACCGCAAGCTGTTTGAGGAACTTGTGCGAGCCTCAAGTCACTCCACAGACCTCATGGAAGCCAT-3'), 10B7F (5'-CCCTAAACCTTACAGATAGCTCGTGAGGCTGAGGCAGCCATGTTCCACCGCAAGCTGTTTGAAGAACTCCGCCGAGCCTCAAGTCACTCCACAGACCTCATGGAAGCCAT-3') with Exon 9Rev oligo (5'-CCCTTAGGGCCCTACCTGCCAGACTCCGTCAGAACTATCAAAGCTGCTGCTAAACACTTATAAGAAGCCTCCACGCTGCCCATGGCC ATGGCTTCCATGAGGTCTG -3') and amplifying using Ex10ADupF (5'-TTCCCCATTCTGTCTTCCCATGTGTTGTGTCTCGTTTTTTTCCTCCTCCTTCCCTCTTCCTTGCCCCCTCTTCCCCTAAACCTTACAG-3') and Ex10ADupR (5'-AGTGTTACCTGCCCTTAGGGCCCTAC-3'). The 106-nt oligonucleotide carries mutations that duplicate specific stretches of exon 10 over the corresponding region of exon 9. Another fragment was amplified from the wild-type minigene using the following primer pairs: Ex10BF: 5'-GTAGGGCCCTAAGGGCAGGTAACAC-3' and RKpnI (5'-GGGGAAGGTACCACTGAGCAGGGCATT-3'). Both fragments were then gel-purified, and subjected to a second OE PCR reaction using the end primers FEcoRV (5'-GGGGAAGATATCAATTCCCCATTCTGTCTTCCCATGT-3') and RKpnI.

To generate the 9G7 minigene construct, a modified exon 10 fragment was constructed by annealing 9G7F (5'-ATGTTGCTCCCCTAGATTGCCCGTGAGGCAGAGGCTGCCATCTACCACTTGCAATTATTTGAAGAACTTGTGCGCCTGGCGCCCATTACCAGCGACCCCACAGAAGCCAC-3') with Exon 9 Rev (5'-CGCTGCCGCCTCCTACCTGCCAGACTTGGTGAGGACGATTATGGCCCCACTGCAGCACTTGAAGGAGGCCTCCACGGCACCCACGGCG GTGGCTTCTGTGGGGTCGCT-3;) and amplifying using Ex9ADupF (5'-TGGACGGATGTTGCTCCCCTAG-3') and Ex9ADupR (5'-GGTACCACTGAGCAGGGCATTCCAGGGAGCCGCTGCCGCCTCCTAC-3'). The 108-nt oligonucleotide carries mutations that duplicate specific stretches of exon 9 over the corresponding region in exon 10. Another fragment was amplified from the wild-type minigene using the following primer pairs: FEcoRV and Ex9BR (5'-GTAGGGCCCTAAGGGCAGGTAACAC-3'). Both fragments were then gel-purified and subjected to a second OE PCR reaction using the FEcoRV and RKpnI primers.

To generate the dB12 mutant, two fragments were generated from the wildtype minigene construct, using the following primer pairs: FEcoRV and PKMdelB12R (5' TGCCCTGCCATGACCTCCCAGACGAGAAGAGGCTCTGTGCCCAG-3') and PKMdelB125 (5'- ACA GAG CCT CTT CTC GTC T GG GAG GTC ATG GCAGGGCAG-3'). To generate the DMGB double mutant, the same two fragments were generated from the 9G7 minigene. Both fragments were then gel purified and subjected to a second OE PCR using FEcoRV and RKpnI. All generated fragments were then cloned between the EcoRV and KpnI sites of the modified wild-type minigene plasmid.

3.4.7 RT-PCR

2-5 μg of total RNA was extracted from cell lines using Trizol (Invitrogen). Contaminating DNA was removed with DNAase I (Promega). Reverse transcription was carried out using ImPromp-II reverse transcriptase (Promega). Semiquantitative PCR using Amplitaq polymerase (Applied Biosystems) was performed by including [α-^{32}P]-dCTP in the reactions. The human-specific primer sets used to amplify endogenous transcripts anneal to *PK-M* exons 8 and 11, and their sequences are: hPKMF: 5'-AGAAACAGCCAAAGGGGACT-3'; hPKMR: 5'-CATTCATGGCAAAGTTCACC-3'. To amplify minigene-specific transcripts, the forward primer was replaced with a primer annealing to the pcDNA3.1(+) vector, pcDNAF: 5'-TAATACGACTCACTATAGGG-3'. After 28 amplification cycles for minigene-derived transcripts, and 27 cycles for endogenous transcripts, the reactions were divided into two aliquots for digestion with PstI (New England Biolabs) or undigested control. The products were analyzed on a 5% native polyacrylamide gel, visualized by autoradiography, and quantified on a FLA-5100 phosphoimager (Fuji Medical Systems) using Multi Gauge software Version 2.3. The % M1 mRNA in endogenous transcripts was calculated using the GC-content-normalized intensities of the top undigested band (M1, A), the bottom two digested bands (M2, B1 B2) in the PstI-digest lanes and the double skipped species (D), if detectable. The % M1 mRNA from minigene-transcripts was calculated using the GC-content-normalized intensities of the top undigested band (**a,** M1) and other higher-mobility digested bands corresponding to M2 and its variant species (**b – g**, as described above) in the PstI-digest lanes. All the PCR products were gel-

purified, cloned, and sequenced to verify their identities.

3.5 Figure Legends

Figure 3.5-1

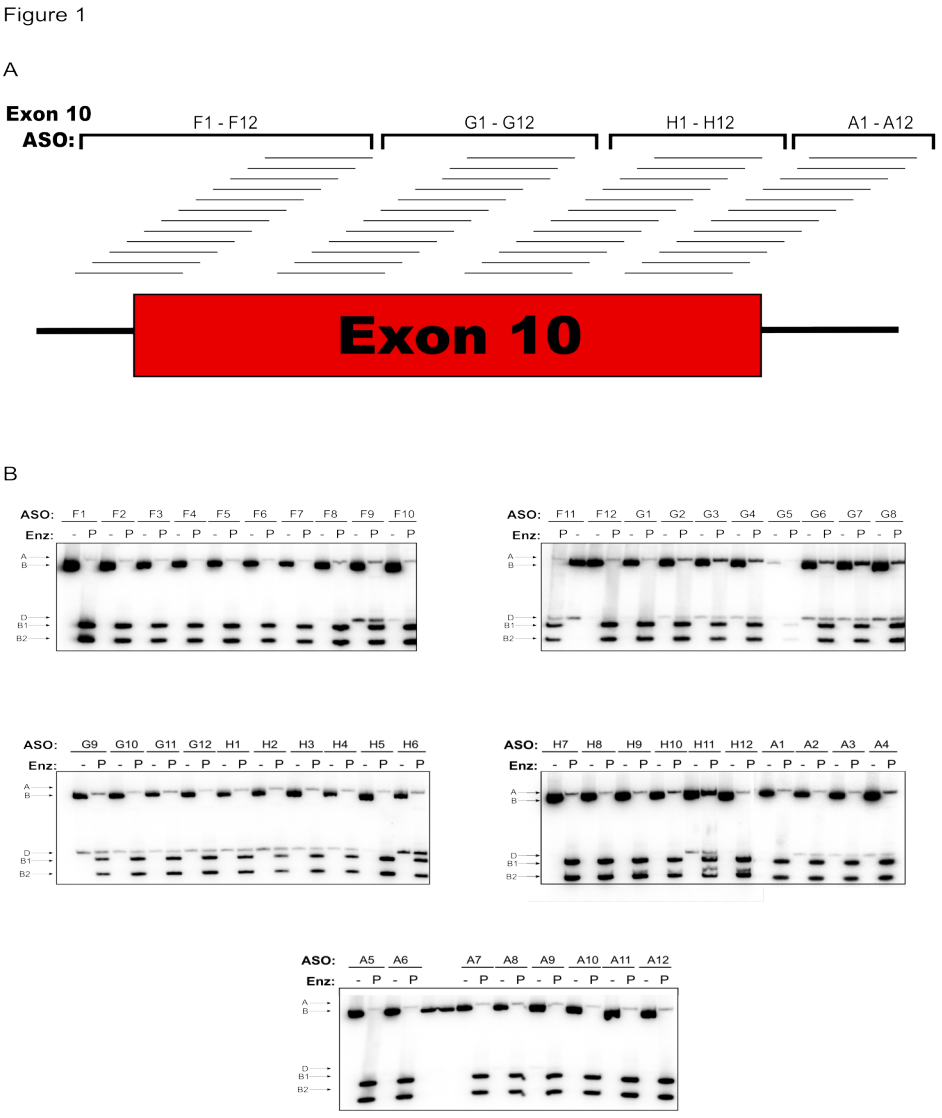

3.5.1 Fig 1. Initial ASO walk along PK-M exon 10.

(A) Schematic representation of the initial ASO walk along exon 10 and flanking regions. Exon 10 is indicated by the red box, while flanking regions (~100 bp of introns 8 and 9) are represented by the thick line. Stacked thin lines above the box represent an individual ASO. Names of the ASOs are indicated at the top of each stack, from bottom to top. Their approximate binding sites are aligned with the exon 10/intron 8/intron 9 diagrams. **(B)** Radioactive RT-PCR and restriction digests of endogenous *PK-M* transcripts in HEK-293 cells (as in Clower et. al. 2009) after ASO transfection at a final concentration of 30 nM. RNA was harvested from cells 48 hours after transfection. The identity of the transfected ASO is indicated at the top. cDNAs and fragements from endogenous mRNAs are indicated on the left. Because PK-M2 is sensitive to PstI digestion (indicated as "P"), the uncut 398 nt A fragment corresponds to full-length PK-M1. B1 (213 nt) and B2 (185 nt) are 3' and 5' PstI digested fragments of the full-length PK-M2 B (398 nt). D (271 nt) is a PstI resistant cDNA that lacks both exons 9 or 10. Both ASO G7 and H11 show the highest amount of M1 inclusion upon transfection.

Figure 3.5-2

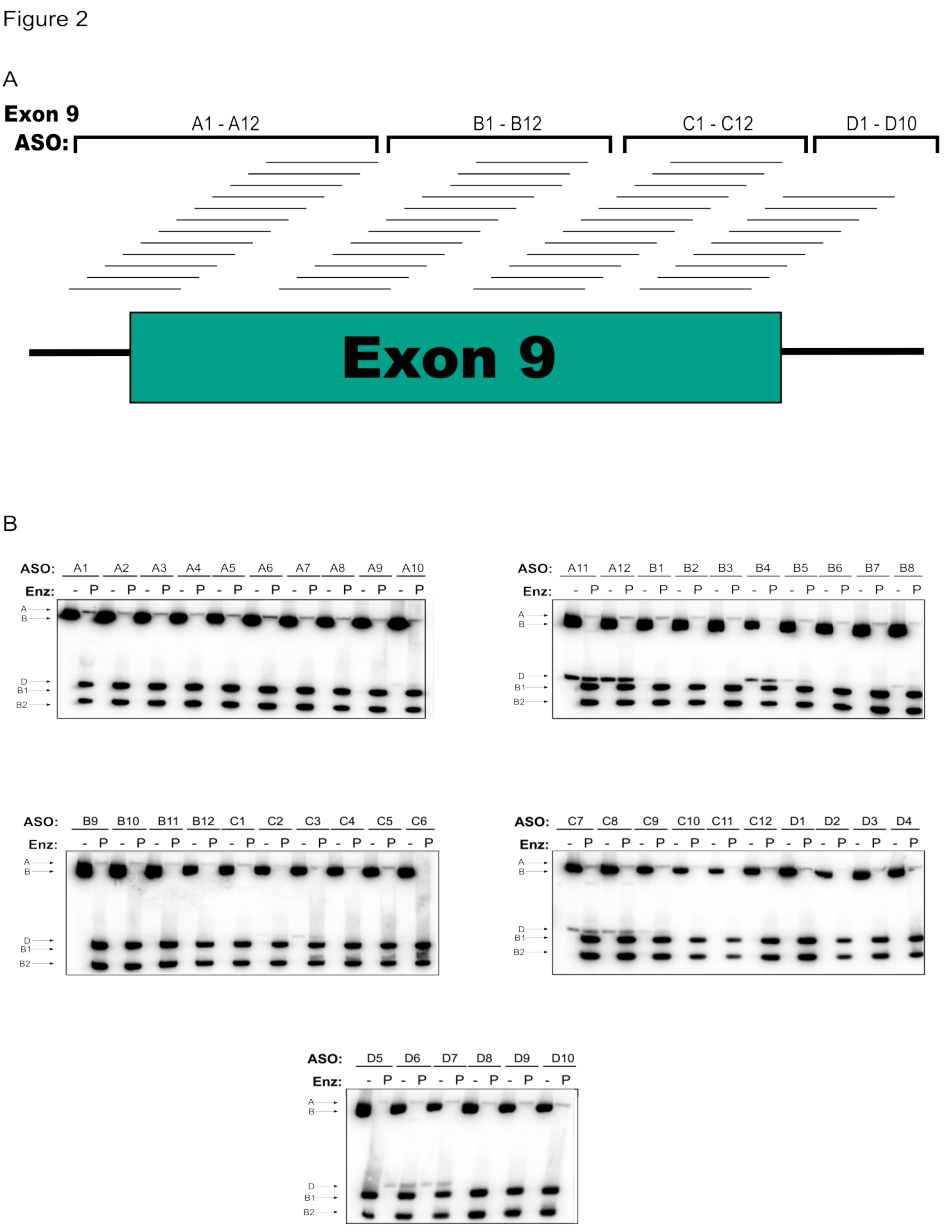
Figure 2
A
Exon 9
ASO:
A1 - A12
B1 - B12
C1 - C12
D1 - D10
Exon 9
B
ASO: A1 A2 A3 A4 A5 A6 A7 A8 A9 A10
Enz: - P - P - P - P - P - P - P - P - P - P
A
B
D
B1
B2
ASO: A11 A12 B1 B2 B3 B4 B5 B6 B7 B8
Enz: - P - P - P - P - P - P - P - P - P - P
ASO: B9 B10 B11 B12 C1 C2 C3 C4 C5 C6
Enz: - P - P - P - P - P - P - P - P - P - P
ASO: C7 C8 C9 C10 C11 C12 D1 D2 D3 D4
Enz: - P - P - P - P - P - P - P - P - P - P
ASO: D5 D6 D7 D8 D9 D10
Enz: - P - P - P - P - P - P

3.5.2 Fig 2. Initial ASO walk along PK-M exon 9.

(A) Schematic representation of the initial ASO walk along exon 9 and flanking regions. Exon 9 and its flanking regions (~100 bp of introns 9 and 10) is indicated by the green box and thick line, respectively. Stacked thin lines above the box represent an individual ASO. Names of the ASOs are indicated at the top of each stack, from bottom to top. Their approximate binding sites are aligned with the exon 9/intron 9/intron 10 diagrams. **(B)** Radioactive RT-PCR and restriction digest of endogenous *PK-M* transcripts in HEK-293 cells after ASO transfection at a final concentration of 30 nM. RNA was harvested from cells 48 hours after transfection. The identity of the transfected ASO is indicated at the top. cDNAs and fragments from endogenous mRNAs are indicated on the left.

Figure 3.5-3

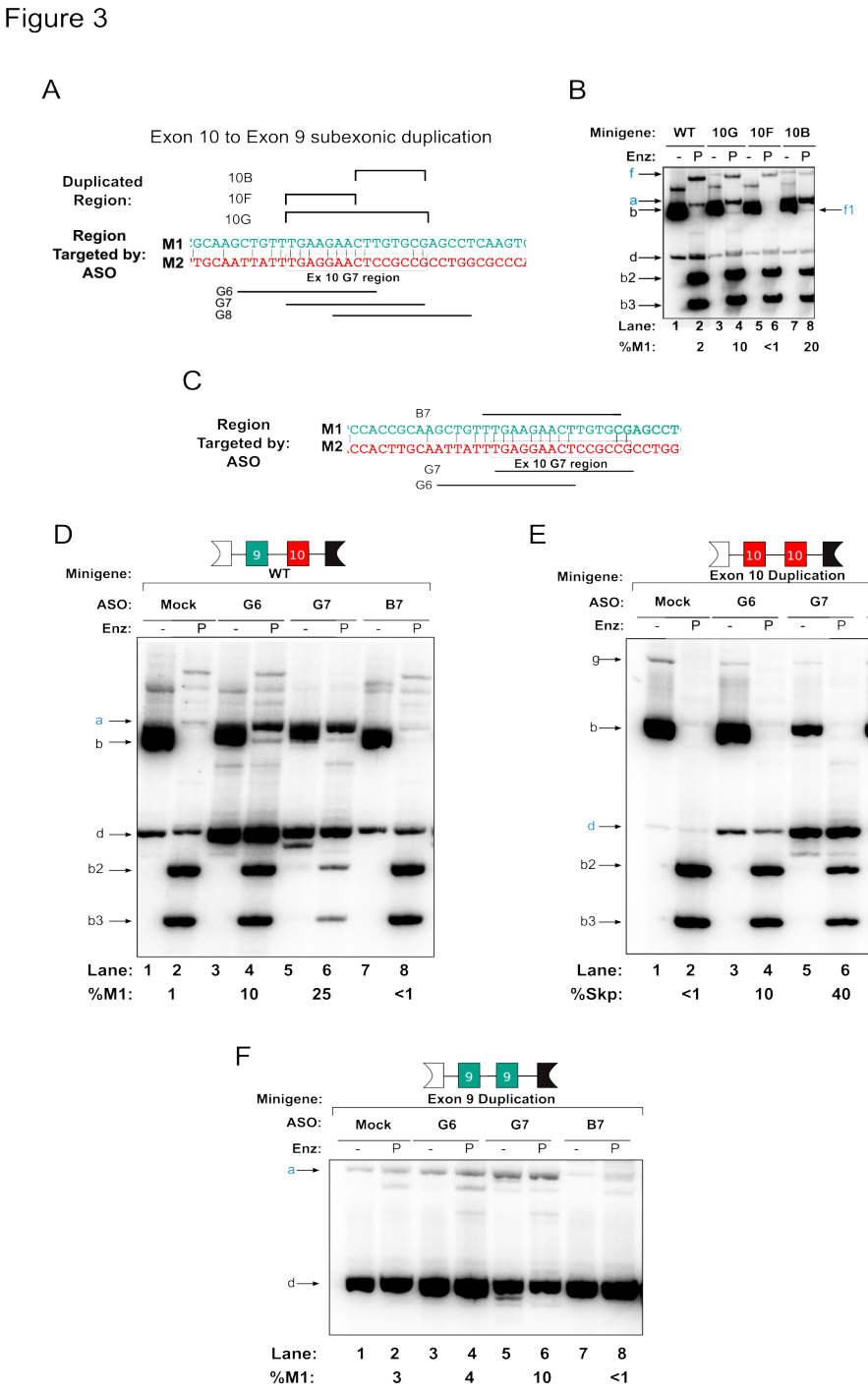
Figure 3
A
Exon 10 to Exon 9 subexonic duplication
Duplicated Region:
10B
10F
10G
Region Targeted by: ASO
M1
M2
Ex 10 G7 region
G6
G7
G8
B
Minigene: WT 10G 10F 10B
Enz: - P - P - P - P
f
a
b
f1
d
b2
b3
Lane: 1 2 3 4 5 6 7 8
%M1: 2 10 <1 20
C
Region Targeted by: ASO
B7
M1
M2
Ex 10 G7 region
G7
G6
D
Minigene: WT
ASO: Mock G6 G7 B7
Enz: - P - P - P - P
a
b
d
b2
b3
Lane: 1 2 3 4 5 6 7 8
%M1: 1 10 25 <1
E
Minigene: Exon 10 Duplication
ASO: Mock G6 G7 B7
Enz: - P - P - P - P
g
b
d
b2
b3
Lane: 1 2 3 4 5 6 7 8
%Skp: <1 10 40 <1
F
Minigene: Exon 9 Duplication
ASO: Mock G6 G7 B7
Enz: - P - P - P - P
a
d
Lane: 1 2 3 4 5 6 7 8
%M1: 3 4 10 <1

3.5.3 Fig 3. Characterizing the G7 ASO target region.

(A) Schematic of method used to duplicate the exon 10 G7 region. The indicated exon 9 (green) nucleotides at the top were mutated to the corresponding exon 10 (red) sequences. The 10G minigene duplicates the entire G7 region into exon 9, the 10F minigene duplicates the first 8 nt, and the 10B minigene duplicates the last 7 nt of G7. The ASOs that target G7 and flanking regions are indicated below. **(B)** The G7 motif is an exon 10 ESE. Mutant minigenes were analyzed by transient transfection into HEK-293 cells, followed by radioactive RT-PCR and restriction digests, as in Fig. 1. To amplify minigene transcripts, a primer annealing to a vector-specific sequence, pcDNAF, was used, as in Wang et. al. 2011. Constructs from (A) are labeled at the top. Labeled bands are indicated in lower case on the left and right, with important bands in blue font. %M1 is indicated at the bottom. Bands are as follows: uncut M1 fragment (**a**, 481 nt); uncut M2 fragment (**b**, 481 nt); PstI-cleaved M2 5' fragment (**b2**, 268 nt); PstI-cleaved M2 3' fragment (**b3,** 213 nt); spliced mRNA that skips both exons 9 and 10 (**d**, 314 nt); an exon 9 – exon 10 doubly-included mRNA are indicated on the left (**f**, 648 nt). This band is sensitive to PstI (**f1**, 435 nt) **(C)** Schematic of ASOs and their binding sites used for minigene experiments in (D). G6 and G7 ASOs target exon 10 and are indicated at the bottom. The B7 ASO indicated at the top targets the exon 9 region that corresponds to exon 10 G7. **(D),(E),(F)** Minigene transcript level changes as a result of ASO co-transfection in HEK-293 cells. ASOs were transfected at a final concentration of 30 nM. The wild-type (D), exon 10 (E) duplication, and exon 9 (F) duplication (Wang et. al. 2011) minigenes, together with the identity of ASOs, are indicated at the top. Labeled bands are indicated in lower case on the left, with important bands in blue font. %M1 is indicated at

the bottom. The exon 10 – exon 10 doubly-included mRNA in (E) expressed from the exon 10 Dup minigene is indicated on the left (**g**, 648 nt).

Figure 3.5-4

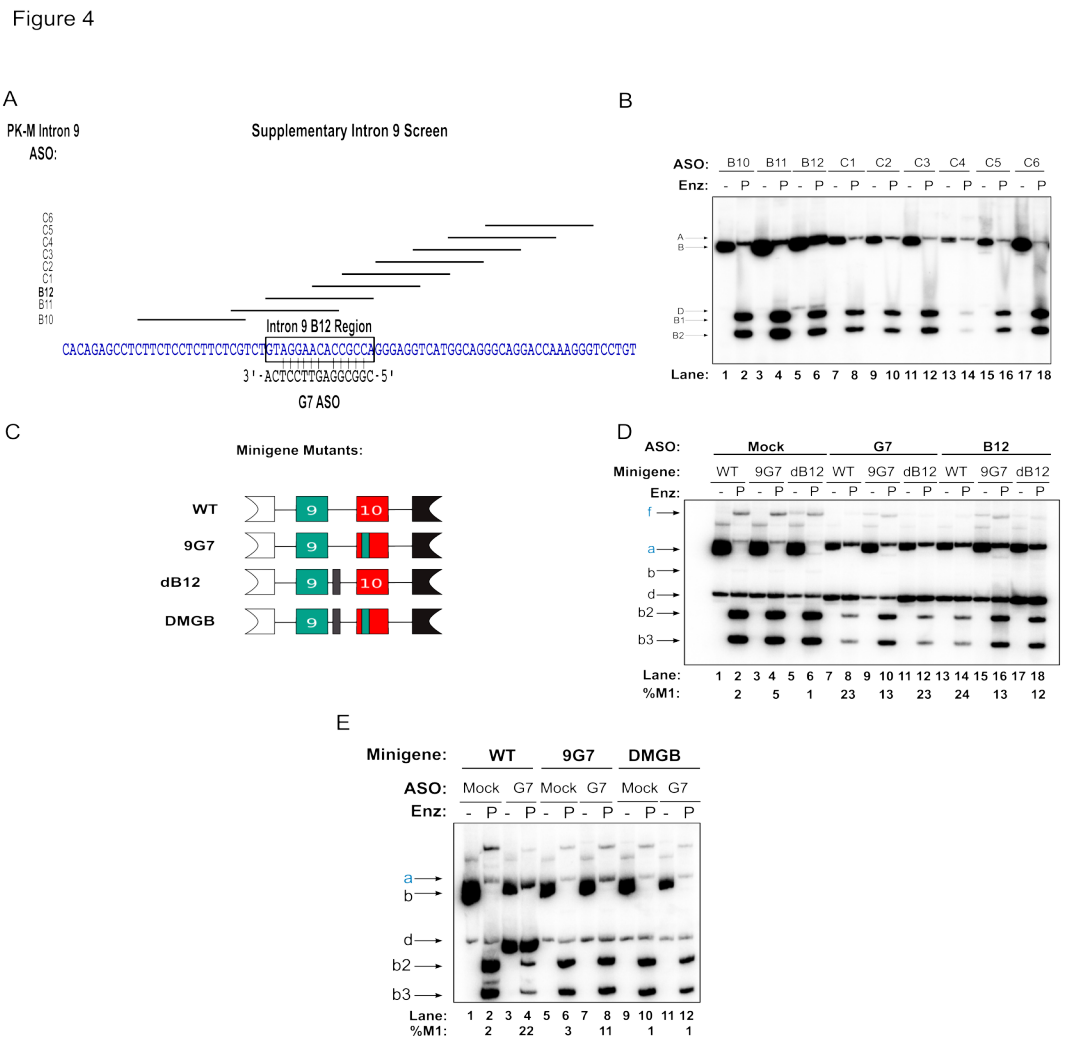
Figure 4
A
PK-M Intron 9
ASO:
Supplementary Intron 9 Screen
C6
C5
C4
C3
C2
C1
B12
B11
B10
Intron 9 B12 Region
CACAGAGCCTCTTCTCCTCTTCTCGTCTGTAGGAACACCGCCAGGGAGGTCATGGCAGGGCAGGACCAAAGGGTCCTGT
3'-ACTCCTTGAGGCGGC-5'
G7 ASO
B
ASO: B10 B11 B12 C1 C2 C3 C4 C5 C6
Enz: - P - P - P - P - P - P - P - P - P
A
B
D
B1
B2
Lane: 1 2 3 4 5 6 7 8 9 10 11 12 13 14 15 16 17 18
C
Minigene Mutants:
WT
9G7
dB12
DMGB
9
10
D
ASO: Mock G7 B12
Minigene: WT 9G7 dB12 WT 9G7 dB12 WT 9G7 dB12
Enz: - P - P - P - P - P - P - P - P - P
f
a
b
d
b2
b3
Lane: 1 2 3 4 5 6 7 8 9 10 11 12 13 14 15 16 17 18
%M1: 2 5 1 23 13 23 24 13 12
E
Minigene: WT 9G7 DMGB
ASO: Mock G7 Mock G7 Mock G7
Enz: - P - P - P - P - P - P
a
b
d
b2
b3
Lane: 1 2 3 4 5 6 7 8 9 10 11 12
%M1: 2 22 3 11 1 1

3.5.4 Fig 4 A second binding site for G7 ASO.

(A) Schematic of the supplementary intron 9 ASO walk centered on an intron 9 region (in blue letters) that is nearly homologous to the G7 ASO binding site, indicated at the bottom. Stacked lines indicate ASOs and their binding sites are aligned with intron 9. ASO names are indicated on the left. **(B)** Radioactive RT-PCR and restriction digest of endogenous *PK-M* transcripts in HEK-293 cells (as in Clower et. al. 2009) after ASO transfection at a final concentration of 30 nM. RNA was harvested from cells 48 hours after transfection. The identity of the transfected ASO is indicated at the top. cDNAs and fragements from endogenous mRNAs are indicated from on the left. **(C)**. Schematic of minigene mutants used in (D) and (E). 9G7 has the G7 ASO binding site in exon 10 removed and replaced by the corresponding region in exon 9. dB12 contains a 15-nt deletion of the intron 9 region targeted by ASO B12 in (A). DMGB contains both the mutations. **(D),(E)** Minigene transcript level changes as a result of ASO co-transfection in HEK-293 cells. ASOs were transfected at a final concentration of 30 nM. ASOs and minigenes in (C) are indicated at the top %M1 is indicated at the bottom, and bands are indicated on the left.

Figure 3.5-5

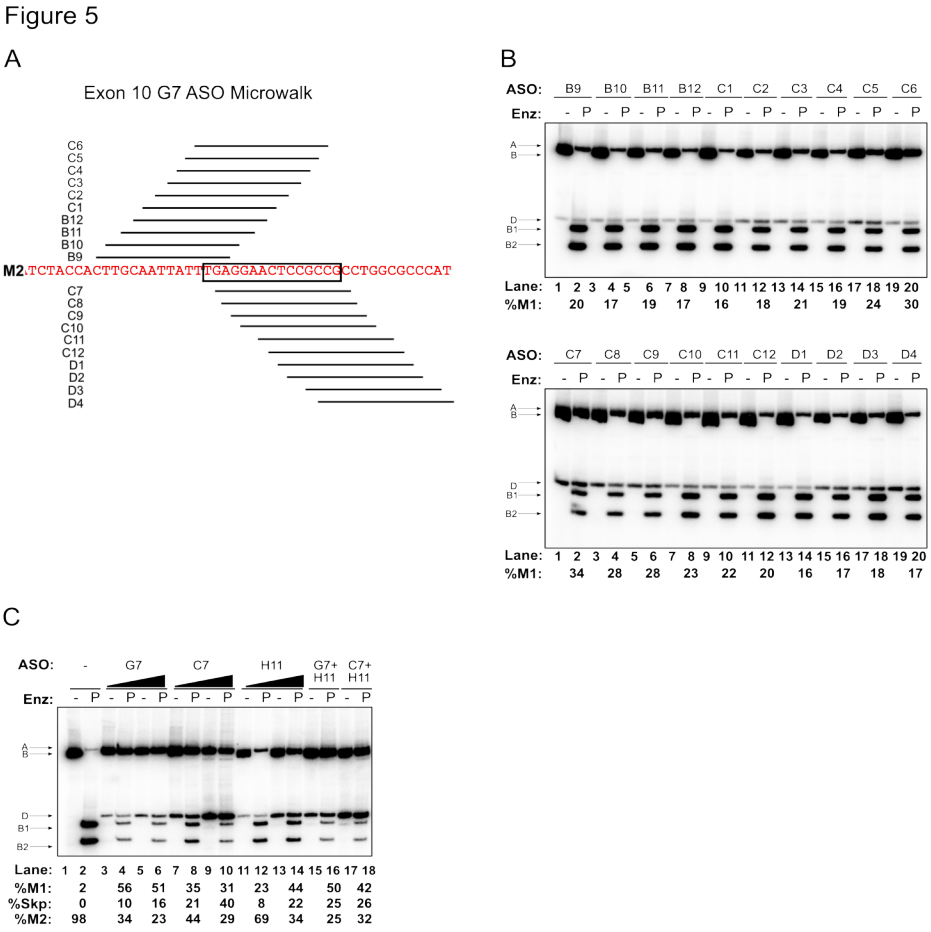
Figure 5
A
Exon 10 G7 ASO Microwalk
C6
C5
C4
C3
C2
C1
B12
B11
B10
B9
M2 TCTACCACTTGCAATTATTTGAGGAACTCCGCCGCCTGGCGCCCAT
C7
C8
C9
C10
C11
C12
D1
D2
D3
D4
B
ASO: B9 B10 B11 B12 C1 C2 C3 C4 C5 C6
Enz: - P - P - P - P - P - P - P - P - P - P
A
B
D
B1
B2
Lane: 1 2 3 4 5 6 7 8 9 10 11 12 13 14 15 16 17 18 19 20
%M1: 20 17 19 17 16 18 21 19 24 30
ASO: C7 C8 C9 C10 C11 C12 D1 D2 D3 D4
Enz: - P - P - P - P - P - P - P - P - P - P
A
B
D
B1
B2
Lane: 1 2 3 4 5 6 7 8 9 10 11 12 13 14 15 16 17 18 19 20
%M1: 34 28 28 23 22 20 16 17 18 17
C
ASO: - G7 C7 H11 G7+ H11 C7+ H11
Enz: - P - P - P - P - P - P - P - P - P
A
B
D
B1
B2
Lane: 1 2 3 4 5 6 7 8 9 10 11 12 13 14 15 16 17 18
%M1: 2 56 51 35 31 23 44 50 42
%Skp: 0 10 16 21 40 8 22 25 26
%M2: 98 34 23 44 29 69 34 25 32

3.5.5 Fig 5. G7-centered ASO microwalks.

(A),(C) Schematic representation of the 1 nt ASO microwalk along exon 10. Red letters indicate the exon 10 sequence. Stacked thin lines represent an individual ASO. Names of the ASOs are indicated on the left, from the bottom to top. Their approximate binding sites are aligned with the exon 10/intron 8/intron9 diagrams. The G7 region and the previously described SRSF3 ESE (Wang et. al. 2011) are indicated by rectangles in (A) and (C), respectively. **(B),(D)** Radioactive RT-PCR and restriction digest of endogenous *PK-M* transcripts in HEK-293 cells after ASO transfection at a final concentration of 30 nM. RNA was harvested from cells 48 hours after transfection. The identity of the transfected ASO is indicated at the top. cDNAs and fragments from endogenous mRNAs are indicated on the left. **(E)** Dose dependent effects of C7, G7 and H11 ASOs in 293 cells. Radioactive RT-PCR and restriction digest of endogenous *PK-M* transcripts in HEK-293 cells after ASO transfection at a final concentration of 60 and 120 nM. RNA was harvested from cells 48 hours after transfection. The identity of the transfected ASO is indicated at the top. cDNAs and fragments from endogenous mRNAs are indicated on the left. %M1 is indicated at the bottom. For combination experiments, each ASO was transfected at 60 nM each, for a final total ASO concentration of 120 nM.

Figure 3.5-6

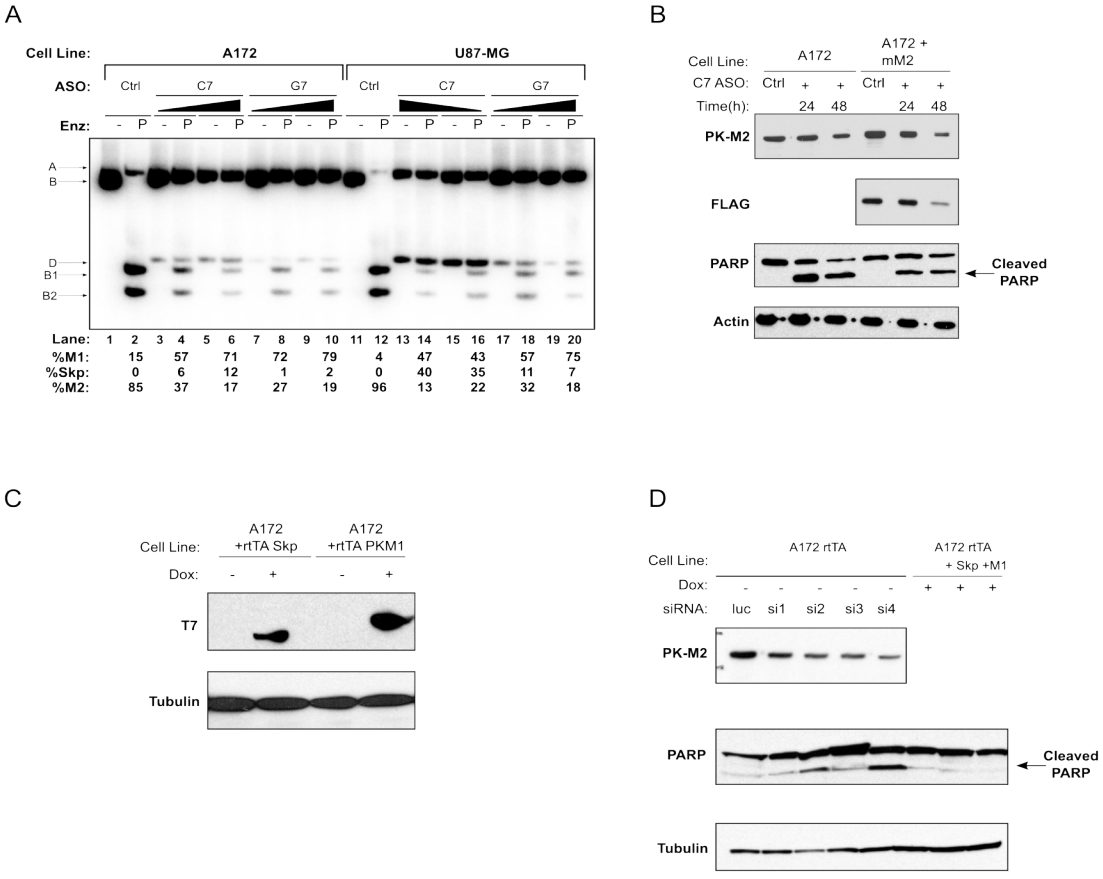
Figure 6
A
Cell Line:
A172
U87-MG
ASO:
Ctrl
C7
G7
Ctrl
C7
G7
Enz:
- P - P - P - P - P - P - P - P - P - P
A
B
D
B1
B2
Lane: 1 2 3 4 5 6 7 8 9 10 11 12 13 14 15 16 17 18 19 20
%M1: 15 57 71 72 79 4 47 43 57 75
%Skp: 0 6 12 1 2 0 40 35 11 7
%M2: 85 37 17 27 19 96 13 22 32 18
B
Cell Line:
A172
A172 + mM2
C7 ASO:
Ctrl + + Ctrl + +
Time(h):
24 48 24 48
PK-M2
FLAG
PARP
Cleaved PARP
Actin
C
Cell Line:
A172 +rtTA Skp
A172 +rtTA PKM1
Dox:
- + - +
T7
Tubulin
D
Cell Line:
A172 rtTA
A172 rtTA + Skp +M1
Dox:
- - - - - + + +
siRNA:
luc si1 si2 si3 si4
PK-M2
PARP
Cleaved PARP
Tubulin

3.5.6 Fig 6. Effects of ASOs on glioblastoma cells.

(A) Dose-dependent effects of C7 and G7 ASOs in A172 and U87-MG glioblastoma cells. Radioactive RT-PCR and restriction digests of endogenous *PK-M* transcripts from the indicated cell lines, 48 hours after transfection of the indicated ASOs at final concentrations of 60 or 120 nM. The control ASO (Ctrl) is an ASO targeting exon 7 of the SMN2 gene (Hua et. al. 2008). %M1 is indicated at the bottom. **(B)** Immunoblot analysis of A172 cells or A172 cells stably transduced with mouse PK-M2 cDNA, transfected with C7 or Control ASOs at a final concentration of 60 nM. C7-transfected cells were harvested 24 and 48 hours after transfection, while control cells were harvested after 48 hours. Antibodies used are indicated on the left. **(C)** Immunoblot analysis of A172 cells stably transduced with rtTA and doxycycline (dox)-inducible human PK-M1 or human Skp cDNA. Cells were harvested 48 hours after addition of doxycylin. Antibodies used are indicated on the left. **(D)** Immunoblot analysis of A172 cells transfected with 4 different PK-M2 siRNAs or A172 cells with dox-induced PK-M1 or Skp as in (C). Antibodies used are indicated on the left.

4 Chapter 4. Conclusions and Perspectives

4.1 Summary of conclusions

I have analyzed the alternative splicing of the mutually exclusive (ME) PK-M gene in cancer cells. I have demonstrated that exons 9 and 10 are repressed and activated, respectively, in cancer cells, and the elements involved in both processes are located mainly in the exons. These elements are critical in maintaining the PK-M2 dominant splicing pattern in proliferating and cancer cells. Through sub-exonic duplications, I have isolated a potent ESE in exon 10 and demonstrated that SRSF3, a known splicing factor, is its cognate activator. Making use of the discovery that critical splicing *cis*-elements are in the ME exons, I conducted an ASO walk along both exons, and discovered potent ASOs targeting exon 10 that switch the splicing of PK-M in cancer cells from a PK-M2 dominant pattern to a PK-M1 dominant pattern. I then tested the ASOs in glioblastoma cells and found that these ASOs induced apoptosis.

4.2 Future directions

Even though the mechanism PK-M alternative splicing is still incompletely understood, these discoveries represent an advance in the understanding of PK-M splicing in cancer cells. However, there are more specific areas of PK-M splicing that have yet to be explored, which I will outline below.

4.2.1 Analysis of PK-M splicing in a PK-M1 dominant system

All of the analyses of PK-M splicing were done in cancer cells, which predominantly express PK-M2. In order to fully understand the splicing switch from terminally

differentiated cells to cancer cells, an analysis of PK-M splicing must also be done in a PK-M1 dominant system. These cell lines exist, specifically the C2C12 myoblast differentiation system (Clower et al., 2010; David et al., 2010). Minigene constructs could be transfected into these cells when they are still proliferating, and induced to differentiate, before harvesting to analyze minigene splicing.

4.2.2 Uncovering exon 9 ESSs

Although the ASO walks and sub-exonic duplications have uncovered exon 10 enhancer elements, exon 9 exonic silencers have yet to be discovered. The exon 9 ASOs could have interfered with exon 9 splicing (as discussed in Chapter 3), but systematic exon 9 sub-duplications have yet to be done. The other problem is that the sub-exonic duplication approach is dependent on the duplicated region having a weaker or opposite type of element, which further confounds analysis and/or discovery.

4.2.3 Prevention of exon 9 and exon 10 double splicing

The predominant species from the exon 10 duplication minigene is the singly spliced PK-M2 isoform. This is unexpected, because it has been shown that exon 10 is strongly activated in cancer cells, and hence, if there were no repression of exon 9 and exon 10 double splicing, the predominant species should be the exon 10-exon 10 double-spliced isoform. Mutation of the B12 intron 9 region (Chapter 3) has also led to some double splicing. This implies that there could be elements in the flanking introns that prevent the double splicing of exon 9 to exon 10. Clearly, minigene mutagenesis analysis should be carried out to find elements that when deleted or mutated, lead to increased abundance of double-spliced species. In addition,

given the importance of RNA secondary structure in the maintenance of ME splicing in other systems (McManus and Graveley, 2011), a systematic analysis of endogenous RNA structure could be carried out, in order to find elements that might mediate ME maintenance via long-distance base pairing.

4.2.4 Effects of transcription and signaling pathways on PK-M splicing

Recently, specific histone modifications present in genomic portions encoding PK-M exon 9 have been reported to recruit PTB to intron 8 to repress exon 9 inclusion in HeLa cells (Luco et al., 2010). Since the effect of histone modifications and transcriptional elongation on ME splicing is relatively unexplored, experiments to determine if these factors play a major role in determining M1/M2 ratios could be performed. For example, a well characterized RNA polymerase II elongation mutant (de la Mata et al., 2003) could be expressed in HeLa cells together with the minigene to see if the slower Pol II elongation mutant could affect M1/M2 ratios. Similarly, signaling pathways have been shown to affect the activity of splicing factors (Blaustein et al., 2005). Since PK-M2 and signaling pathways are intimately related (Hitosugi et al., 2009; Yang et al., 2011), inhibition of selected pathways that are involved in cellular metabolism, growth and survival, for example, the mTOR, PI3K, EGFR and HGF pathways by widely available small-molecule inhibitors and assessing M1/M2 transcript ratios upon inhibition might be informative in determining which signaling pathways are important in the modulation of M1/M2 transcript ratios.

4.2.5 Tissue-specific mechanisms of PK-M splicing

I have found that an exon 10 3'ss minigene mutant (Chapter 2) behaves differently in different cell lines. In HeLa (data not shown) and 293 (Fig 1A) cell lines, the %M1 upon transfection is small (less than 10%). However, in cell lines derived from brain and muscle tissue, such as the glioblastoma A172 (Fig 1B), neuroblastoma SK-N-BE2 (Fig 1C) and rhabdomyosarcoma A204 (Fig 1D) cell lines, the extent of PK-M1 inclusion is drastically increased. It seems that the switch to the use of the exon 9 3'ss upon abrogation of the exon 10 3'ss is much more efficient in these cell lines. However, I have not begun experiments to find out why this is so, and this is a potentially interesting project in the future.

4.2.6 Establishment of *in vitro* splicing system to find trans-acting factors involved in PK-M splicing

A complementary approach to finding critical *cis*-elements is to establish *in vitro* splicing systems in a PK-M2 dominant context, such as in HeLa nuclear extracts, a fully PK-M1 dominant context, such as the rat brain splicing extract (Grabowski, 2005) or partial PK-M1 dominant system such as WERI-Rb1 extracts (Fig 1E). The different extracts could be mixed together to see if there are any changes in the M1/M2 splicing pattern, and fractionation of extracts could be carried out in order to isolate the factors involved in eliciting such a change. However, in order to establish such a system, the 6.4 kb minigene must be shortened to about 1.5 kb. Even though the critical *cis* elements are found in the exons, more work needs to be done to isolate other important splicing elements in the introns in order to find the minimal set of elements that are sufficient to recapitulate endogenous splicing patterns in all systems.

4.3 Figures and Legends

Figure 4.3-1

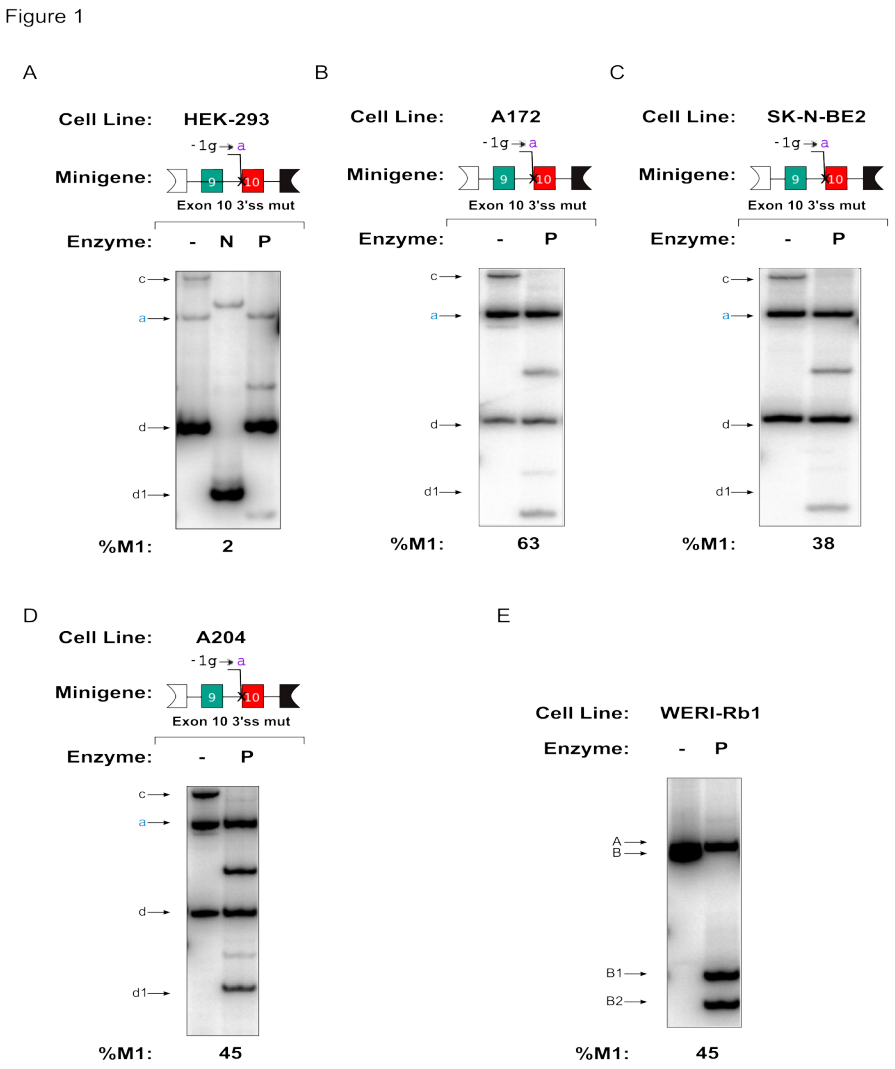

4.3.1 Fig 1. Unpublished data and future directions.

(A), (B), (C), (D). Behavior of the exon 10 3'ss mutant minigene in different cell lines. RT-PCR analysis of the exon 10 3'ss mutant minigene transfected in the cell lines indicated above, and harvested 48 hours later. % M1 is indicated at the bottom, while minigene species are indicated on the left in lower case, with important species in blue font. (E) Endogenous splicing pattern for the WERI-Rb1 retinoblastoma cell line. RT-PCR analysis of endogenous PK-M splicing. %M1 is indicated at the bottom, while endogenous species are indicated on the left in capital letters.

5 List of Abbreviations

ASO	antisense oligonucleotide
ATP	adenosine triphosphate
A172	A172 human glioblastoma cells
BPS	branch point Sequence
cDNA	complementary DNA
CTD	C-terminal domain of RNA polymerase II
CLIP	Cross-linking and immunoprecipitation
DMEM	Dubelcco's modified Eagle medium
DNA	deoxyribonucleic acid
dNTP	deoxynucleotide triphosphate
Dox	doxycycline
ECL	enhanced chemiluminescence
EJC	exon junction complex
ESE	exonic splicing enhancer
ESS	exonic splicing silencer
FBS	fetal bovine serum
HeLa	ovarian cancer cells from Henrietta Lacks
HEK 293	human embryonic kidney cells
HIF1α	hypoxia inducible factor 1-alpha
hnRNP	heterogenous nuclear ribonucleoprotein
ISE	intronic splicing enhancer
ISS	intronic splicing silencer
kDa	kilodalton
MOE	2'-O-methoxyethyl
mRNA	messenger ribonucleic acid
MSCV	murine stem cell virus
mTOR	mammalian target of rapamycin
Mut	Mutant
NMD	nonsense-mediated mRNA decay
PCR	polymerase chain reaction
PI3K	phosphoinositide 3-kinase
PK-M	Pyruvate kinase M gene
PK-M1	splicing isoform 1 of pyruvate kinase M
PK-M2	splicing isoform 2 of pyruvate kinase M
PMO	phosphorodiamidate morpholino oligonucleotide
PNA	peptide nucleic acid
Pol II	RNA polymerase II
Poly(A)	polyadenylation
PPT	polypyrimidine tract
PTC	premature termination codon
RNA	ribonucleic acid
RNAi	RNA interference
RRM	RNA recognition motif
RS	arginine and serine rich domain

SDS-PAGE	sodium dodecyl sulphate polyacrylamide gel electrophoresis
SR	serine and arginine domain containing protein
SRSF1	Serine and arginine rich, splicing factor 1
SRSF3	Serine and arginine rich, splicing factor 3
siRNA	small interfering RNAs
snRNP	small nuclear ribonucleoprotein
ss	splice site
U87-MG	U87-MG human glioblastoma cells
WT	wild-type

6 Appendix: Bibliography

Akerman, M., David-Eden, H., Pinter, R. Y., and Mandel-Gutfreund, Y. (2009). A computational approach for genome-wide mapping of splicing factor binding sites. Genome Biol *10*, R30.

Alter, J., Lou, F., Rabinowitz, A., Yin, H., Rosenfeld, J., Wilton, S. D., Partridge, T. A., and Lu, Q. L. (2006). Systemic delivery of morpholino oligonucleotide restores dystrophin expression bodywide and improves dystrophic pathology. Nat Med *12*, 175-177.

Anastasiou, D., Poulogiannis, G., Asara, J. M., Boxer, M. B., Jiang, J. K., Shen, M., Bellinger, G., Sasaki, A. T., Locasale, J. W., Auld, D. S.*, et al.* (2011). Inhibition of pyruvate kinase M2 by reactive oxygen species contributes to antioxidant responses. Science.

Belverud, S., Mogilner, A., and Schulder, M. (2008). Intrathecal pumps. Neurotherapeutics *5*, 114-122.

Black, D. L. (2003). Mechanisms of alternative pre-mRNA splicing. Annu Rev Biochem *72*, 291-336.

Black, D. L. (2000). Protein diversity from alternative splicing: a challenge for bioinformatics and post-genome biology. Cell *103*, 367-370.

Blanchette, M., and Chabot, B. (1999). Modulation of exon skipping by high-affinity hnRNP A1-binding sites and by intron elements that repress splice site utilization. EMBO J *18*, 1939-1952.

Blaustein, M., Pelisch, F., Tanos, T., Munoz, M. J., Wengier, D., Quadrana, L., Sanford, J. R., Muschietti, J. P., Kornblihtt, A. R., Caceres, J. F.*, et al.* (2005). Concerted regulation of nuclear and cytoplasmic activities of SR proteins by AKT. Nat Struct Mol Biol *12*, 1037-1044.

Bluemlein, K., Gruning, N. M., Feichtinger, R. G., Lehrach, H., Kofler, B., and Ralser, M. (2011). No evidence for a shift in pyruvate kinase PKM1 to PKM2 expression during tumorigenesis. Oncotarget *2*, 393-400.

Bonnet, S., Archer, S. L., Allalunis-Turner, J., Haromy, A., Beaulieu, C., Thompson, R., Lee, C. T., Lopaschuk, G. D., Puttagunta, L., Bonnet, S.*, et al.* (2007). A mitochondria-K+ channel axis is suppressed in cancer and its normalization promotes apoptosis and inhibits cancer growth. Cancer Cell *11*, 37-51.

Cáceres, J. F., and Kornblihtt, A. R. (2002). Alternative splicing: multiple control mechanisms and involvement in human disease. Trends Genet *18*, 186-193.

Cáceres, J. F., Screaton, G. R., and Krainer, A. R. (1998). A specific subset of SR proteins shuttles continuously between the nucleus and the cytoplasm. Genes Dev *12*, 55-66.

Cairns, R. A., Harris, I. S., and Mak, T. W. (2011). Regulation of cancer cell metabolism. Nat Rev Cancer *11*, 85-95.

Caputi, M., Mayeda, A., Krainer, A. R., and Zahler, A. M. (1999). hnRNP A/B proteins are required for inhibition of HIV-1 pre-mRNA splicing. EMBO J *18*, 4060-4067.

Cartegni, L., Chew, S. L., and Krainer, A. R. (2002). Listening to silence and understanding nonsense: exonic mutations that affect splicing. Nat Rev Genet *3*, 285-298.

Cartegni, L., Hastings, M., Calarco, J. A., de Stanchina, E., and Krainer, A. R. (2006). Determinants of exon 7 splicing in the spinal muscular atrophy genes, SMN1 and SMN2. Am J Hum Genet *78*, 63-77.

Chacko, E., and Ranganathan, S. (2009). Comprehensive splicing graph analysis of alternative splicing patterns in chicken, compared to human and mouse. BMC Genomics *10 Suppl 1*, S5.

Chang, Y. F., Imam, J. S., and Wilkinson, M. F. (2007). The nonsense-mediated decay RNA surveillance pathway. Annu Rev Biochem *76*, 51-74.

Choo, A. Y., Kim, S. G., Vander Heiden, M. G., Mahoney, S. J., Vu, H., Yoon, S. O., Cantley, L. C., and Blenis, J. (2010). Glucose addiction of TSC null cells is caused by failed mTORC1-dependent balancing of metabolic demand with supply. Mol Cell *38*, 487-499.

Christofk, H., Vander Heiden, M., Harris, M. H., Ramanathan, A., Gerszten, R. E., Wei, R., Fleming, M. D., Schreiber, S. L., and Cantley, L. (2008a). The M2 splice isoform of pyruvate kinase is important for cancer metabolism and tumour growth. Nature *452*, 230-233.

Christofk, H., Vander Heiden, M., Wu, N., Asara, J., and Cantley, L. (2008b). Pyruvate kinase M2 is a phosphotyrosine-binding protein. Nature *452*, 181-186.

Clower, C. V., Chatterjee, D., Wang, Z., Cantley, L. C., Vander Heiden, M. G., and Krainer, A. R. (2010). The alternative splicing repressors hnRNP A1/A2 and PTB influence pyruvate kinase isoform expression and cell metabolism. Proc Natl Acad Sci USA *107*, 1894-1899.

Crooke, S. (2001). Basic principles of antisense technology, In Antisense drug technology: Principles, strategies, and applications. , S. Crooke, ed. (New York: Marcel Dekker), pp. 1-28.

Dang, C. V., Kim, J. W., Gao, P., and Yustein, J. (2008). The interplay between MYC and HIF in cancer. Nat Rev Cancer *8*, 51-56.

David, C. J., Chen, M., Assanah, M., Canoll, P., and Manley, J. L. (2010). HnRNP proteins controlled by c-Myc deregulate pyruvate kinase mRNA splicing in cancer. Nature *463*, 364-368.

de la Mata, M., Alonso, C. R., Kadener, S., Fededa, J. P., Blaustein, M., Pelisch, F., Cramer, P., Bentley, D., and Kornblihtt, A. R. (2003). A slow RNA polymerase II affects alternative splicing in vivo. Mol Cell *12*, 525-532.

Dean, N., McKay, R., Miraglia, L., Howard, R., Cooper, S., Giddings, J., Nicklin, P., Meister, L., Ziel, R., Geiger, T.*, et al.* (1996). Inhibition of growth of human tumor cell lines in nude mice by an antisense of oligonucleotide inhibitor of protein kinase C-alpha expression. Cancer Res *56*, 3499-3507.

Dombrauckas, J. D., Santarsiero, B. D., and Mesecar, A. D. (2005). Structural basis for tumor pyruvate kinase M2 allosteric regulation and catalysis. Biochemistry *44*, 9417-9429.

Eldridge, A. G., Li, Y., Sharp, P. A., and Blencowe, B. J. (1999). The SRm160/300 splicing coactivator is required for exon-enhancer function. Proc Natl Acad Sci USA *96*, 6125-6130.

Elstrom, R. L., Bauer, D. E., Buzzai, M., Karnauskas, R., Harris, M. H., Plas, D. R., Zhuang, H., Cinalli, R. M., Alavi, A., Rudin, C. M., and Thompson, C. B. (2004). Akt stimulates aerobic glycolysis in cancer cells. Cancer Res *64*, 3892-3899.

Fischer, D. C., Noack, K., Runnebaum, I. B., Watermann, D. O., Kieback, D. G., Stamm, S., and Stickeler, E. (2004). Expression of splicing factors in human ovarian cancer. Oncology Reports *11*, 1085-1090.

Ge, K., DuHadaway, J., Du, W., Herlyn, M., Rodeck, U., and Prendergast, G. C. (1999). Mechanism for elimination of a tumor suppressor: aberrant splicing of a brain-specific exon causes loss of function of Bin1 in melanoma. Proc Natl Acad Sci U S A *96*, 9689-9694.

Ghigna, C., Giordano, S., Shen, H., Benvenuto, F., Castiglioni, F., Comoglio, P. M., Green, M. R., Riva, S., and Biamonti, G. (2005). Cell motility is controlled by SF2/ASF through alternative splicing of the Ron protooncogene. Molecular Cell *20*, 881-890.

Goncalves, V., Matos, P., and Jordan, P. (2008). The beta-catenin/TCF4 pathway modifies alternative splicing through modulation of SRp20 expression. RNA *14*, 2538-2549.

Grabowski, P. J. (2005). Splicing-active nuclear extracts from rat brain. Methods *37*, 323-330.

Graveley, B. (2005). Mutually exclusive splicing of the insect Dscam pre-mRNA directed by competing intronic RNA secondary structures. Cell *123*, 65-73.

Graveley, B. R. (2000). Sorting out the complexity of SR protein functions. RNA *6*, 1197-1211.

Graveley, B. R., Hertel, K. J., and Maniatis, T. (2001). The role of U2AF35 and U2AF65 in enhancer-dependent splicing. RNA *7*, 806-818.

Guertin, D. A., and Sabatini, D. M. (2007). Defining the role of mTOR in cancer. Cancer Cell *12*, 9-22.

Hammes, A., Guo, J. K., Lutsch, G., Leheste, J. R., Landrock, D., Ziegler, U., Gubler, M. C., and Schedl, A. (2001). Two splice variants of the Wilms' tumor 1 gene have distinct functions during sex determination and nephron formation. Cell *106*, 319-329.

Hammond, S. M., and Wood, M. J. (2011). Genetic therapies for RNA mis-splicing diseases. Trends Genet *27*, 196-205.

Hastings, M., Resta, N., Traum, D., Stella, A., Guanti, G., and Krainer, A. R. (2005). An LKB1 AT-AC intron mutation causes Peutz-Jeghers syndrome via splicing at noncanonical cryptic splice sites. Nat Struct Mol Biol *12*, 54-59.

Hastings, M. L., and Krainer, A. R. (2001). Pre-mRNA splicing in the new millennium. Curr Opin Cell Biol *13*, 302-309.

He, X., Ee, P. L., Coon, J. S., and Beck, W. T. (2004). Alternative splicing of the multidrug resistance protein 1/ATP binding cassette transporter subfamily gene in ovarian cancer creates functional splice variants and is associated with increased expression of the splicing factors PTB and SRp20. Clin Cancer Res *10*, 4652-4660.

Hitosugi, T., Kang, S., Vander Heiden, M. G., Chung, T. W., Elf, S., Lythgoe, K., Dong, S., Lonial, S., Wang, X., Chen, G. Z.*, et al.* (2009). Tyrosine phosphorylation inhibits PKM2 to promote the Warburg effect and tumor growth. Sci Signal *2*, ra73.

Hua, Y., Sahashi, K., Hung, G., Rigo, F., Passini, M. A., Bennett, C. F., and Krainer, A. R. (2010). Antisense correction of SMN2 splicing in the CNS rescues necrosis in a type III SMA mouse model. Genes Dev *24*, 1634-1644.

Hua, Y., Sahashi, K., Rigo, F., Hung, G., Horev, G., Bennett, C. F., and Krainer, A. R. (2011). Peripheral SMN restoration is essential for long-term rescue of a severe spinal muscular atrophy mouse model. Nature *478*, 123-126.

Hua, Y., Vickers, T. A., Okunola, H. L., Bennett, C. F., and Krainer, A. R. (2008). Antisense masking of an hnRNP A1/A2 intronic splicing silencer corrects SMN2 splicing in transgenic mice. Am J Hum Genet *82*, 834-848.

Huang, Y., and Steitz, J. (2005). SRprises along a Messenger's Journey. Molecular Cell *17*, 613-615.

Jelluma, N., Yang, X., Stokoe, D., Evan, G. I., Dansen, T. B., and Haas-Kogan, D. A. (2006). Glucose withdrawal induces oxidative stress followed by apoptosis in glioblastoma cells but not in normal human astrocytes. Mol Cancer Res *4*, 319-330.

Jia, R., Li, C., McCoy, J. P., Deng, C. X., and Zheng, Z. M. (2010). SRp20 is a proto-oncogene critical for cell proliferation and tumor induction and maintenance. Int J Biol Sci *6*, 806-826.

Jia, R., Liu, X., Tao, M., Kruhlak, M., Guo, M., Meyers, C., Baker, C. C., and Zheng, Z. M. (2009). Control of the papillomavirus early-to-late switch by differentially expressed SRp20. J Virol *83*, 167-180.

Johnson, J. M., Castle, J., Garrett-Engele, P., Kan, Z., Loerch, P. M., Armour, C. D., Santos, R., Schadt, E. E., Stoughton, R., and Shoemaker, D. D. (2003). Genome-wide survey of human alternative pre-mRNA splicing with exon junction microarrays. Science *302*, 2141-2144.

Kaelin, W. G., Jr. (2008). The von Hippel-Lindau tumour suppressor protein: O2 sensing and cancer. Nat Rev Cancer *8*, 865-873.

Kan, J. L., and Green, M. R. (1999). Pre-mRNA splicing of IgM exons M1 and M2 is directed by a juxtaposed splicing enhancer and inhibitor. Genes Dev *13*, 462-471.

Karni, R., Hippo, Y., Lowe, S. W., and Krainer, A. R. (2008). The splicing-factor oncoprotein SF2/ASF activates mTORC1. Proc Natl Acad Sci U S A *105*, 15323-15327.

Kim, J. W., Tchernyshyov, I., Semenza, G. L., and Dang, C. V. (2006). HIF-1-mediated expression of pyruvate dehydrogenase kinase: a metabolic switch required for cellular adaptation to hypoxia. Cell Metab *3*, 177-185.

Kreahling, J. M., and Graveley, B. R. (2005). The iStem, a long-range RNA secondary structure element required for efficient exon inclusion in the Drosophila Dscam pre-mRNA. Mol Cell Biol *25*, 10251-10260.

Le Hir, H., Izaurralde, E., Maquat, L. E., and Moore, M. J. (2000). The spliceosome deposits multiple proteins 20-24 nucleotides upstream of mRNA exon-exon junctions. EMBO J *19*, 6860-6869.

Letunic, I., Copley, R. R., and Bork, P. (2002). Common exon duplication in animals and its role in alternative splicing. Hum Mol Genet *11*, 1561-1567.

Licatalosi, D. D., and Darnell, R. B. (2010). RNA processing and its regulation: global insights into biological networks. Nat Rev Genet *11*, 75-87.

Licatalosi, D. D., Mele, A., Fak, J. J., Ule, J., Kayikci, M., Chi, S. W., Clark, T. A., Schweitzer, A. C., Blume, J. E., Wang, X.*, et al.* (2008). HITS-CLIP yields genome-wide insights into brain alternative RNA processing. Nature *456*, 464-469.

Long, J., and Caceres, J. (2009). The SR protein family of splicing factors: master regulators of gene expression. Biochemical J *417*, 15.

Lu, Q. L., Mann, C. J., Lou, F., Bou-Gharios, G., Morris, G. E., Xue, S. A., Fletcher, S., Partridge, T. A., and Wilton, S. D. (2003). Functional amounts of dystrophin produced by skipping the mutated exon in the mdx dystrophic mouse. Nat Med *9*, 1009-1014.

Lu, Q. L., Rabinowitz, A., Chen, Y. C., Yokota, T., Yin, H., Alter, J., Jadoon, A., Bou-Gharios, G., and Partridge, T. (2005). Systemic delivery of antisense oligoribonucleotide restores dystrophin expression in body-wide skeletal muscles. Proc Natl Acad Sci U S A *102*, 198-203.

Luco, R. F., Allo, M., Schor, I. E., Kornblihtt, A. R., and Misteli, T. (2011). Epigenetics in alternative pre-mRNA splicing. Cell *144*, 16-26.

Luco, R. F., Pan, Q., Tominaga, K., Blencowe, B. J., Pereira-Smith, O. M., and Misteli, T. (2010). Regulation of alternative splicing by histone modifications. Science *327*, 996-1000.

Luo, W., Hu, H., Chang, R., Zhong, J., Knabel, M., O'Meally, R., Cole, R. N., Pandey, A., and Semenza, G. L. (2011). Pyruvate kinase M2 is a PHD3-stimulated coactivator for hypoxia-inducible factor 1. Cell *145*, 732-744.

Luo, W., and Semenza, G. L. (2011). Pyruvate kinase M2 regulates glucose metabolism by functioning as a coactivator for hypoxia-inducible factor 1 in cancer cells. Oncotarget *2*, 551-556.

Lv, L., Li, D., Zhao, D., Lin, R., Chu, Y., Zhang, H., Zha, Z., Liu, Y., Li, Z., Xu, Y.*, et al.* (2011). Acetylation targets the M2 isoform of pyruvate kinase for degradation through chaperone-mediated autophagy and promotes tumor growth. Mol Cell *42*, 719-730.

Matlin, A. J., Clark, F., and Smith, C. W. (2005). Understanding alternative splicing: towards a cellular code. Nat Rev Mol Cell Biol *6*, 386-398.

May, G. E., Olson, S., McManus, C. J., and Graveley, B. R. (2011). Competing RNA secondary structures are required for mutually exclusive splicing of the Dscam exon 6 cluster. RNA *17*, 222-229.

Mayeda, A., and Krainer, A. R. (1999). Mammalian in vitro splicing assays. Methods Mol Biol *118*, 315-321.

Mazurek, S., Boschek, C. B., Hugo, F., and Eigenbrodt, E. (2005). Pyruvate kinase type M2 and its role in tumor growth and spreading. Semin Cancer Biol *15*, 300-308.

McGlincy, N., and Smith, C. (2008). Alternative splicing resulting in nonsense-mediated mRNA decay: what is the meaning of nonsense? Trends Biochem Sci *33*, 385-393.

McKay, R. A., Miraglia, L. J., Cummins, L. L., Owens, S. R., Sasmor, H., and Dean, N. M. (1999). Characterization of a potent and specific class of antisense oligonucleotide inhibitor of human protein kinase C-alpha expression. J Biol Chem *274*, 1715-1722.

McManus, C. J., and Graveley, B. R. (2011). RNA structure and the mechanisms of alternative splicing. Curr Opin Genet Dev *21*, 373-379.

Mercatante, D. R., Bortner, C. D., Cidlowski, J. A., and Kole, R. (2001). Modification of alternative splicing of Bcl-x pre-mRNA in prostate and breast cancer cells. analysis of apoptosis and cell death. J Biol Chem *276*, 16411-16417.

Michelakis, E. D., Sutendra, G., Dromparis, P., Webster, L., Haromy, A., Niven, E., Maguire, C., Gammer, T. L., Mackey, J. R., Fulton, D.*, et al.* (2010). Metabolic modulation of glioblastoma with dichloroacetate. Sci Transl Med *2*, 31ra34.

Michlewski, G., Sanford, J. R., and Cáceres, J. F. (2008). The splicing factor SF2/ASF regulates translation initiation by enhancing phosphorylation of 4E-BP1. Molecular Cell *30*, 179-189.

Monia, B. P., Lesnik, E. A., Gonzalez, C., Lima, W. F., McGee, D., Guinosso, C. J., Kawasaki, A. M., Cook, P. D., and Freier, S. M. (1993). Evaluation of 2'-modified oligonucleotides containing 2'-deoxy gaps as antisense inhibitors of gene expression. J Biol Chem *268*, 14514-14522.

Moore, M. J., and Proudfoot, N. J. (2009). Pre-mRNA processing reaches back to transcription and ahead to translation. Cell *136*, 688-700.

Muntoni, F., and Wood, M. J. (2011). Targeting RNA to treat neuromuscular disease. Nat Rev Drug Discov *10*, 621-637.

Noguchi, T., Inoue, H., and Tanaka, T. (1986). The M1- and M2-type isozymes of rat pyruvate kinase are produced from the same gene by alternative RNA splicing. J Biol Chem *261*, 13807-13812.

Olson, S., Blanchette, M., Park, J., Savva, Y., Yeo, G. W., Yeakley, J. M., Rio, D. C., and Graveley, B. (2007). A regulator of Dscam mutually exclusive splicing fidelity. Nat Struct Mol Biol *14*, 1134-1140.

Opalinska, J. B., and Gewirtz, A. M. (2002). Nucleic-acid therapeutics: basic principles and recent applications. Nat Rev Drug Discov *1*, 503-514.

Pan, Q., Shai, O., Lee, L. J., Frey, B. J., and Blencowe, B. J. (2008). Deep surveying of alternative splicing complexity in the human transcriptome by high-throughput sequencing. Nat Genet *40*, 1413-1415.

Papandreou, I., Cairns, R. A., Fontana, L., Lim, A. L., and Denko, N. C. (2006). HIF-1 mediates adaptation to hypoxia by actively downregulating mitochondrial oxygen consumption. Cell Metab *3*, 187-197.

Passini, M. A., Bu, J., Richards, A. M., Kinnecom, C., Sardi, S. P., Stanek, L. M., Hua, Y., Rigo, F., Matson, J., Hung, G.*, et al.* (2011). Antisense oligonucleotides delivered to the mouse CNS ameliorate symptoms of severe spinal muscular atrophy. Sci Transl Med *3*, 72ra18.

Patel, A. A., and Steitz, J. A. (2003). Splicing double: insights from the second spliceosome. Nat Rev Mol Cell Biol *4*, 960-970.

Paz, I., Akerman, M., Dror, I., Kosti, I., and Mandel-Gutfreund, Y. (2010). SFmap: a web server for motif analysis and prediction of splicing factor binding sites. Nucleic Acids Research *38 Suppl*, W281-285.

Robey, R. B., and Hay, N. (2009). Is Akt the "Warburg kinase"?-Akt-energy metabolism interactions and oncogenesis. Semin Cancer Biol *19*, 25-31.

Roca, X., Sachidanandam, R., and Krainer, A. R. (2005). Determinants of the inherent strength of human 5' splice sites. RNA *11*, 683-698.

Sakamuro, D., Elliott, K. J., Wechsler-Reya, R., and Prendergast, G. C. (1996). BIN1 is a novel MYC-interacting protein with features of a tumour suppressor. Nat Genet *14*, 69-77.

Sakharkar, M. K., Chow, V. T., and Kangueane, P. (2004). Distributions of exons and introns in the human genome. In Silico Biol *4*, 387-393.

Sazani, P., and Kole, R. (2003). Therapeutic potential of antisense oligonucleotides as modulators of alternative splicing. J Clin Invest *112*, 481-486.

Schaal, T. D., and Maniatis, T. (1999). Selection and characterization of pre-mRNA splicing enhancers: identification of novel SR protein-specific enhancer sequences. Mol Cell Biol *19*, 1705-1719.

Semenza, G. L. (2010). HIF-1: upstream and downstream of cancer metabolism. Curr Opin Genet Dev *20*, 51-56.

Sendoel, A., Kohler, I., Fellmann, C., Lowe, S. W., and Hengartner, M. O. (2010). HIF-1 antagonizes p53-mediated apoptosis through a secreted neuronal tyrosinase. Nature *465*, 577-583.

Smith, C. W. (2005). Alternative splicing--when two's a crowd. Cell *123*, 1-3.

Smith, C. W., and Nadal-Ginard, B. (1989). Mutually exclusive splicing of alpha-tropomyosin exons enforced by an unusual lariat branch point location: implications for constitutive splicing. Cell *56*, 749-758.

Stalder, L., and Muhlemann, O. (2008). The meaning of nonsense. Trends Cell Biol *18*, 315-321.

Sun, Q., Chen, X., Ma, J., Peng, H., Wang, F., Zha, X., Wang, Y., Jing, Y., Yang, H., Chen, R., *et al.* (2011). Mammalian target of rapamycin up-regulation of pyruvate kinase isoenzyme type M2 is critical for aerobic glycolysis and tumor growth. Proc Natl Acad Sci U S A *108*, 4129-4134.

Takenaka, M., Yamada, K., Lu, T., Kang, R., Tanaka, T., and Noguchi, T. (1996). Alternative splicing of the pyruvate kinase M gene in a minigene system. Eur J Biochem / FEBS *235*, 366-371.

Taylor, J. K., Zhang, Q. Q., Wyatt, J. R., and Dean, N. M. (1999). Induction of endogenous Bcl-xS through the control of Bcl-x pre-mRNA splicing by antisense oligonucleotides. Nat Biotechnol *17*, 1097-1100.

Vander Heiden, M., Cantley, L., and Thompson, C. B. (2009). Understanding the Warburg effect: the metabolic requirements of cell proliferation. Science *324*, 1029-1033.

Venables, J. P. (2004). Aberrant and alternative splicing in cancer. Cancer Research *64*, 7647-7654.

Venkitaraman, A. R. (2002). Cancer susceptibility and the functions of BRCA1 and BRCA2. Cell *108*, 171-182.

Verhaak, R. G., Hoadley, K. A., Purdom, E., Wang, V., Qi, Y., Wilkerson, M. D., Miller, C. R., Ding, L., Golub, T., Mesirov, J. P., *et al.* (2010). Integrated genomic analysis identifies clinically relevant subtypes of glioblastoma characterized by abnormalities in PDGFRA, IDH1, EGFR, and NF1. Cancer Cell *17*, 98-110.

Wagner, E. J., and Garcia-Blanco, M. A. (2001). Polypyrimidine tract binding protein antagonizes exon definition. Mol Cell Biol *21*, 3281-3288.

Wang, E. T., Sandberg, R., Luo, S., Khrebtukova, I., Zhang, L., Mayr, C., Kingsmore, S. F., Schroth, G. P., and Burge, C. B. (2008). Alternative isoform regulation in human tissue transcriptomes. Nature *456*, 470-476.

Wang, Z., Chatterjee, D., Jeon, H. Y., Akerman, M., Vander Heiden, M. G., Cantley, L. C., and Krainer, A. R. (2011). Exon-centric regulation of pyruvate kinase M alternative splicing via mutually exclusive exons. J Mol Cell Biol.

Wang, Z., Kayikci, M., Briese, M., Zarnack, K., Luscombe, N. M., Rot, G., Zupan, B., Curk, T., and Ule, J. (2010). iCLIP predicts the dual splicing effects of TIA-RNA interactions. PLoS Biol *8*, e1000530.

Warburg, O. (1956). On the origin of cancer cells. Science *123*, 309-314.

Will, C. L., and Luhrmann, R. (2011). Spliceosome structure and function. Cold Spring Harb Perspect Biol *3*.

Witten, J. T., and Ule, J. (2011). Understanding splicing regulation through RNA splicing maps. Trends Genet *27*, 89-97.

Xue, Y., Zhou, Y., Wu, T., Zhu, T., Ji, X., Kwon, Y. S., Zhang, C., Yeo, G., Black, D. L., Sun, H., *et al.* (2009). Genome-wide analysis of PTB-RNA interactions reveals a strategy used by the general splicing repressor to modulate exon inclusion or skipping. Mol Cell *36*, 996-1006.

Yang, W., Xia, Y., Ji, H., Zheng, Y., Liang, J., Huang, W., Gao, X., Aldape, K., and Lu, Z. (2011). Nuclear PKM2 regulates beta-catenin transactivation upon EGFR activation. Nature.

Yeo, G., and Burge, C. B. (2004). Maximum entropy modeling of short sequence motifs with applications to RNA splicing signals. J Comput Biol *11*, 377-394.

Zhang, Z., and Krainer, A. R. (2004). Involvement of SR proteins in mRNA surveillance. Molecular Cell *16*, 597-607.

Zhu, J., Mayeda, A., and Krainer, A. R. (2001). Exon identity established through differential antagonism between exonic splicing silencer-bound hnRNP A1 and enhancer-bound SR proteins. Molecular Cell *8*, 1351-1361.

Zuo, P., and Maniatis, T. (1996). The splicing factor U2AF35 mediates critical protein-protein interactions in constitutive and enhancer-dependent splicing. Genes Dev *10*, 1356-1368.